Powered Addition as Modelling Technique for Flow Processes

by

Pierré de Wet

Thesis presented in partial fulfilment of the requirements for the degree of Master of Sciences

at

Stellenbosch University

Supervisor: Prof. J P du Plessis

Department of Mathematical Sciences
Applied Mathematics Division
Faculty of Natural Sciences

March 2010

Declaration

By submitting this thesis electronically, I declare that the entirety of the work contained therein is my own, original work, that I am the owner of the copyright thereof (unless to the extent explicitly otherwise stated) and that I have not previously in its entirety or in part submitted it for obtaining any qualification.

Signature: ..... Date: ...../...../.....

Abstract

The interpretation – and compilation of predictive equations to represent the general trend – of collected data is aided immensely by its graphical representation. Whilst, by and large, predictive equations are more accurate and convenient for use in applications than graphs, the latter is often preferable since it visually illustrates deviations in the data, thereby giving an indication of reliability and the range of validity of the equation. Combination of these two tools – a graph for demonstration and an equation for use – is desirable to ensure optimal understanding. Often, however, the functional dependencies of the dependent variable are only known for large and small values of the independent variable; solutions for intermediate quantities being obscure for various reasons (e.g. narrow band within which the transition from one regime to the other occurs, inadequate knowledge of the physics in this area, etc.). The limiting solutions may be regarded as asymptotic and the powered addition to a power, s, of such asymptotes, f_0 and f_∞ , leads to a single correlating equation that is applicable over the entire domain of the dependent variable. This procedure circumvents the introduction of *ad hoc* curve fitting measures for the different regions and subsequent, unwanted jumps in piecewise fitted correlative equations for the dependent variable(s). Approaches to successfully implement the technique for different combinations of asymptotic conditions are discussed. The aforementioned method of powered addition is applied to experimental data and the semblances and discrepancies with literature and analytical models are discussed; the underlying motivation being the aspiration towards establishing a sound modelling framework for analytical and computational predictive measures. The purported procedure is revealed to be highly useful in the summarising and interpretation of experimental data in an elegant and simplistic manner.

Opsomming

Die interpretasie – en samestelling van vergelykings om die algemene tendens voor te stel – van versamelde data word onoorsienbaar bygestaan deur die grafiese voorstelling daarvan. Ten spyte daarvan dat vergelykings meer akkuraat en geskik is vir die gebruik in toepassings as grafieke, is laasgenoemde dikwels verskieslik aangesien dit afwykings in die data visueel illustreer en sodoende 'n aanduiding van die betroubaarheid en omvang van geldigheid van die vergelyking bied. 'n Kombinasie van hierdie twee instrumente – 'n grafiek vir demonstrasie en 'n vergelyking vir aanwending – is wenslik om optimale begrip te verseker. Die funksionele afhanklikheid van die afhanklike veranderlike is egter dikwels slegs bekend vir groot en klein waardes van die onafhanklike veranderlike; die oplossings by intermediêre hoeveelhede onduidelik as gevolg van verskeie redes (waaronder, bv. 'n smal band van waardes waarbinne die oorgang tussen prosesse plaasvind, onvoldoende kennis van die fisika in hierdie area, ens.). Beperkende oplossings / vergelykings kan as asimptote beskou word en magsaddisie tot 'n mag, s, van sodanige asimptote, f_0 en f_∞, lei tot 'n enkel, saamgestelde oplossing wat toepaslik is oor die algehele domein van die onafhanklike veranderlike. Dié prosedure voorkom die instelling van ad hoc passingstegnieke vir die verskillende gebiede en die gevolglike ongewensde spronge in stuksgewyspassende vergelykings van die afhankilke veranderlike(s). Na aanleiding van die moontlike kombinasies van asimptotiese toestande word verskillende benaderings vir die suksesvolle toepassing van hierdie tegniek bespreek. Die bogemelde metode van magsaddisie word toegepas op eksperimentele data en die ooreenkomste en verskille met literatuur en analitiese modelle bespreek; die onderliggend motivering 'n strewe na die daarstelling van 'n modellerings-raamwerk vir analitiese- en rekenaarvoorspellingsmaatreëls. Die voorgestelde prosedure word aangetoon om, op 'n elegante en eenvoudige wyse, hoogs bruikbaar te wees vir die lesing en interpretasie van eksperimentele data.

Acknowledgements

I would like to express my sincere gratitude to the following people for their contribution:

- My supervisor, Prof. Jean Prieur du Plessis, for patient academic guidance, longanimity and an open-door policy throughout the course of both my undergraduate and postgraduate studies at Stellenbosch University;
- Prof. Britt Halvorsen at Høgskolen i Telemark (Telemark University College), Porsgrunn, Norway, for being my host and generous financial assistance during my visit to their institution during the months of August – October 2008; for encouraging me to write a paper for submission to The 5th International Conference on Computational & Experimental Methods in Multiphase and Complex Flow (Multiphase Flow V); and for making it financially possible to attend the conference in New Forest, UK, form 15 - 17 June 2009;
- Dr. Finn Haugen for writing the experiment-specific software in LabVIEW that we required to perform the experiments at Høgskolen i Telemark (Telemark University College), Porsgrunn, Norway.
- The South African National Research Foundation (NRF) for financial support.

vir die Twee Outes

Contents

Nomenclature

Constants

π	3.141 592 654
e	2.718 281 828

Variables

a_v	particle specific surface	$[m^{-1}]$
A	arbitrary coefficient	$[-]$
A_{ann}	area of annulus	$[m^2]$
A_c	cross-sectional area of bed	$[m^2]$
A_p	surface area of single, non-spherical particle	$[m^2]$
A_{plug}	area of plug	$[m^2]$
A_{sp}	surface area of an equivalent volume sphere	$[m^2]$
B	arbitrary coefficient	$[-]$
c	constant	$[-]$
c_d	form drag coefficient	$[-]$
C_Ω	new constant / model parameter of Mbiya	$[-]$
d	linear dimension of RUC	$[m]$
d_p	mean particle diameter	$[m]$
d_s	linear dimension of solid in RUC	$[m]$
d_{sv}	diameter of sphere with equivalent surface area / volume ratio as particle	$[m]$
d_v	volume diameter	$[m]$
D	diameter	$[m]$
D_h	hydraulic diameter	$[m]$
D_{plug}	plug diameter	$[m]$
$D_{\mathtt{s}}$	diameter of sphere (perfectly spherical particle)	$[m]$
D_{shear}	sheared diameter	$[m]$
$f\{x\}$	original dependent variable	$[-]$

f_0	asymptotic solution or correlation for $x \to 0$	$[-]$
f_∞	asymptotic solution or correlation for $x \to \infty$	$[-]$
g	acceleration due to gravity	$[m/s^2]$
$g\{x\}$	canonical dependent variable	$[-]$
$h\{x^*\}$	logarithmic dependent variable	$[-]$
h_v	velocity head	$[m]$
h_s	static head	$[m]$
h_t	total head	$[m]$
H	bed height	$[m]$
k	pressure loss coefficient	$[-]$
k_v	pressure loss coefficient for valve	$[-]$
$k_{v,c}$	pressure loss coefficient for valve at critical point	$[-]$
K	fluid consistency index	$[Pa.s^n]$
L	length of straight channel / bed height	$[m]$
m_0	total or bulk mass	$[kg]$
m_f	mass of traversing fluid	$[kg]$
m_s	solid mass	$[kg]$
M	empirically determined, constant coefficient	$[-]$
n	fluid behaviour index	$[-]$
N	empirically determined, constant coefficient	$[-]$
p	pressure	$[N/m^2]$
p_H	total pressure head	$[N/m^2]$
q	superficial velocity / specific discharge	$[m/s]$
q_A	arbitrary constant	$[-]$
q_{mf}	minimum fluidisation velocity	$[m/s]$
Q_{ann}	flux through annulus	$[m^3/s]$
Q_{plug}	flux through plug	$[m^3/s]$
r	radius	$[m]$
r_{plug}	plug radius	$[m]$
R	pipe radius	$[m]$
Re	general Reynolds number	$[-]$
Re_3	Slatter Reynolds number	$[-]$
$Re_{3,c}$	Slatter Reynolds number at critical point	$[-]$
Re_p	particle Reynolds number	$[-]$
$Re_{\mathtt{s}}$	Reynolds number for packed bed of spheres	$[-]$
s	arbitrary shifting exponent	$[-]$
t	arbitrary shifting exponent	$[-]$
U_0	total or bulk volume	$[m^3]$
U_f	volume of fluid phase	$[m^3]$
U_s	volume of solid phase	$[m^3]$
$\underline{v}$	velocity	$[m/s]$

$\overline{v}_{\text{ann}}$	corrected mean velocity in the annulus	$[m/s]$
$\underline{v}_{\text{plug}}$	velocity of plug	$[m/s]$
v_x	velocity component in x-direction	$[m/s]$
v_y	velocity component in y-direction	$[m/s]$
v_z	velocity component in z-direction	$[m/s]$
V_p	volume of single, non-spherical particle	$[m^3]$
w	specific weight	$[kg/m^2s^2]$
x	independent variable	$[-]$
x^*	logarithmic independent variable	$[-]$
x_A	arbitrary constant	$[-]$
x_B	arbitrary constant	$[-]$
x_c	independent variable at central or critical point	$[-]$
Y	normalised dependent variable	$[-]$
z	height above arbitrary reference point	$[m]$
Z	normalised independent variable	$[-]$

Greek letters

α	exponent in asymptotic solution for $x \to 0$ / arbitrary exponent	$[-]$
β	exponent in asymptotic solution for $x \to \infty$ / arbitrary exponent	$[-]$
$\dot{\gamma}$	shear rate	$[s^{-1}]$
Δ	change in stream-wise property	$[-]$
ε	bed porosity / void fraction	$[-]$
ε_0	porosity at incipient fluidisation	$[-]$
η	apparent viscosity	$[N.s/m^2]$
θ	valve opening coefficient	$[-]$
κ	hydrodynamic permeability	$[-]$
λ_Ω	nominal turbulent loss coefficient	$[-]$
μ	fluid dynamic viscosity	$[N.s/m^2]$
ν	kinematic viscosity	$[s^{-1}]$
$\zeta_0\{q\}$	functional dependence of pressure drop for $q \to 0$	$[N/m^3]$
$\zeta_\infty\{q\}$	functional dependence of pressure drop for $q \to \infty$	$[N/m^3]$
ρ	mass density	$[kg/m^3]$
ρ_0	total or bulk mass density	$[kg/m^3]$
ρ_f	mass density of traversing fluid	$[kg/m^3]$
ρ_s	mass density of solids	$[kg/m^3]$
τ	shear stress	$[N/m^2]$
τ_0	shear stress at the pipe wall	$[N/m^2]$

τ_y	yield stress	$[N/m^2]$
ϕ_p	particle shape factor (sphericity)	$[-]$
Φ	variable defined for simplicity in Ergun equation	$[-]$
ψ	geometric factor	$[-]$
Ψ	Waddell sphericity factor	$[-]$

Vectors and Tensors

$\underline{f_b}$	body forces	$[N/kg]$
$\underline{\hat{n}}$	unit vector in stream-wise direction	$[-]$
∇	del operator	$[m^{-1}]$
$\underline{\underline{\sigma}}$	stress tensor	$[N/m^2]$
$\underline{\underline{\tau}}$	viscous stress dyadic	$[N/m^2]$

Acronyms

CHE	Churchill-Usagi Equation
RUC	Representative Unit Cell

Introduction

The dependence of modern engineering research on precise, credible experimental and computational practices is undeniable. These procedures provide the requisite predictive information needed for design purposes and the in-depth understanding of complex processes. It is common practice to represent the general trend in a set of such collected data by drawing a line through the individual datum points on the plot. Correlation between the drawn predictive curve and the data is then evaluated against some norm, e.g. least squares fit to a straight line or polynomial function passing through the data, visual inspection, etc. Theoretical knowledge of the functional behaviour is helpful but not a prerequisite for the construction of graphical correlation and thus a line best suited to the particular problem is chosen – the better the predictive line on the graphical presentation corresponds to the physical reality, especially in the limits of the independent variable, the greater the trustworthiness of obtained results.

If it is possible to accurately determine or predict the asymptotic behaviour – traits at extreme values of the independent variable – of the dependent variable under consideration, the results can usually be presented in a neat and elegant format. The basic procedure of asymptotic matching by straightforward addition of the expressions for the asymptotic conditions is a method that has been been in use for some time, especially in engineering practice. However, the article by Churchill & Usagi [1], which appeared in 1972, for the first time really formalised the use and accentuated the wide application possibilities of the method and variations thereof. Their method yields an equation of simple form with one arbitrary constant that interpolates between the limiting solutions; the value of which may be determined by either experimental or theoretical procedure. The routine is applicable to any phenomenon which varies uniformly between known, limiting solutions and is especially useful for the evaluation and summarising of experimental and computational data. Furthermore it is particularly convenient for design purposes as it yields an expression that is relevant over the entire domain of the dependent variable and has the same form for all correlations. Whether it presents an exact representation of the transfer process cannot be proven scientifically, yet the method is widely applicable and accepted.

In the first chapter an outline is given of powered addition. The articles by Churchill & Usagi [1; 2] form the backbone of this chapter. Different scenarios of the limiting functions and / or values are investigated and simple examples provided. Curve adjustment and the importance of the point of intersection of the asymptotes are discussed. Chapter 2 and 4 sees the application of the method to the collected experimental data for two diverse processes. The results of the former chapter were presented at The 2nd Southern African Conference on Rheology (SASOR), Cape Peninsula University of Technology, Cape Town, 6 - 8 October 2008 [3]; those of the latter were published in the proceedings of The 5th International Conference on Computational & Experimental Methods in Multiphase and Complex Flow (Multiphase Flow V), New Forest, UK, 15 - 17 June 2009 [4]. Chapter 3 serves as précis of two approaches used in predicting pressure drop over a packed bed or porous medium – the one (Ergun equation) being itself an example of powered addition with an exponent of unity, the other (RUC model) forming a keystone to the work of the following chapter. Supplementary material and the original data sets of the experimental investigations conducted at Høgskolen i Telemark (Telemark University College), Porsgrunn, Norway are collected in the appendices.

Chapter 1

Powered addition as curve fitting technique

Powered addition of expressions valid for two opposing ranges as described by Churchill and Usagi [1; 2; 5; 6] is a procedure used to produce a combined result which is valid for both of these ranges. Since each of the limiting expressions predominates in their respective regions of applicability, a unified model can be obtained using such an 'asymptote matching' technique.

1.1 Asymptotic behaviour of transfer processes

In many continuum processes, such as momentum and thermal transfer processes, the value of a sought after parameter is expressible as a function of certain known parameter(s) at low and high values. These limiting solutions for large and small values of the independent variable(s) may be regarded as asymptotic conditions of the dependent variable.

By stating that

$$f\{x\} \to g\{x\} \quad \text{as} \quad x \to a$$

it is meant that

$$\left(\frac{f\{x\}}{g\{x\}}\right) \to 1 \quad \text{as} \quad x \to a.$$

In other words, it is said that f is *asymptotic* to g as $x \to a$ [7]. Very often the functional expression of the dependent variable is in the form of a power dependency upon some independent variable, x.

Let the functional dependence, f, of such a process be described by

$$f \to f_0\{x\} = Ax^{\alpha} \qquad \text{as} \quad x \to 0, \tag{1.1}$$

$$f \to f_\infty\{x\} = Bx^{\beta} \qquad \text{as} \quad x \to \infty. \tag{1.2}$$

Here equations (1.1) and (1.2) denote the functional expressions at the lower and upper extremal values of x respectively. However, solutions for intermediate cases are seldom as simply expressed. (It is important to take note that, for the discussion to follow, the explicit expression of the asymptotes in terms of a power dependency is not permutable, i.e. the lower asymptote is always associated with coefficient A and exponent α; the upper with B and β).

The direct summation of two such asymptotic solutions or approximations is often effected to obtain a single solution that holds over the entire range of the independent variable, i.e.

$$f\{x\} = f_0\{x\} + f_\infty\{x\} = Ax^{\alpha} + Bx^{\beta}. \tag{1.3}$$

Equation (1.3) may now be considered as a *matching* or *coupled* curve connecting the two dependencies as it satisfies the asymptotic conditions and also provides values for f at intermediate values of the independent variable, x.

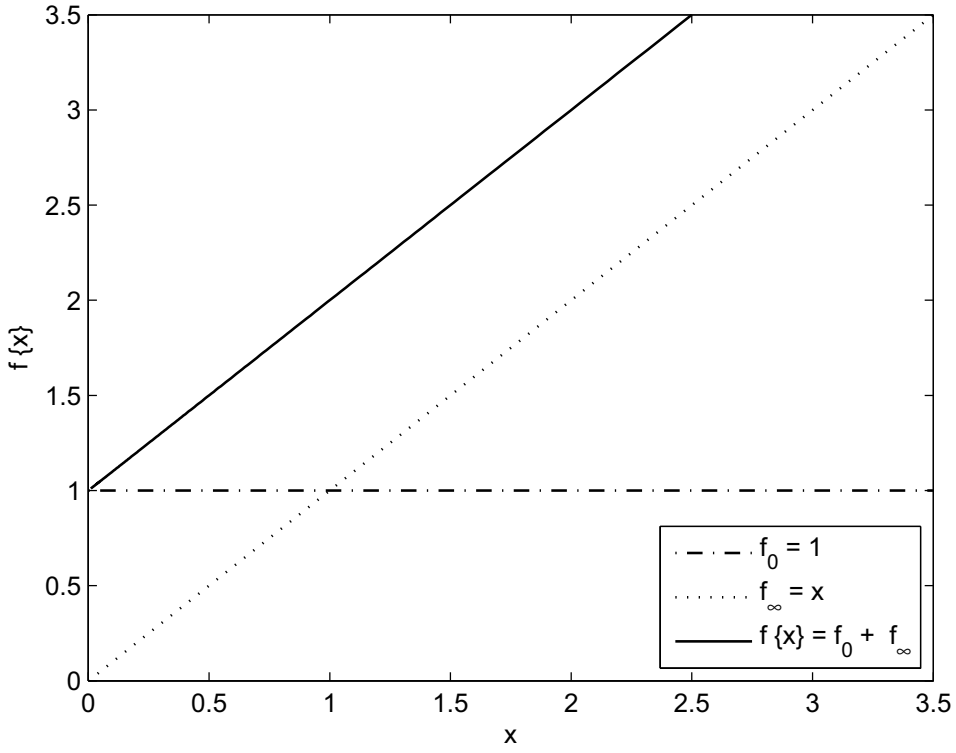

Figure 1.1: Linear plot of the function $f\{x\} = 1 + x$.

As an example, consider the very simple case of a function $f\{x\} = 1 + x$; i.e. $A = 1$, $B = 1$, $\alpha = 0$ and $\beta = 1$ in equation (1.3). In the above formulation this corresponds to the case,

$$f\{x\} \to 1 \quad \text{as} \quad x \to 0, \tag{1.4}$$

$$f\{x\} \to x \quad \text{as} \quad x \to \infty. \tag{1.5}$$

Hence the asymptotes governing the behaviour of the coupled function will be given by

$$f_0\{x\} = 1$$
$$f_\infty\{x\} = x.$$

Plotting this relation on a linear-linear Cartesian scale, generates a straight line as shown in Figure 1.1. It is only once the function is drawn on a log-log graph that more insight is gained; the asymptotic behaviour that results from addition of the functional expressions at the extremal values now becomes apparent. This is illustrated in Figure 1.2.

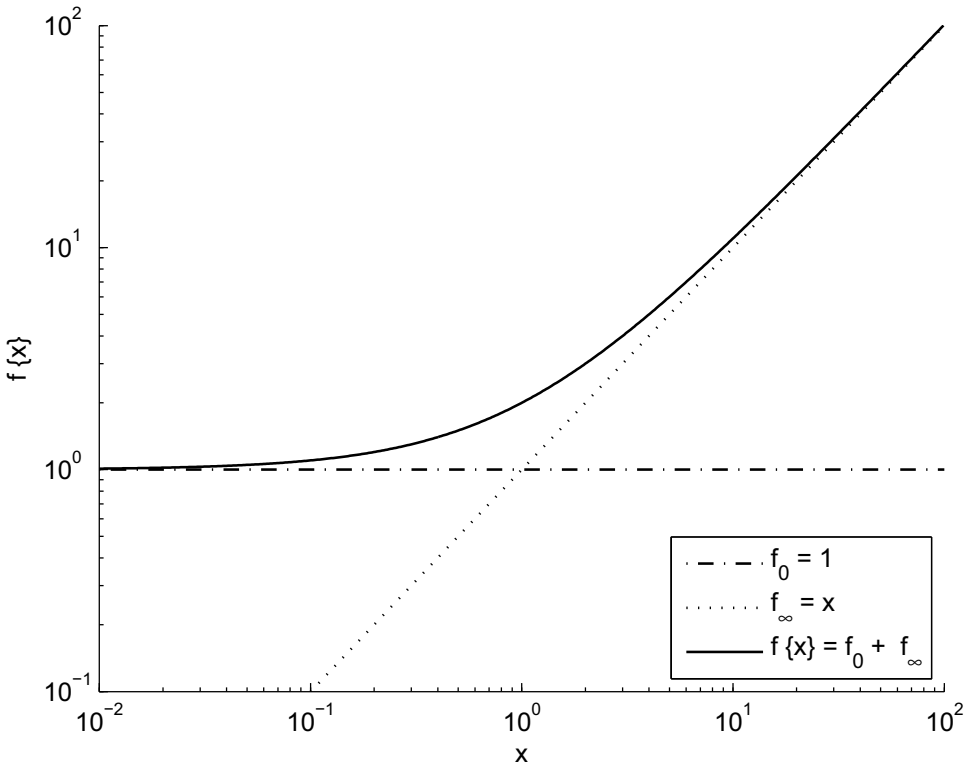

Figure 1.2: Log-log plot of the function $f\{x\} = 1 + x$.

The advantage of using logarithmic coordinates when plotting data is that equal percentage changes yield equal displacements over the entire range, where-as with

arithmetic coordinates (Cartesian axes) on the other hand, the displacement increases in accordance with the magnitude of the variable. In other words, logarithmic coordinates display percentage deviations and perceptually suppress these deviations compared to arithmetic plots – the former may thus obscure the magnitude of scatter in the data, the latter distort such scatter unduly by displaying absolute differences. [5].

It is important to note that, as seen in Figure 1.1, the matched curve merely approaches, yet never reaches, the upper limiting functional value. An increase in the independent variable leads to the diminishing influence of the lower asymptotic function on the overall solution, which only becomes visually apparent once the solution is plotted on log-log axes as in Figure 1.2. The method is therefore best suited to approximate the general trend in a process, rather than predict the exact values of the constituent limiting functions.

1.2 Shifting of the matching curve

Frequently the values of the dependent variable at the transition between the asymptotic extremities do not lie exactly on this matching solution. Churchill & Usagi [1; 2; 5; 6] demonstrated that the use of powered addition, the most general form of which is shown in equations (1.6) and (1.7) below, may lead to dramatic improvement in correlation with experimental data

$$f^s\{x\} = f_0^s\{x\} + f_\infty^s\{x\}, \tag{1.6}$$

whence

$$f\{x\} = [f_0^s\{x\} + f_\infty^s\{x\}]^{1/s}. \tag{1.7}$$

By adjusting the value of the shifting exponent, s, the level of the solution may be modified so as to more closely trace the expected or empirical values, yielding better correspondence between predictive equation and experimental results. The right hand side of equation (1.7) may be considered as the s^{th} order sum of the asymptotic solutions [1; 2; 5].

1.2.1 Increasing dependence

When the dependent variable is an increasing power of the independent variable, in other words if the power of x in equation (1.3) is greater at the higher limit, that is

$$\alpha < \beta, \tag{1.8}$$

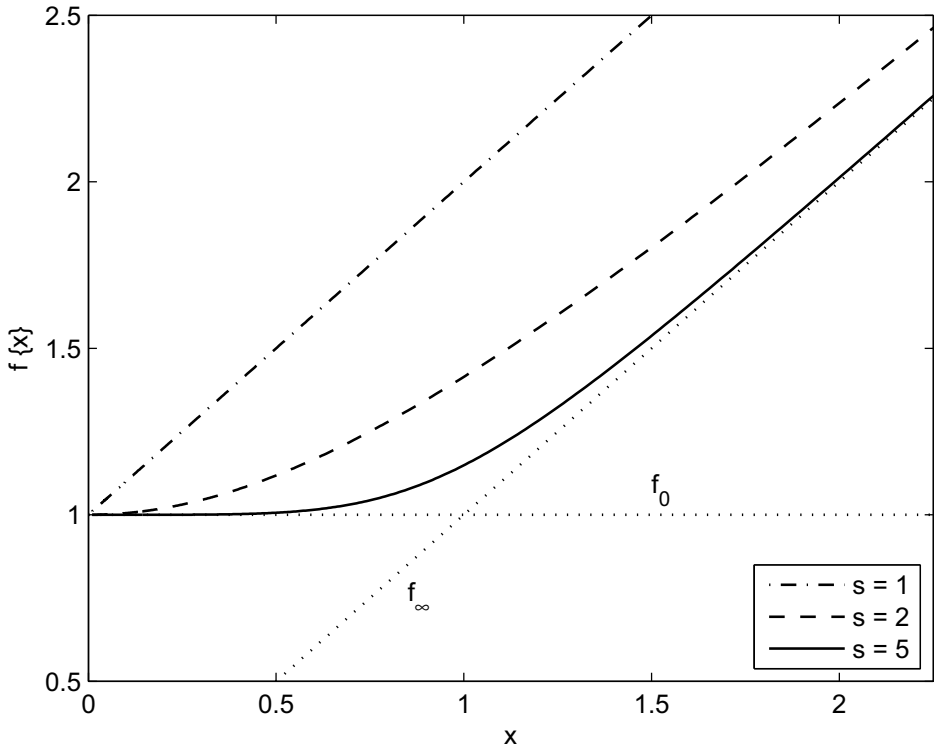

Figure 1.3: Linear plot of the function $f\{x\} = [f_0^s\{x\} + f_\infty^s\{x\}]^{1/s} = [1 + x^s]^{1/s}$ for varying values of the shifting exponent, s.

the expression

$$f\{x\} = [(Ax^\alpha)^s + (Bx^\beta)^s]^{1/s}, \tag{1.9}$$

is usually desirable for interpolation between the extremal values.

Theoretically the matched function in equation (1.9) will have no upper bound and will only be bounded from below by the the functional expression for small values of x; i.e the term Ax^α in equation (1.3) will form a lower bound on the values that the independent variable may take on. The arbitrary exponent, s will now have a positive value. The shifting effect obtained is illustrated in Figures 1.3 and 1.4; the same conditions were used as in equations (1.4) and (1.5) to obtain

$$f\{x\} = [f_0^s\{x\} + f_\infty^s\{x\}]^{1/s} = [1 + x^s]^{1/s}. \tag{1.10}$$

For the sake of simplicity, the function-notation (f_0 and f_∞) will henceforth be favoured over the explicit expression in terms of power dependencies.

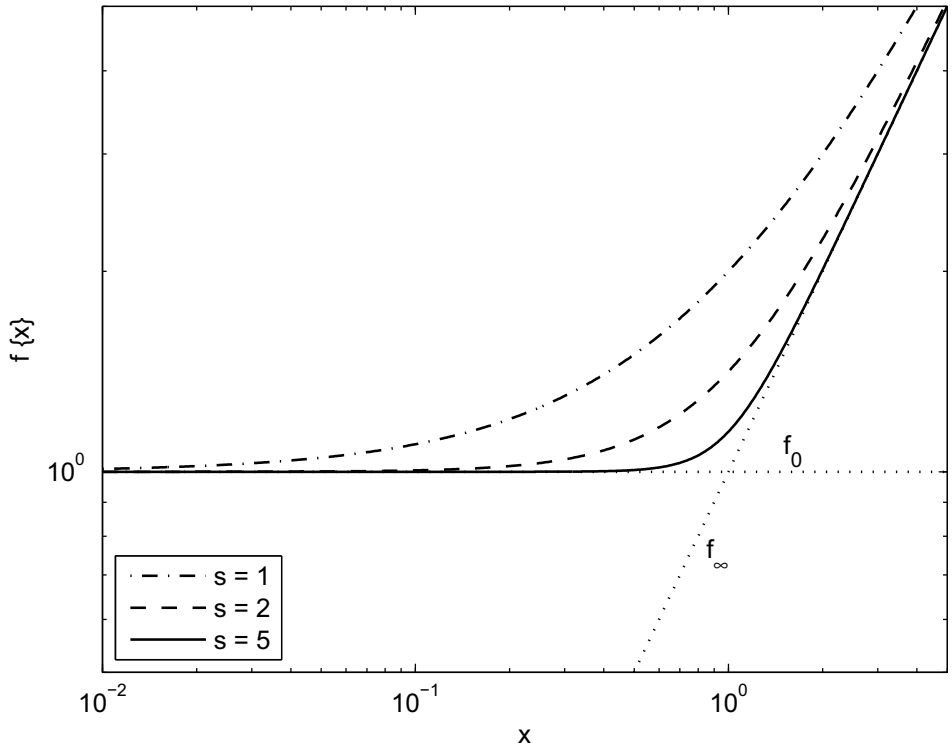

Figure 1.4: Log-log plot of the function $f\{x\} = [f_0^s\{x\} + f_\infty^s\{x\}]^{1/s} = [1 + x^s]^{1/s}$ for varying values of the shifting exponent, s.

1.2.2 Decreasing dependence

In some instances the dependence of $f\{x\}$ decreases with an increase in the independent variable, i.e.

$$\alpha > \beta, \tag{1.11}$$

in equation (1.3). Two possibilities now exist – the asymptotes may either form the lower bound or the upper bound of the resulting matched curve; knowledge of the process being modelled and/or experimental data will dictate the specific case.

1.2.2.1 Bounded from below

Decreasing dependence upon the independent variable is such that the solutions for extremal values – i.e. the functional expressions for the asymptotes – bind all possible solutions to the process from below. Suppose, for the sake of an illustrative example,

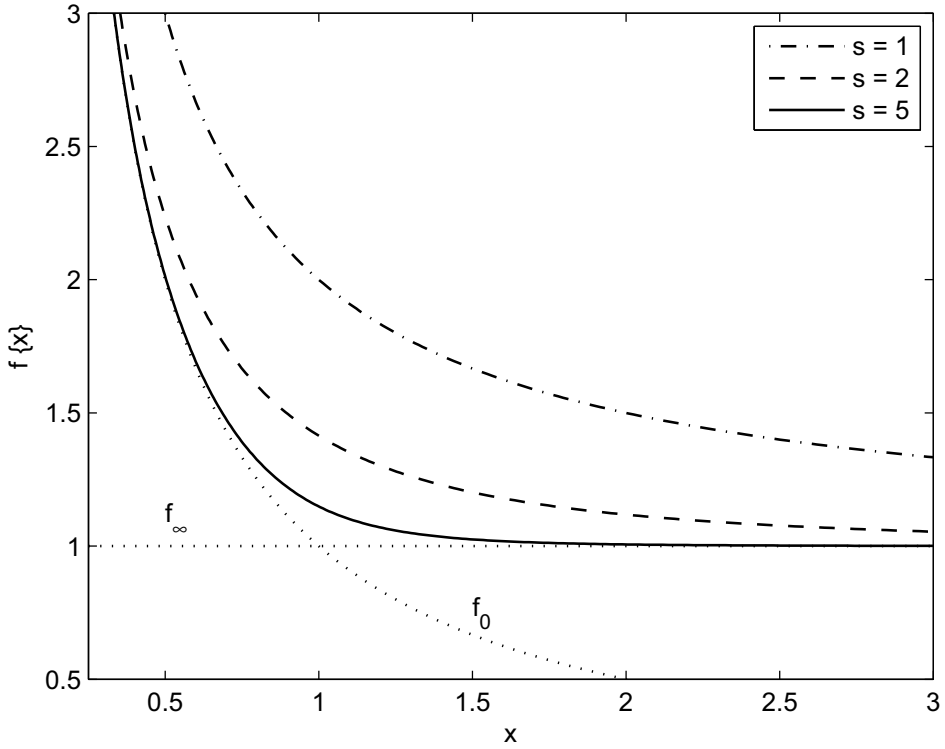

Figure 1.5: Linear plot of the function $f\{x\} = \left[\left(\frac{1}{x}\right)^s + 1\right]^{1/s}$ for varying values of the shifting exponent, s.

that the limiting solutions to such a process are given by the simple relations

$$f\{x\} \to \frac{1}{x} \quad \text{as} \quad x \to 0, \tag{1.12}$$

$$f\{x\} \to 1 \quad \text{as} \quad x \to \infty. \tag{1.13}$$

This corresponds to equation (1.3) with coefficients $A = 1$, $B = 1$ and exponents, $\alpha = -1$ and $\beta = 0$. The matched solution, raised to the shifting exponent will thus be

$$f\{x\} = \left[\left(\frac{1}{x}\right)^s + 1\right]^{1/s}. \tag{1.14}$$

The result of varying the values of the shifter, s, is graphically represented on Cartesian and log-log axes in Figures 1.5 and 1.6 respectively.

1.2.2.2 Bounded from above

The asymptotes, $f_0\{x\}$ and $f_\infty\{x\}$, of the process being modelled form an upper bound on the possible values that the function can assume. Using the formulation of

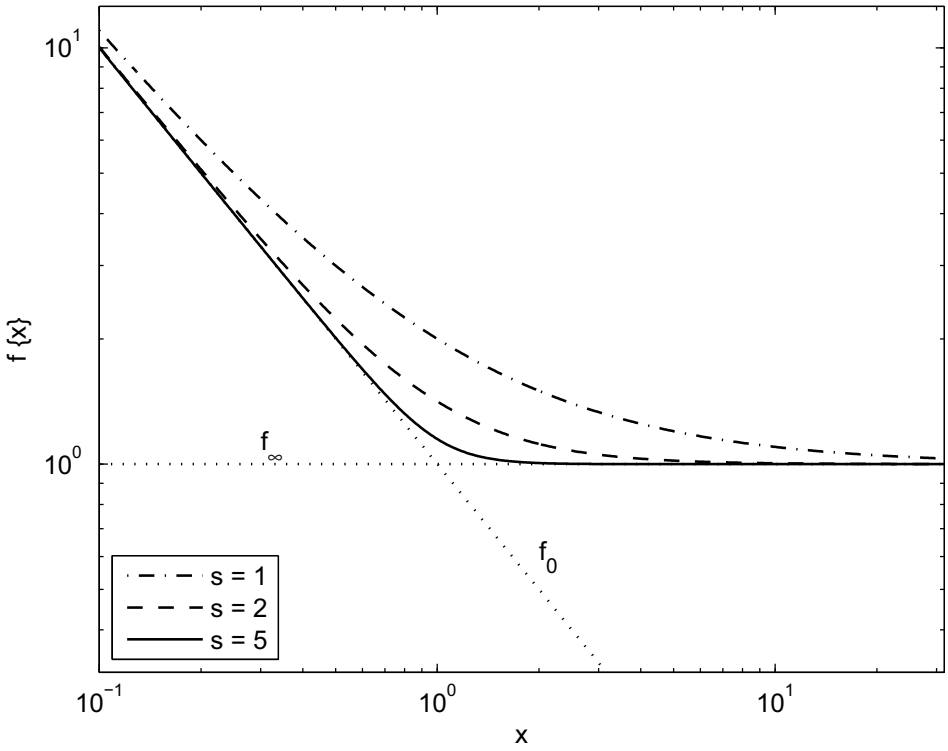

Figure 1.6: Log-log plot of the function $f\{x\} = \left[\left(\frac{1}{x}\right)^s + 1\right]^{1/s}$ for varying values of the shifting exponent, s.

equation (1.3) consider, as an example, the very simple case in which the asymptotes constituting the matched equation are given by

$$f\{x\} \to x \quad \text{as} \quad x \to 0, \tag{1.15}$$

$$f\{x\} \to 1 \quad \text{as} \quad x \to \infty. \tag{1.16}$$

To ensure that the matched solution approaches the limiting functions from below, the shifting exponent now needs to take on a negative value. However, the obtained curve will still approach the asymptotes as $|s|$ increases; illustrated in Figures 1.7 and 1.8.

The introduction of a negative value for s may be circumvented by taking the reciprocal of the original dependent variable, i.e. by defining

$$\frac{1}{g\{x\}} = \frac{1}{Ax^p} + \frac{1}{Bx^q} = \frac{1}{g_0\{x\}} + \frac{1}{g_\infty\{x\}}, \tag{1.17}$$

before it is raised to s, ensures that $s > 0$. Applying this to the above example, outlined in equations (1.15) and (1.16), yields the function

$$f\{x\} = \frac{x}{1+x}, \tag{1.18}$$

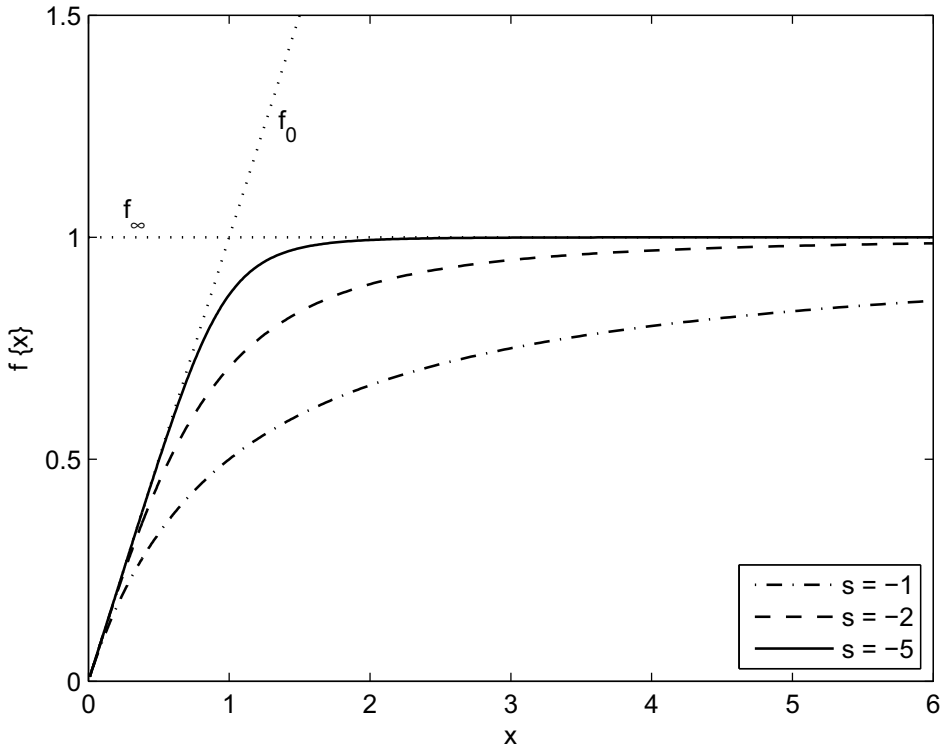

Figure 1.7: Linear plot of the function $f\{x\} = [x^s + 1]^{1/s}$ for varying negative values of the shifting exponent, s.

and in so doing Figures 1.7 and 1.8 in $g\{x\}$ are converted to Figures 1.5 and 1.6 in $f\{x\} = 1/g\{x\}$.

1.2.3 Only limiting values known

In many cases the functional dependence of the independent variable is known at the extremal values. Often, however, only the limiting values in both limits, i.e. $f\{0\}$ and $f\{\infty\}$, are known beforehand. In cases such as these the straight-forward application of equation (1.6) is not possible and an alternative approach is to be followed.

To commence, a functional dependence of the dependent variable upon the independent variable is postulated for either $x \to 0$ or $x \to \infty$. Any convenient function which approximates the behaviour of the data may be chosen. Churchill & Usagi [2] recommend the use of a power function since its use is widely applicable and the simplicity of such a function ties in with that of equation (1.6) and the philosophy behind the method in general. Once an applicable function for either of the limiting values has been chosen it is, as per the discussion in Section 1.1, matched to the constant value

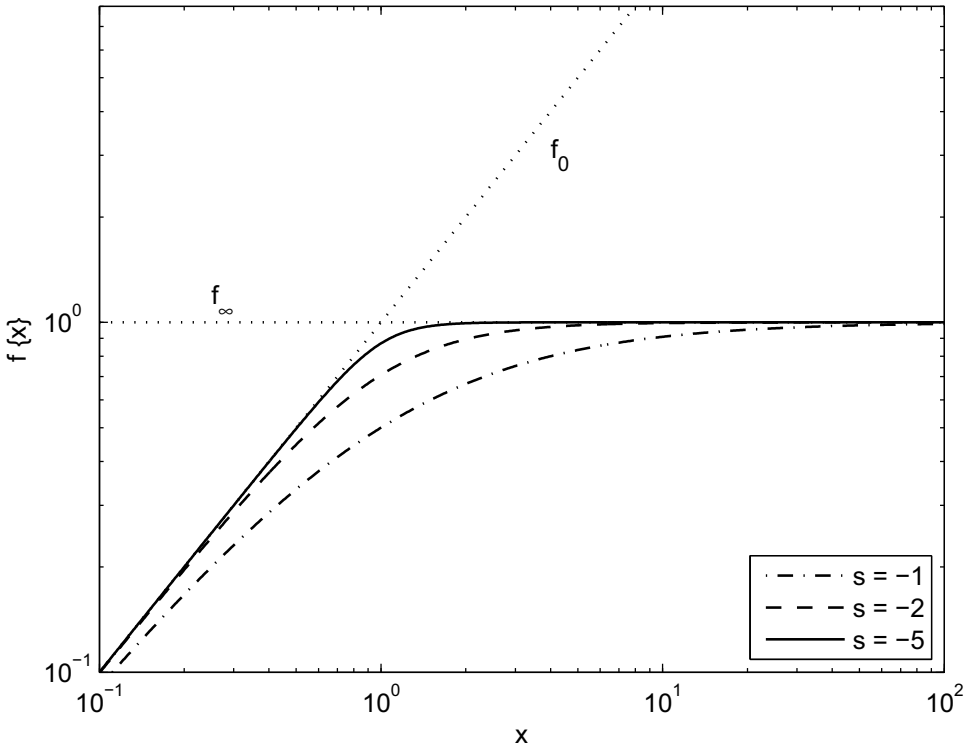

Figure 1.8: Log-log plot of the function $f\{x\} = [x^s + 1]^{1/s}$ for varying negative values of the shifting exponent, s.

that binds the process in the other limit (it is important to choose the approximating function such that no singularities are introduced once the functions are combined).

As an example, the power function

$$f_0\{x\} = f\{0\} + (f\{\infty\} - f\{0\}) \left(\frac{x}{x_A}\right)^{\alpha}, \tag{1.19}$$

may be suggested to represent the functional dependence at the lower limiting value [2]. Here x_A is an arbitrary constant and α an arbitrary exponent; the influence of these values on the obtained curves will be discussed shortly. The function in equation (1.19) is chosen such that

$$f_0\{x\} \to f\{0\} \qquad \text{as} \quad x \to 0,$$

$$\text{i.e.} \quad (f\{\infty\} - f\{0\}) \left(\frac{x}{x_A}\right)^{\alpha} \to 0 \qquad \text{as} \quad x \to 0. \tag{1.20}$$

In equation (1.20) the coefficient $(f\{\infty\} - f\{0\})$ is a constant value and therefore it should hold that

$$\left(\frac{x}{x_A}\right)^{\alpha} \to 0 \quad \text{as} \quad x \to 0, \tag{1.21}$$

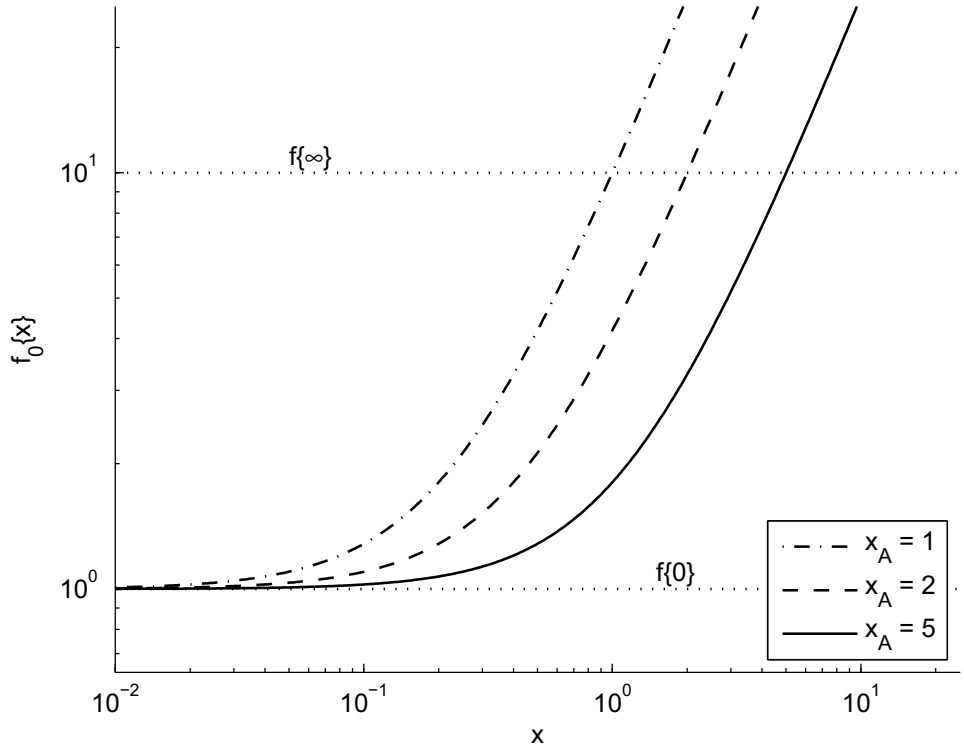

Figure 1.9: Postulated function $f_0\{x\} = f\{0\} + (f\{\infty\} - f\{0\})(x/x_A)^\alpha$ for constant value of arbitrary exponent, $\alpha = 1.5$, and varying values of the arbitrary constant, x_A.

which will only be the case if both the arbitrary constant and exponent is such that $x_A > 0$ and $\alpha \geq 0$; a restriction that should be kept in mind when choosing these values.

The postulated function and upper limiting asymptote will now intersect where

$$f_0\{x\} = f_\infty\{x\}, \tag{1.22}$$

that is

$$f\{0\} + (f\{\infty\} - f\{0\}) \left(\frac{x}{x_A}\right)^\alpha = f\{\infty\}, \tag{1.23}$$

whence, after rearrangement and division,

$$\left(\frac{x}{x_A}\right)^\alpha = 1. \tag{1.24}$$

It thus follows from equation (1.24) that $x = x_A$ at the intersection of these two functions; by changing the value of x_A the point of intersection may be altered. In Section 1.4 the importance of this value, the so-called *critical point*, will be discussed. Plotting of the postulated function in equation (1.19) for different values of the arbitrary constant x_A – illustrated in Figure 1.9 – graphically clarifies its influence.

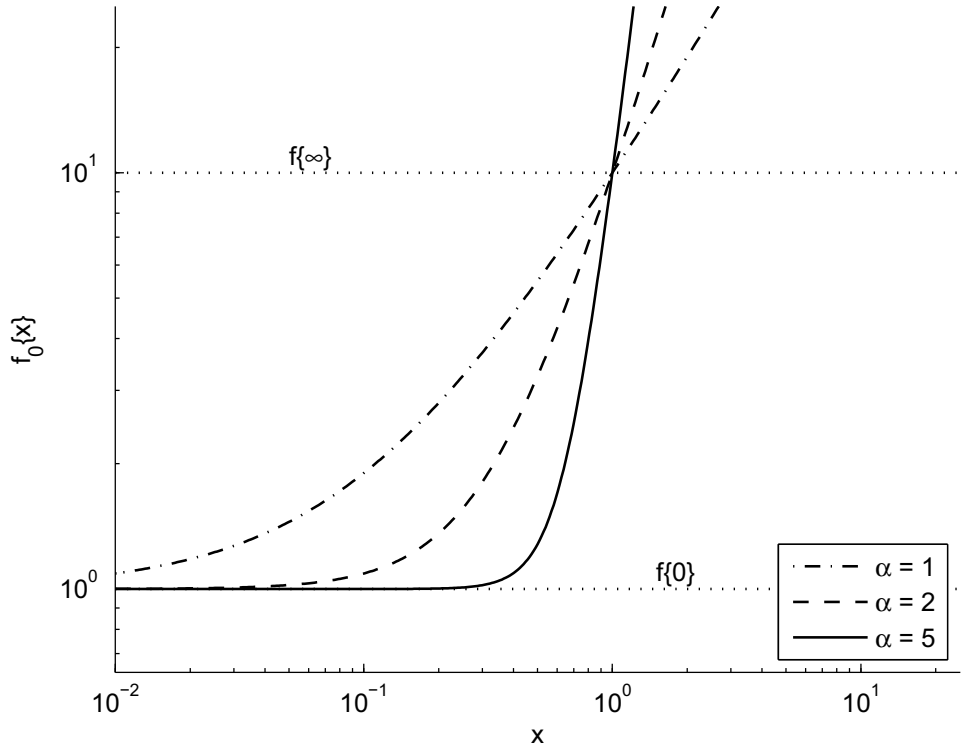

Figure 1.10: Postulated function $f_0\{x\} = f\{0\} + (f\{\infty\} - f\{0\})(x/x_A)^\alpha$ for constant value of the arbitrary constant, $x_A = 1$, and varying values of the arbitrary exponent, α.

The influence of the arbitrary exponent, α, becomes clear when equation (1.19) is rearranged as

$$\left(\frac{x}{x_A}\right)^\alpha = \frac{f_0\{x\} - f\{0\}}{f\{\infty\} - f\{0\}}, \tag{1.25}$$

and the logarithm taken on either side to yield

$$\log\left(\frac{x}{x_A}\right)^\alpha = \log\left(\frac{f_0\{x\} - f\{0\}}{f\{\infty\} - f\{0\}}\right),$$

$$\text{i.e.} \quad \alpha(\log x - \log x_A) = \log(f_0\{x\} - f\{0\}) - \log(f\{\infty\} - f\{0\}). \tag{1.26}$$

Defining a new variable, x^*, equation (1.26) thus takes the form of a linear depen-

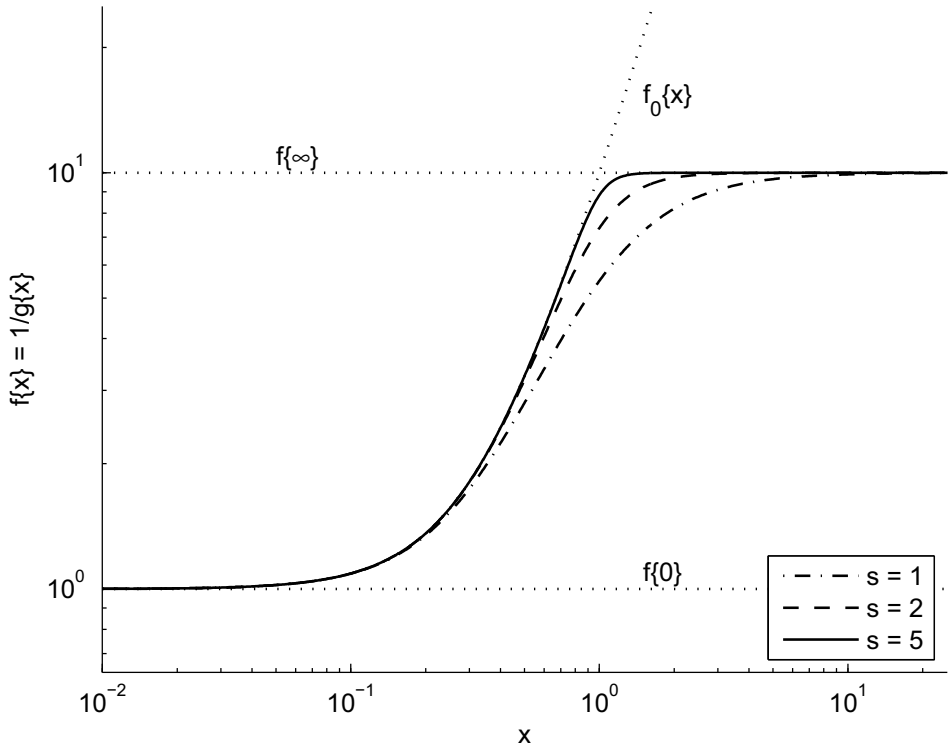

Figure 1.11: Application of powered addition with only limiting values known. A function of the form $f_0\{x\} = f\{0\} + (f\{\infty\} - f\{0\})(x/x_A)^{\alpha}$ was postulated for the lower limiting dependency. The effect of varying the value of the shifting exponent, s, on the solution is shown ($x_A = 1$ and $\alpha = 2$ were kept constant).

dency in x^* (straight line graph in Cartesian coordinates), such that

$$h\{x^*\} = \alpha x^* + c, \tag{1.27}$$

$$\text{where} \quad h\{x^*\} = \log(f_0\{x\} - f\{0\}), \tag{1.28}$$

$$x^* = \log x, \tag{1.29}$$

and c is a constant value

$$c = \log(f\{\infty\} - f\{0\}) - \alpha \log x_A = \log\left(\frac{f\{\infty\} - f\{0\}}{x_A^{\alpha}}\right). \tag{1.30}$$

As can be seen from equation (1.27), altering the value of α thus influences the 'curvature' of the postulated function; this is illustrated graphically in Figure 1.10.

The postulated function of equation (1.19) will thus form an upper bound on the possible values that the dependent variable may take in the lower limit. Furthermore

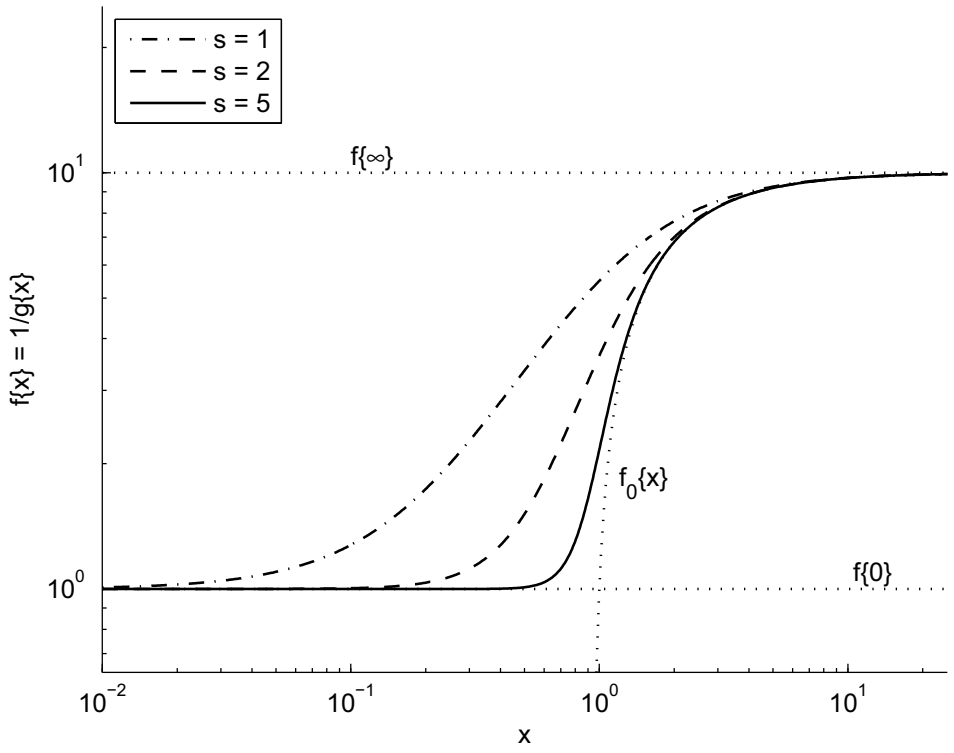

Figure 1.12: Application of powered addition with only limiting values known. A function of the form $f_\infty\{x\} = f\{\infty\} - (f\{\infty\} - f\{0\})(x_B/x)^\beta$ was postulated for the upper limit. The effect on the matched solution for selected values of the shifting exponent, s, is demonstrated ($x_B = 1$ and $\beta = 1.5$ were kept constant).

its contribution to the final solution should diminish as the value of the independent variable increases, in other words, once *matched*, the solution should show a decreasing dependence upon this function: a decreasing dependence, bounded from above as outlined in Section 1.2.2. By setting $g\{x\} = 1/f\{x\}$, cf. equation (1.17), the expressions $g_0\{x\} = 1/f_0\{x\}$ and $g_\infty\{x\} = 1/f_\infty\{x\} = 1/f\{\infty\}$ are obtained for the respective dependencies; the latter being a constant value. Inserting the aforementioned together with the proposed dependency of equation (1.19) into equation (1.6), yields

$$\frac{1}{f^s\{x\}} = \frac{1}{f_0^s\{x\}} + \frac{1}{f_\infty^s\{x\}} = \frac{1}{\left[f\{0\} + (f\{\infty\} - f\{0\})\left(\dfrac{x}{x_A}\right)^\alpha\right]^s} + \frac{1}{f^s\{\infty\}}. \tag{1.31}$$

A plot of equation (1.31) for different values of the shifting exponent, s, is shown in Figure 1.11.

Instead of postulating a function for the lower limit, the behaviour of the process in

the upper limit may be considered. The function is now required to act such that

$$f_\infty\{x\} \to f\{\infty\} \quad \text{as} \quad x \to \infty. \tag{1.32}$$

Once again a power function, now of the form

$$f_\infty\{x\} = f\{\infty\} - (f\{\infty\} - f\{0\}) \left(\frac{x_B}{x}\right)^\beta, \tag{1.33}$$

may be utilised as arbitrary function, approximating the dependency at upper extremal values. Applying the same reasoning as above to equation (1.32) imposes the restrictions $x_B > 0$ and $\beta \geq 0$ (the function now forming a lower bound). A power-added function, similar to that of equation (1.31), covering the entire range of the independent variable, may now be constructed by choosing $g\{x\} = 1/f\{x\}$, $g_0\{x\} = 1/f_0\{x\} = 1/f\{0\}$ and $g_\infty\{x\} = 1/f_\infty\{x\}$, where $1/f_0\{x\}$ is now given by equation (1.33). Figure 1.12 illustrates the use of the function proposed in equation (1.33) for approximation of the behaviour at upper extremal values; altering the value of the shifting exponent, s, having the desired effect.

1.2.4 Crossing of one limiting solution

In some phenomena the data is not bound completely by the limiting solutions; one of the limiting functions may be crossed as the solution approaches it. Although it is presumed that both the lower functional dependency, $f_0\{x\}$, and the upper limiting value, $f\{\infty\}$, is known, equation (1.6) is not directly applicable, since for any positive values of the shifting exponent, equation (1.6) gives values that fall above $f_0\{x\}$ and $f\{\infty\}$ (see Sections 1.2.1 and 1.2.2.1). As in the preceding section, a function is postulated viz.,

$$f_\infty\{x\} \to f\{\infty\} \quad \text{as} \quad x \to \infty, \tag{1.34}$$

but it should now differ from equation (1.33) in that it not only forms an upper bound on attainable values of the dependent variable, but also approaches the limiting value from above. Using a function of the form [1; 2],

$$f_\infty\{x\} = f\{\infty\} \left[1 + \left(\frac{x_A}{x}\right)^\alpha\right], \tag{1.35}$$

in stead of $f\{\infty\}$, solves this problem, since as $x \to \infty$ the second term in square brackets on the left hand side of equation (1.35) approaches zero (once again, provided that $\alpha \geq 0$).

Constructing a new dependency of the form suggested by equation (1.6), with $g\{x\} = 1/f\{x\}$, $g_0\{x\} = 1/f_0\{x\}$ and $g_\infty\{x\} = 1/f_\infty\{x\}$, with $f_\infty\{x\}$ the newly defined re-

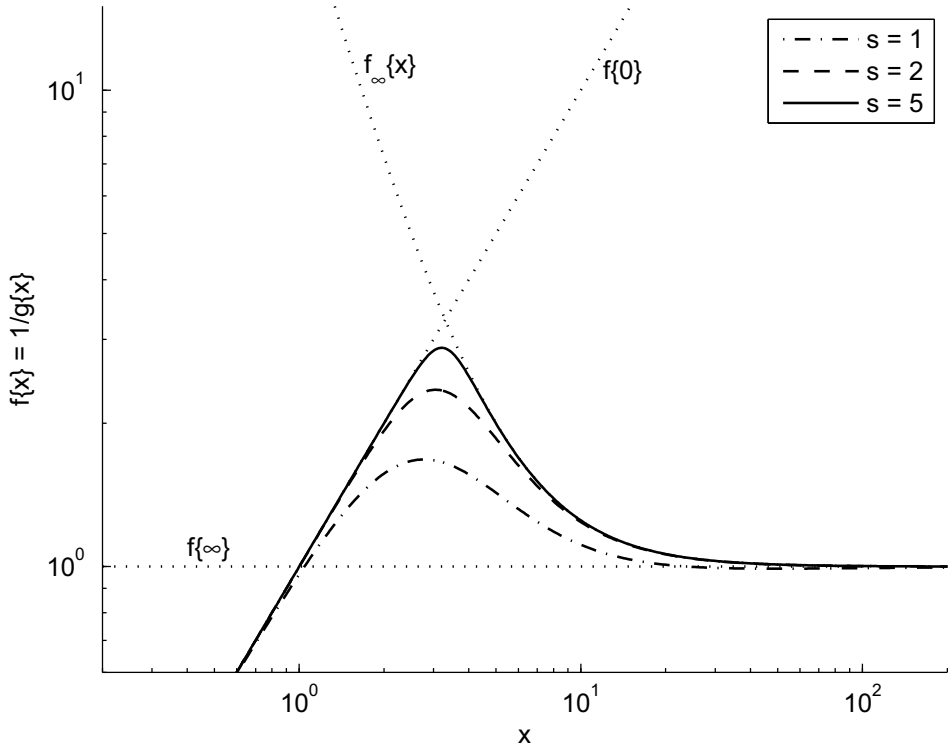

Figure 1.13: Application of powered addition when the solution crosses one of the limiting functions; a function of the form $f_\infty\{x\} = [1 + (x_A/x)^\alpha]$ utilized to approximate the upper limit. The effect on the matched solution for selected values of the shifting exponent, s, is demonstrated ($x_A = 5$ and $\alpha = 2$ were kept constant).

lation of equation (1.35), yields

$$\left(\frac{f_0\{x\}}{f\{x\}}\right)^s = 1 + \left(\frac{f_0\{x\}}{f\{\infty\}\left[1 + \left(\frac{x_A}{x}\right)^\alpha\right]}\right)^s \tag{1.36}$$

after simplification. In Figure 1.13 the family of curves found for selected values of the shifting exponent, s is illustrated; the arbitrary variables, $x_A = 5$ and $\alpha = 2$, were kept constant, their allocated values having been selected purely for demonstrative purposes. Investigation of the influence of the arbitrary constant, x_A, and arbitrary exponent, α, in equation (1.36) can be done in a fashion similar to the procedures followed to obtain equations (1.26) and (1.27) – the graphical representation of a change in the values assigned to these constants are illustrated by Figures 1.14 and 1.15. The results are, as was to be expected, akin to those of Figures 1.9 and 1.10.

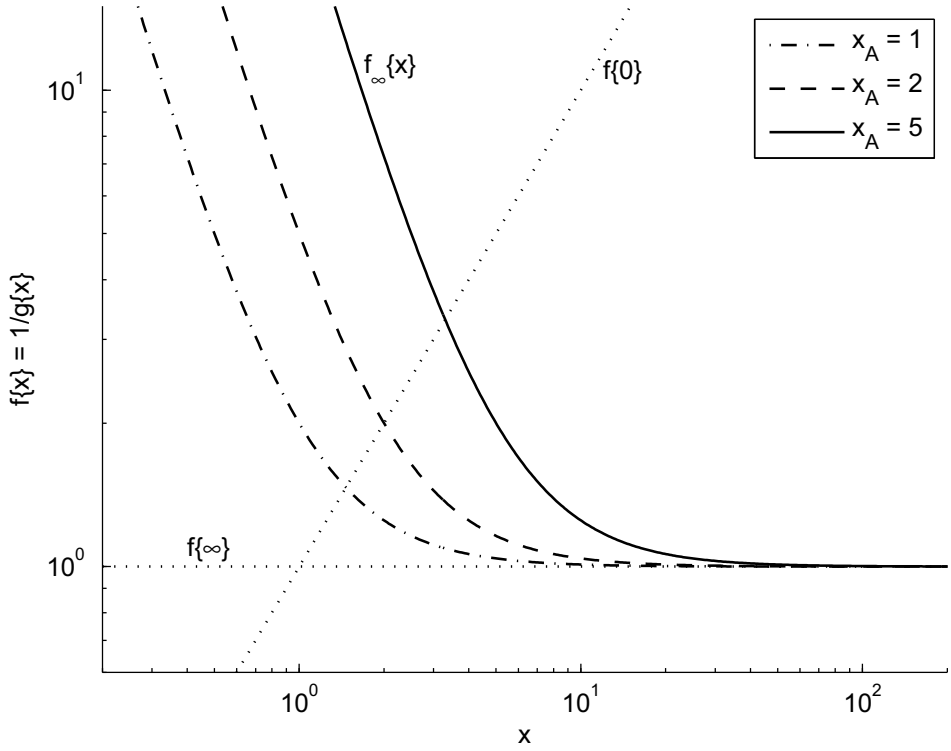

Figure 1.14: Variation of the value of the arbitrary constant, x_A, in equation (1.35) with the value of arbitrary exponent, $\alpha = 2$, being kept constant.

1.3 Normalisation to obtain one horizontal asymptote

Frequently neither of the expressions for the limiting solutions, (1.1) and (1.2), are linear in form or of a constant value. To aide visual interpretation it is often beneficial to divide equation (1.7) by one of the asymptotic expressions, namely

$$\frac{f\{x\}}{f_0\{x\}} = \left[1 + \left(\frac{f_\infty\{x\}}{f_0\{x\}}\right)^s\right]^{1/s}, \tag{1.37}$$

or

$$\frac{f\{x\}}{f_\infty\{x\}} = \left[\left(\frac{f_0\{x\}}{f_\infty\{x\}}\right)^s + 1\right]^{1/s}, \tag{1.38}$$

to obtain non-dimensional, normalised forms of the original function. Both equation (1.37) and (1.38) can now be written in generic form as

$$Y = (1 + Z^s)^{1/s}, \tag{1.39}$$

yielding a horizontal asymptote at $Y = 1$ ($Z \to 0$); the exact functional definition of the newly defined variables, Y and Z, will be case specific. Plotting of the expression

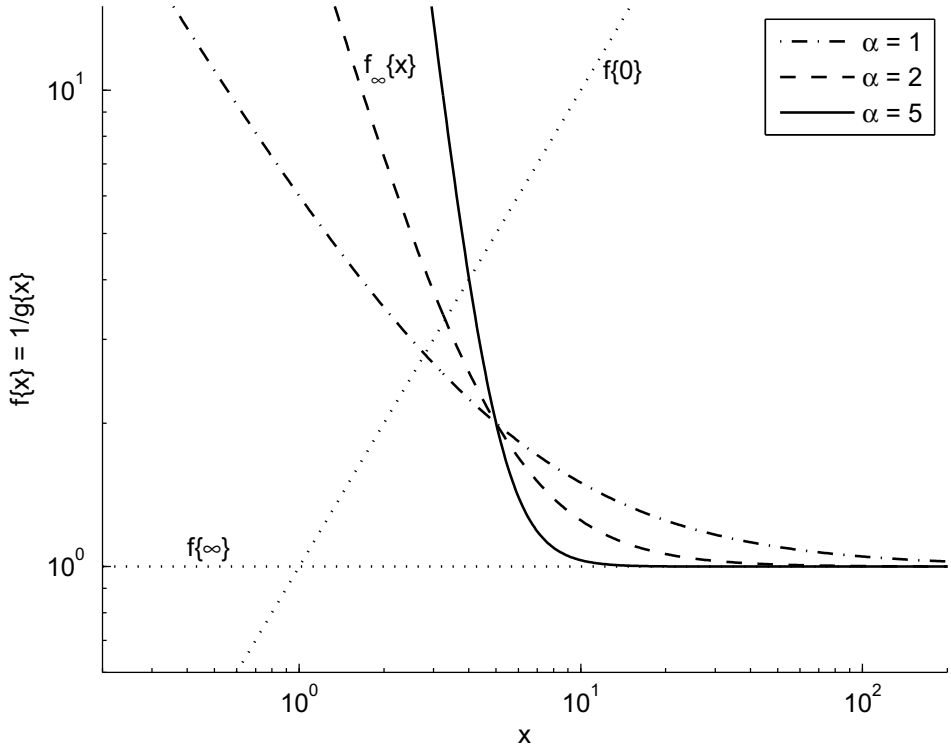

Figure 1.15: The effect of a change in the arbitrary arbitrary exponent, α, on the asymptotes of the Churchill-Usagi equation proposed by equation (1.35). The value of the arbitrary constant, $x_A = 5$, was kept constant.

obtained in equation (1.37) will stretch the curve at low values of the independent variable, whereas plots with equation (1.38) will extend the curve at high values of the independent variable.

1.4 Critical point and shifting-exponent

The *central* or *critical point*, x_c, of the matching curve is the value of the independent variable at which the asymptotes meet. Since the asymptotes intersect here, the numerical value of their respective functional expressions must be equal, that is

$$f_0\{x_c\} = f_\infty\{x_c\}. \tag{1.40}$$

As both functions, f_0 and f_∞, contribute equally to the added solution at this point, the resultant curve is most sensitive to variations in the value of the shifter, s, in the vicinity of x_c. Furthermore, looking at equations (1.37), (1.38) and (1.39), it becomes apparent that the maximal fractional deviation of the matched solution from either of

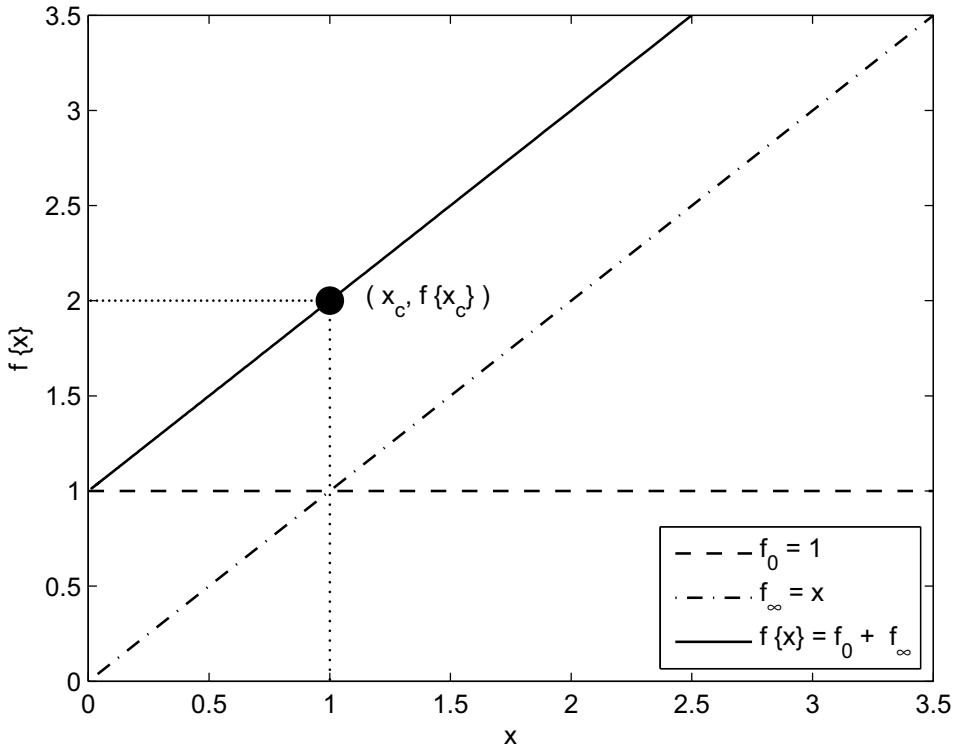

Figure 1.16: Linear plot of the function $f\{x\} = (f_0^s\{x\} + f_\infty^s\{x\})^{1/s} = (1 + x^s)^{1/s}$ to indicate the location of the critical point and equivalent function value.

the limiting solutions or asymptotic values will occur at precisely this point and take on the value

$$Y\{1\} - 1 = 2^{1/s} - 1. \tag{1.41}$$

That is

$$\left(\frac{f\{x_c\}}{f_0\{x_c\}}\right) - 1 = \left(\frac{f\{x_c\}}{f_\infty\{x_c\}}\right) - 1 = 2^{1/s} - 1, \tag{1.42}$$

if written in terms of the original equations for the extremal values.

Determining the value of the shifting-exponent, s, we use the same argument as above in equation (1.40). Thus,

$$f^s\{x_c\} = f_0^s\{x_c\} + f_\infty^s\{x_c\} = 2f_0^s\{x_c\} = 2f_\infty^s\{x_c\} \tag{1.43}$$

whence it follows that

$$\left(\frac{f\{x_c\}}{f_\infty\{x_c\}}\right)^s = \left(\frac{f\{x_c\}}{f_0\{x_c\}}\right)^s = Y\{1\}^s = 2. \tag{1.44}$$

The value of s may now be determined straightforwardly from equation (1.44) as

$$s = \frac{\ln 2}{\ln f\{x_c\} - \ln f_\infty\{x_c\}} = \frac{\ln 2}{\ln f\{x_c\} - \ln f_0\{x_c\}} = \frac{\ln 2}{\ln Y\{1\}}. \tag{1.45}$$

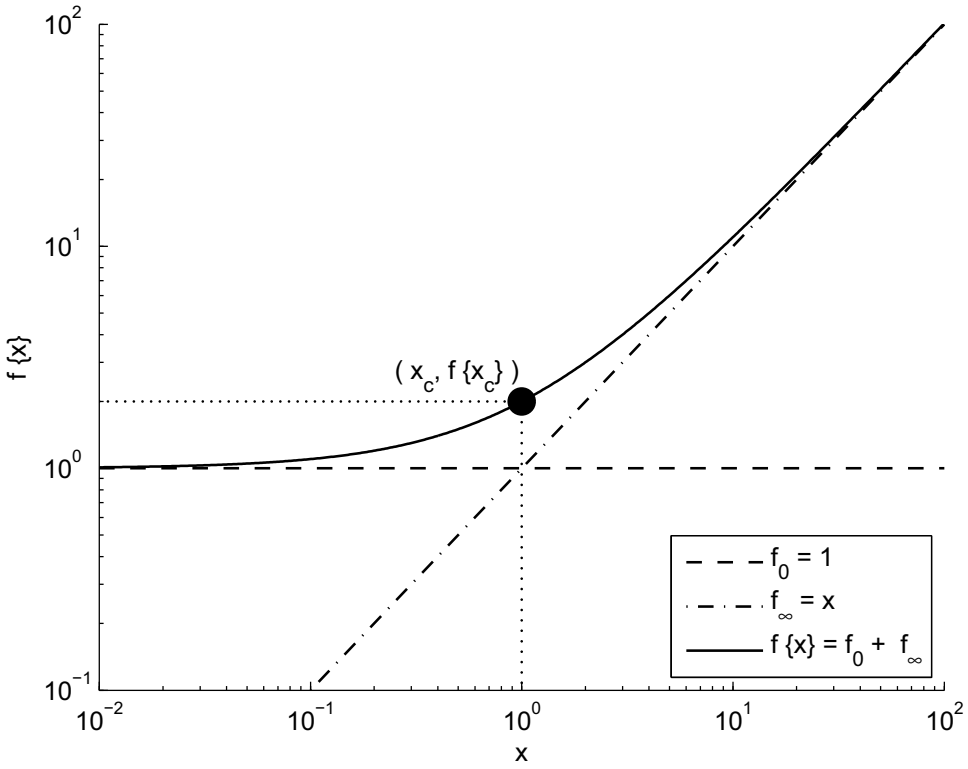

Figure 1.17: Log-log plot of the function $f\{x\} = (f_0^s\{x\} + f_\infty^s\{x\})^{1/s} = (1 + x^s)^{1/s}$ to indicate the location of the critical point and equivalent function value.

In performing an experiment, it is therefore advantageous to arrange the physical conditions in such a manner that the independent variable is in close vicinity of x_c. Whenever the experimental value of $f\{x_c\}$ is known, we proceed to determine the value of the shifter by equation (1.45). In Figures 1.16 and 1.17 the critical point and the corresponding function value at this point is indicated for the illustrative example, $f\{x\} = 1 + x$, that has been used thus far. Note that in this, most simple form, the value of the shifter, $s = 1$.

Alternatively, visual inspection by trial and error adjustment of the correlation between the predictive curve and data points may lead to an assignment of a value to s. As noted by Churchill & Usagi [1] the matched curve is relatively insensitive to variations in s; the required acuity being determined by considerations such as the process involved, tunability of other parameters and allowable error-margin.

Chapter 2

Flow in straight-through diaphragm valves

Diaphragm valves possess several advantages that lead to their extensive use in diverse industrial applications. There are two types of diaphragm valves: the "weir" type used in piping systems that carry less viscous fluids; and the "straight-through" type - a schematic representation of which is shown in Figure 2.1 - suited to slurries and suspensions [8]. The data sets of Mbiya [9; 10], on which this chapter is based, is concerned with the latter type of valve.

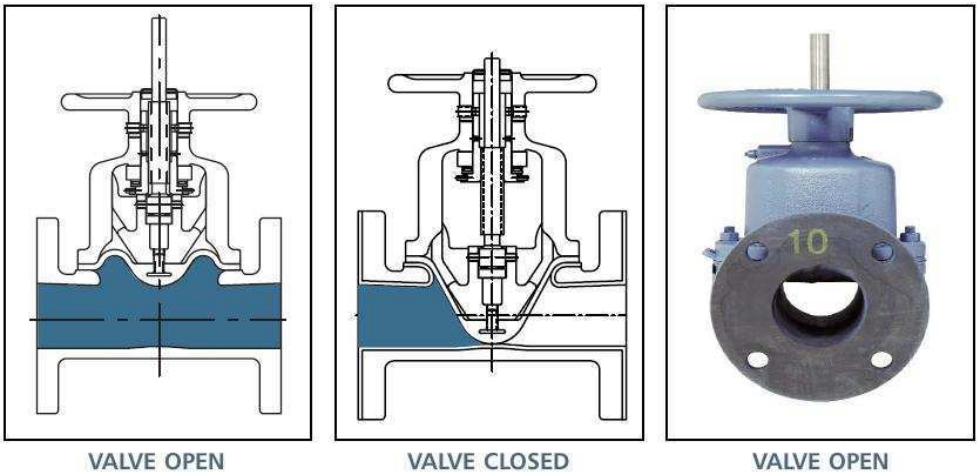

Figure 2.1: Schematic representation showing the cross-section of a straight-through diaphragm valve (http://www.engvalves.com)

Despite the broad scope of their use, Mbiya [9; 11] notes that few studies dealing

with valve openings of aperture less than unity is available in the literature. This limits the use of the information contained therein, rendering it inapplicable to cases where valves are used as flow impeding devices. Furthermore the studies that had been done were restricted to specific intervals of the Reynolds number. The aim of Mbiya's [9; 11] experimental investigation was to more accurately predict the additional pressure loss incurred, for four different opening positions, once a pipe had been fitted with a straight-through diaphragm valve.

A brief outline will be given on the definition of the pressure loss coefficient, the experimental determination of which is one of the main focuses of Mbiya's work [9; 10; 11]. Hereafter the specific Reynolds number used in his study will be discussed shortly (for a complete derivation of the Slatter Reynolds number, refer to Appendix B). In the second half of this chapter Mbiya's [9; 11] results are investigated for possible asymptotic bounds whereafter powered addition is applied to these functional dependencies. The outcomes of powered addition is compared to those of Mbiya's model for a few selected cases (a complete set of comparative graphs are available in Appendix C) and the results discussed.

2.1 Definitions of pressures and heads

The fitting of a valve into a pipe section causes a change in shape of the plane perpendicular to the direction of flow and hence also in that of the flow path, thereby leading to an increase in the pressure drop as the fluid traverses the constriction caused by the valve. In Figure 2.2 this resulting additional pressure loss is graphically illustrated.

A wide variety of parameters are used to express the pressure drop characteristics of the different components in a piping system [12]. The data on pressure losses may be arrived at by either experiment or by theoretical solution of the equations governing flow. Pressure loss data obtained by the former method usually concern measurements taken at two stations, one upstream and one downstream of the component. Reference is seldom made to the details of the change in pressure within the component itself.

The well-known Bernoulli equation for steady, incompressible flow states

$$\frac{1}{2}v_1^2 + \frac{p_1}{\rho_1} + gz_1 = \frac{1}{2}v_2^2 + \frac{p_2}{\rho_2} + gz_2 = \text{constant}, \tag{2.1}$$

where v is the velocity, p the pressure, ρ the fluid density (which is presumed constant), z is the height above some arbitrary reference point and g is the acceleration due to gravity. Division of equation (2.1) by g yields

$$\frac{v_1^2}{2g} + \frac{p_1}{w_1} + z_1 = \frac{v_2^2}{2g} + \frac{p_2}{w_2} + z_2 = \text{constant} = h_t, \tag{2.2}$$

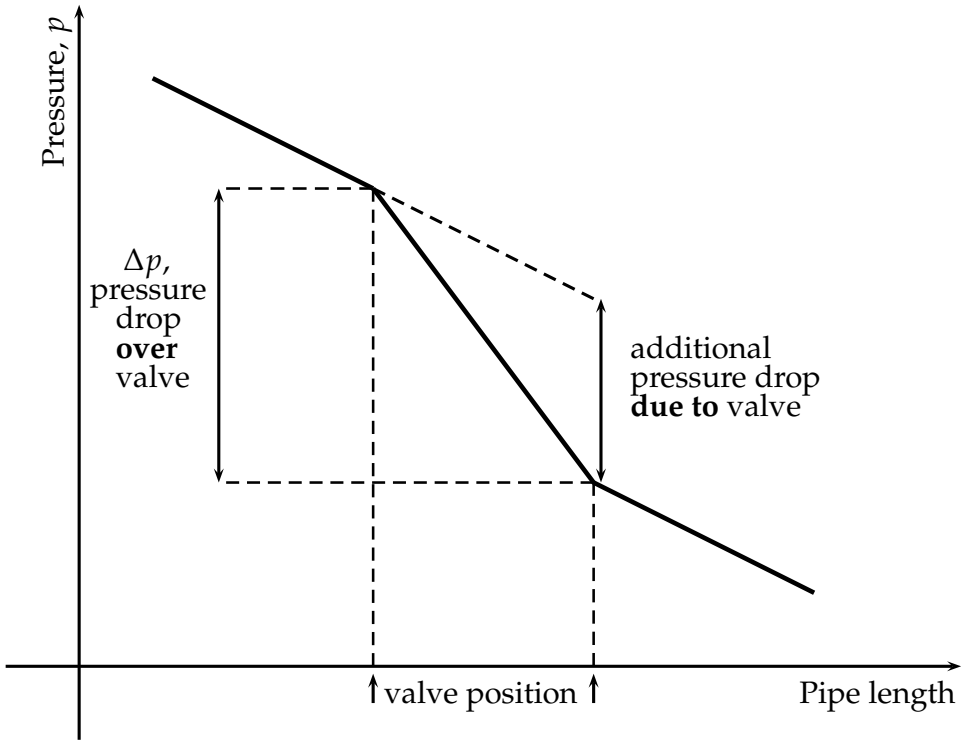

Figure 2.2: Increased pressure drop due to the presence of a valve.

where w, the specific weight, has been written in stead of ρg. The terms in equation (2.2) all have the dimensions of length and are referred to as *heads* in hydraulics. Hence, $v^2/2g$ is known as the velocity head (h_v), p/w the pressure head, z is the position head and their sum, h_t – constant along the stream tube – is called the total head [12]. Frequently the pressure head and position head together are referred to as the static head [13]; the choice of this grouping becomes clear upon regarding Figure 2.3, where the flow in a horizontal pipe is schematically represented.

The height to which a fluid rises in a tube connected to a tapping in the pipe wall is called the static head. The difference between the static head and the head yielded upon placing a forward facing tube (pitot) into the fluid stream, is called the velocity head. The total head is simply the sum of the static and velocity heads. Comparison with equation (2.2) yields an expression for the static head

$$h_s = \frac{p}{w} + z. \tag{2.3}$$

Since it is the same fluid being regarded, and assuming incompressibility (i.e. constant density), that is $\rho = \rho_1 = \rho_2$, equation (2.1) may be multiplied by ρ, resulting in

$$\frac{1}{2}\rho v_1^2 + p + \rho g z_1 = \frac{1}{2}\rho v_2^2 + p + \rho g z_2 = \text{constant} = p_H. \tag{2.4}$$

In equation (2.4) the contribution to the energy balance (the principle on which the

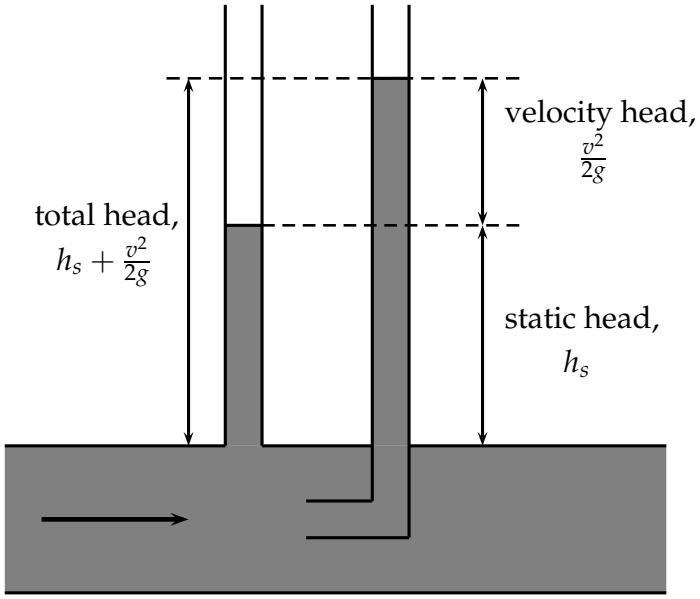

Figure 2.3: Graphical representation of the static, velocity and total heads.

Bernoulli equation is based) of the term $\rho g z$ is negligible [12] and hence it simplifies to

$$\frac{1}{2}\rho v_1^2 + p_1 = \frac{1}{2}\rho v_2^2 + p_2 = \text{constant} = p_H. \tag{2.5}$$

In the form of equation (2.5) all terms have the dimensions of pressure; the first term, $\frac{1}{2}\rho v^2$, is known as the dynamic pressure, the second term, p, as the static pressure and their sum, p_H, (once again a constant along the stream tube) as the total pressure [12].

Considering equation (2.5), it follows that any change in the total or static pressure within the flow will be proportional to the local dynamic pressure. This leads to the definition of the total pressure loss coefficient

$$k \equiv \frac{\bar{p}_{H_2} - \bar{p}_{H_1}}{\frac{1}{2}\rho v^2} = \frac{\Delta p_H}{\frac{1}{2}\rho v^2}. \tag{2.6}$$

Hence, using the change of total head, the head loss, Δh_t, in a straight pipe section is approximately proportional to the square of the velocity, v^2, of the fluid. The relation in equation (2.6) may thus be expressed as

$$k = \frac{h_{t_1} - h_{t_2}}{\bar{v}^2/2g} = \frac{2g\Delta h_t}{\bar{v}^2} = \frac{2gH}{\bar{v}^2}, \tag{2.7}$$

whereby division of the head loss by the mean velocity head, $\bar{v}^2/2g$, yields a non-dimensional loss coefficient [12; 13]. The presence of a component, such as a valve, in a piping system will, via an increase in the loss of dynamic pressure, lead to a

larger head loss. The study of Mbiya [9; 10; 11] concerns the experimental determination of the pressure loss coefficient (or resistance coefficient) and the prediction thereof in terms of an empirical equation expressible as a function of valve opening and Reynolds number.

2.2 Choice of Reynolds number

According to Newton's law of viscosity the shear stress, τ, and viscosity, μ, for one-dimensional flow of a fluid are related by

$$\tau = -\mu \frac{dv_x}{dy}, \tag{2.8}$$

where dv_x/dy is the shear rate or velocity gradient as a function of position [14]. Fluids that obey this criterion are referred to as Newtonian fluids. This is however an idealisation as many fluids exhibit a more complicated relationship than the mere linearity described by equation (2.8). Often the relation between the velocity gradient and shear stress of a fluid is best described by the power dependency,

$$\tau = K \left(-\frac{dv_x}{dy} \right)^n, \tag{2.9}$$

where K is the fluid consistency index and n the flow behaviour index; fluids exhibiting such behaviour are called power-law fluids (for a brief outline on the classification of fluids, refer to Appendix A). Depending on the value of the flow behaviour index, power-law fluids are classified into three broad groups: pseudo-plastic fluids if $n < 1$; Newtonian fluids for $n = 1$, since equation (2.9) reverts to equation (2.8) in this case; and dilatant fluids for $n > 1$. In pseudo-plastic substances shear thinning is observed, in other words the viscosity decreases with an increase in rate of the shear stress.

A true plastic substance has an initial yield stress that needs to be overcome before it assumes fluid-like properties, i.e. continuous deformation when subjected to a (further) shear stress [14]. The constitutive equation for the yield pseudo-plastic model can thus be formulated as

$$\tau = \tau_y + K \left(-\frac{dv_x}{dy} \right)^n, \tag{2.10}$$

with τ_y denoting the yield stress. Setting $n = 1$ in equation (2.10) yields the so-called Bingham-plastic model, while $\tau_y = 0$ results in it reverting back to that for power-law fluids, equation (2.9).

The Slatter Reynolds number, Re_3, is based on the yield pseudo-plastic model and starts from the assumption that, in the presence of a yield stress, the core of the fluid

moves as a solid, unsheared plug [10; 15] resulting in annular flow (see derivation in Appendix B). It can be expressed as

$$Re_3 = \frac{8\rho\overline{v}_{\text{ann}}^2}{\tau_y + K\left(\frac{8\overline{v}_{\text{ann}}}{D_{\text{shear}}}\right)^n} \quad . \tag{2.11}$$

In equation (2.11) $\overline{v}_{\text{ann}}$ denotes the corrected mean velocity in the annulus and D_{shear} the sheared diameter.

2.3 Mbiya's empirical correlation

The addition of a component, such as a valve, to a piping system leads to a local constriction (or dilation) of the cross-sectional area and consequently also to a change in the flow path. Initially, at low Reynolds numbers – the region of laminar flow –

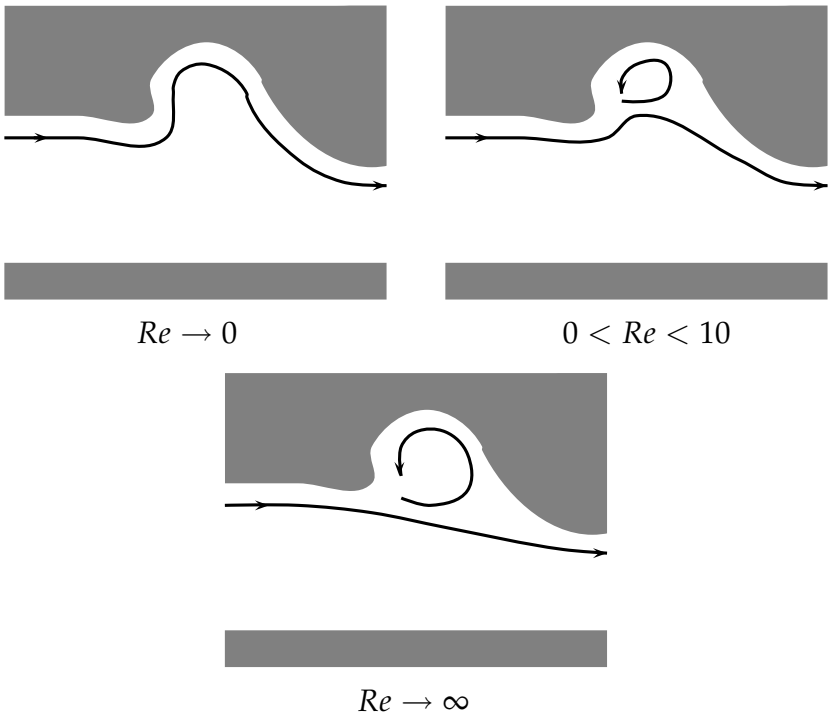

Figure 2.4: Schematic representation of recirculation within the valve section due to an increase in the Reynolds number.

streamlines will trace out the irregular geometry caused by the valve's presence. As the Reynolds number increases however, localised areas of recirculation will gradually develop within the indentations of the diaphragm until, at turbulent flow conditions,

the streamlines bypass these areas altogether; Figure 2.4 represents this schematically. This is an intuitive explanation accounting for the constant resistance coefficients (pressure loss) obtained at high Reynolds numbers, i.e. turbulent flow, and reflected in the data of Mbiya [9; 10; 11].

Mbiya's [9; 10; 11] proposed *two-constant* model is based on a large set of accrued experimental data. A test rig , constructed at the Cape Peninsula University of Technology, consisted of pipes of different diameters ($40mm$, $50mm$, $65mm$, $80mm$ and $100mm$), each of which was fitted with the appropriately sized diagram valve. The fluids carboxymethyl cellulose [CMC] (at 5% and 8% concentration), glycerine or glycerol (concentrations of 75% and 100%), kaolin, a claylike mineral (10% and 13% concentrations) and water were pumped through the pipes for four different valve opening positions (25%, 50%, 75% and 100% open) and the pressure drop in the pipe was recorded. The aim was to predict the pressure loss coefficient, $k_v(Re_3)$, as defined in equation (2.7) – the v-subscript denoting valve – for straight-through diaphragm valves. Mbiya [9; 10; 11] concludes by summarizing his model, as being applicable to all sizes of valves tested, by straight-forward addition of

$$k_v = \begin{cases} \dfrac{1000}{Re_3}, & Re_3 < 10 \\ \dfrac{C_\Omega}{\sqrt{Re_3}\,\theta^2} + \dfrac{\lambda_\Omega}{\theta^2}, & Re_3 \geq 10 \end{cases} \tag{2.12}$$

Here C_Ω is a new constant (model parameter) introduced by Mbiya [9; 11], λ_Ω is the nominal turbulent loss coefficient, and θ is the partial valve opening coefficient as ratio of the fully opened position, i.e. $\theta = 0$ for a closed valve and $\theta = 1$ for a fully opened valve. Note that an open valve does not correspond to an open tube flow condition; the diaphragm still protrudes into the lumen as can be seen in Figure 2.1 (right).

Unfortunately, to obtain good agreement with experimental results, an 'if'-condition had to be introduced at a Slatter Reynolds number of 10. The two different curve fitted solutions on either side of this value lead to an unwanted jump in the values of the dependent variable, i.e. the predicted crossover at this Reynolds number is not smooth; Figure 2.5 shows a typical correlation for such a case – cf equation (2.12) – the 'jump' in the value of the dependent variable evident. This contradicts the expected, intuitive-orderly behaviour of such a continuum transfer process. (The constant C_Ω is an unfortunate fudge factor introduced for proper agreement, in the transitional region, between the experimental data and correlative equations (2.12). It is also this factor that leads to the unwanted jump in the proposed model).

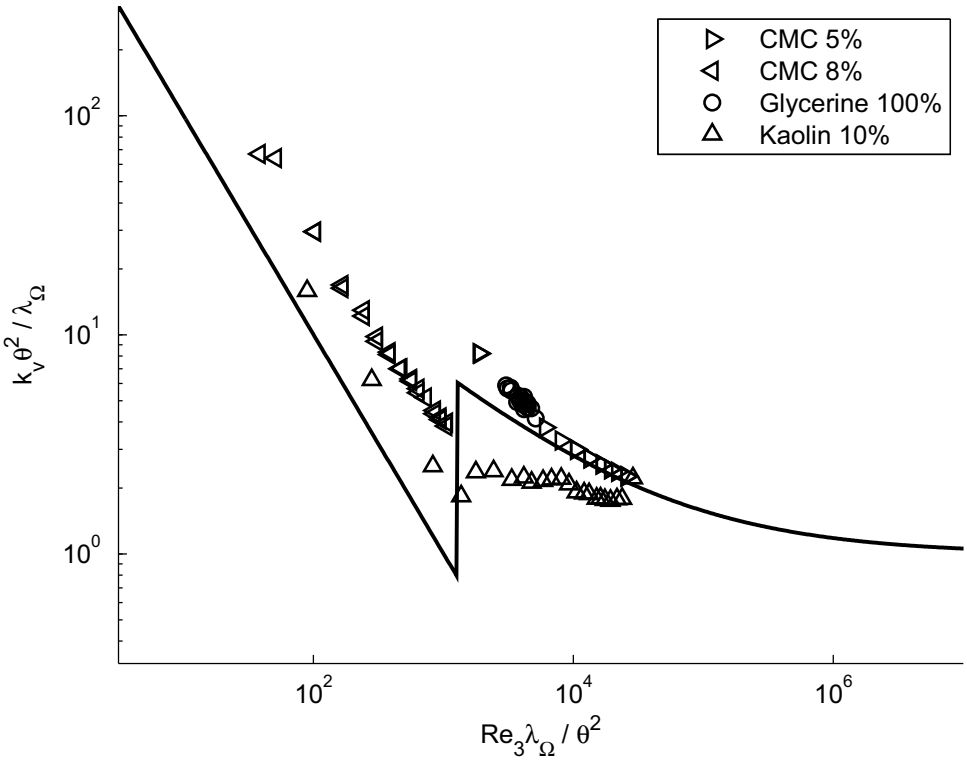

Figure 2.5: Typical correlation of experimental data with equation (2.12), showing the jump at $Re_3 = 10$. The equations were applied to the data sets of Mbiya [9] for a pipe with internal diameter of $40mm$ and a valve opening of 25%.

2.4 Powered addition applied to Mbiya's work

Regarding equation (2.12) in the limit where $Re_3 \to \infty$, it is clear that $k_v \to \lambda_\Omega/\theta^2$. Hence, λ_Ω/θ^2 may be regarded as an asymptotic lower bound on k_v. The direct addition of this result to the dependency of k_v on Re_3 for $Re_3 < 10$, is then considered as a matching between the two asymptotic conditions, yielding a single solution that covers the entire range of the Reynolds numbers, namely

$$k_v = \frac{1000}{Re_3} + \frac{\lambda_\Omega}{\theta^2}. \tag{2.13}$$

Inspection of Mbiya's proposal thus evidently leads to the following definitions

$$k_0 \equiv \frac{1000}{Re_3} \quad \text{for} \quad Re_3 \to 0, \tag{2.14}$$

and

$$k_\infty \equiv \frac{\lambda_\Omega}{\theta^2} \quad \text{for} \quad Re_3 \to \infty, \tag{2.15}$$

whence equation (2.13) becomes

$$k_v = k_0 + k_\infty. \tag{2.16}$$

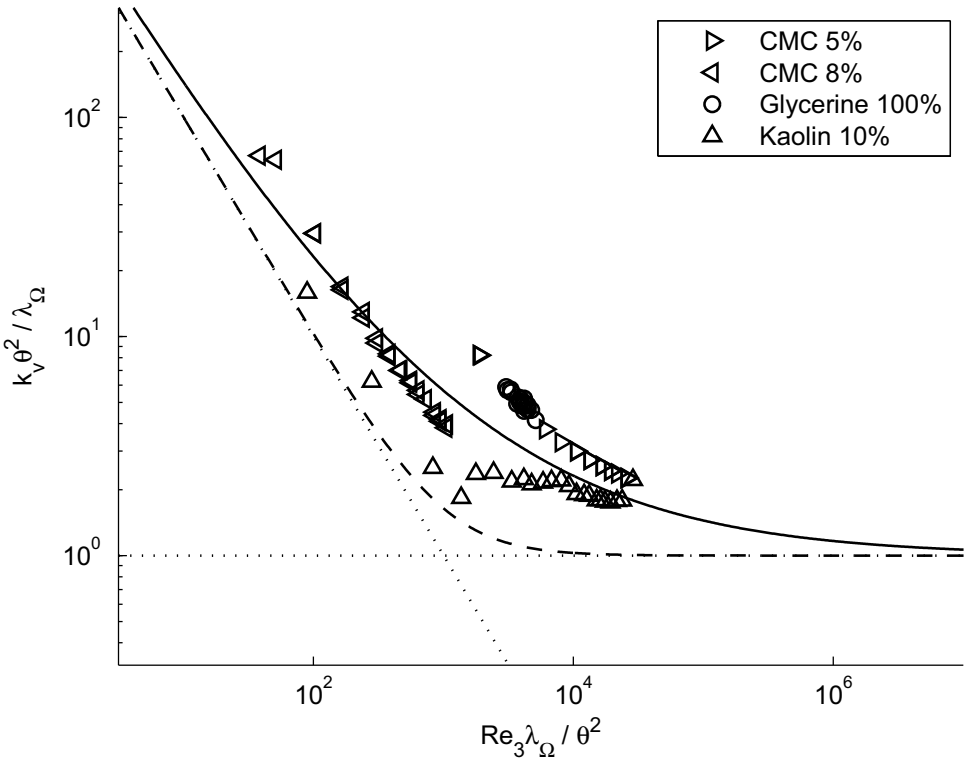

Figure 2.6: Application of powered addition to the data sets generated by Mbiya [9] for a pipe with internal diameter of 40mm and a valve opening of 25%; s-values of 0.4 (solid line) and 1.4 (dashed) are shown for comparison.

Instead of the direct addition of the two asymptotes as in equation (2.13), powered addition, as discussed in Chapter 1, may now be applied to the asymptotic expressions, yielding

$$k_v^s = k_0^s + k_\infty^s, \tag{2.17}$$

which may, analogous to equation (1.38), be re-written as

$$\frac{k_v}{k_\infty} = \left[\left(\frac{k_0}{k_\infty}\right)^s + 1\right]^{1/s}. \tag{2.18}$$

If two new variables, Y and Z, are defined as

$$Y \equiv \frac{k_v}{k_\infty} \tag{2.19}$$

$$Z \equiv \frac{k_0}{k_\infty}, \tag{2.20}$$

equation (2.18) simplifies to

$$Y = [Z^s + 1]^{1/s}, \tag{2.21}$$

cf equation (1.39).

Instead of dividing equation (2.17) by k_∞, one may alternatively have chosen to designate k_0 as denominator, followed by the corresponding redefinition of variables Y and Z in equations (2.19) and (2.20). One extremely useful consequence of this type of modelling is the direct possibility of non-dimensionalisation into either of the following forms

$$\frac{k_v\, Re_3}{1000} = \left[1 + \left(\frac{\lambda_\Omega\, Re_3}{1000\,\theta^2}\right)^s\right]^{(1/s)}, \tag{2.22}$$

or

$$\frac{k_v\,\theta^2}{\lambda_\Omega} = \left[\left(\frac{1000\,\theta^2}{\lambda_\Omega\, Re_3}\right)^s + 1\right]^{(1/s)}. \tag{2.23}$$

Furthermore, in so doing equations (2.22) and (2.23) have been normalized with regards to different values of the nominal turbulent loss coefficient, λ_Ω, and valve flow ratio (or valve opening), θ, and a single horizontal asymptote obtained.

Determination of the critical point and the value of the shifting exponent may now be done in the manner outlined in Section 1.4. The critical point will thus be where

$$k_0 = k_\infty, \tag{2.24}$$

whence

$$\begin{aligned} \frac{1000}{Re_{3,c}} &= \frac{\lambda_\Omega}{\theta^2} \\ \Rightarrow Re_{3,c} &= \frac{1000\,\theta^2}{\lambda_\Omega}. \end{aligned} \tag{2.25}$$

Since both λ_Ω and θ are constants for a given pipe diameter and valve opening, the Slatter Reynolds number at which the critical point is to be found may easily be determined; these values are listed in Table 2.1. The pressure loss coefficient at the critical point is thus given by $k_{v,c} = k_v(Re_{3,c})$, the corresponding functional value obtained by equation (2.25).

The discussion in Section 1.4, equation (1.45), now yields a value for the shifting exponent, i.e.

$$s = \frac{\ln 2}{\ln k_{v,c} - \ln k_{\infty,c}} = \frac{\ln 2}{\ln k_{v,c} - \ln k_{0,c}}, \tag{2.26}$$

or in explicit form as

$$s = \frac{\ln 2}{\ln k_v(Re_{3,c}) - \ln\left(\dfrac{\lambda_\Omega}{\theta^2}\right)} = \frac{\ln 2}{\ln k_v(Re_{3,c}) - \ln\left(\dfrac{1000}{Re_{3,c}}\right)}. \tag{2.27}$$

		valve opening, θ			
		0.25	0.50	0.75	1.00
$40mm$	$(\lambda_\Omega = 8.0)$	7.8594	31.438	70.734	125.75
$50mm$	$(\lambda_\Omega = 3.4)$	18.493	73.971	166.43	295.88
$65mm$	$(\lambda_\Omega = 1.5)$	41.917	167.67	377.25	670.67
$80mm$	$(\lambda_\Omega = 2.9)$	21.681	86.724	195.13	346.90
$100mm$	$(\lambda_\Omega = 4.1)$	15.335	61.341	138.02	245.37

Table 2.1: Calculated values $Re_{3,c} = (1000\,\theta^2)/\lambda_\Omega$ for all possible combinations of pipe diameter and valve opening. The λ_Ω-values in this table were obtained from Mbiya [9].

Traversal of the data sets in search of the $Re_{3,c}$-value closest to those listed in Table 2.1 may now be effected, the objective being to find the corresponding value of the dependent variable, $k_{v,c}$, at this point. Plugging these values into equation (2.27) will then yield a possible value for the shifting exponent. However, the datum point chosen may be a poor choice (an outlier, the result of a poor reading, etc.) and grounding the s-value solely on this one, single reading may lead to erroneous results. It is therefore recommended that the value of the intersection of the asymptotes be determined beforehand and the bulk of experimentation conducted in the area of the yielded independent variable, i.e. $Re_{3,c}$. In so doing a more accurate prediction will be obtained (from averaging numerous data points) and the fractional deviation of the matched solution from either of the limiting solutions or asymptotic values minimized (see Section 1.4). It is nevertheless important to note that the method is still an empirical one, based on experimental results; the wish being for an analytical expression in which this shifting exponent is linked to some quantifiable parameter in the process under consideration.

Since Mbiya's experimental readings were not arranged in such a manner as to focus on the transitional area between the asymptotes, the aforementioned methodical approach was not used. In lieu, to circumvent the shifting exponent being based on an incorrect or inaccurate reading, a trial-and-error graphical approach was used. The results of two such curve fittings for different pipe diameters and valve openings are shown in Figures 2.6 and 2.7, with s-values of 0.4 (solid line) and 1.4 (dashed) plotted for comparison.

Ideally, the normalised, non-dimensional expressions of equations (2.22) and (2.23) would also allow for the experimental data of all valve sizes to be plotted on a single plot, irrespective of the valve flow ratio, θ. However, as can be seen in Table 2.1, there is no discernable relation between the valve diameter and the λ_Ω-values. Mbiya

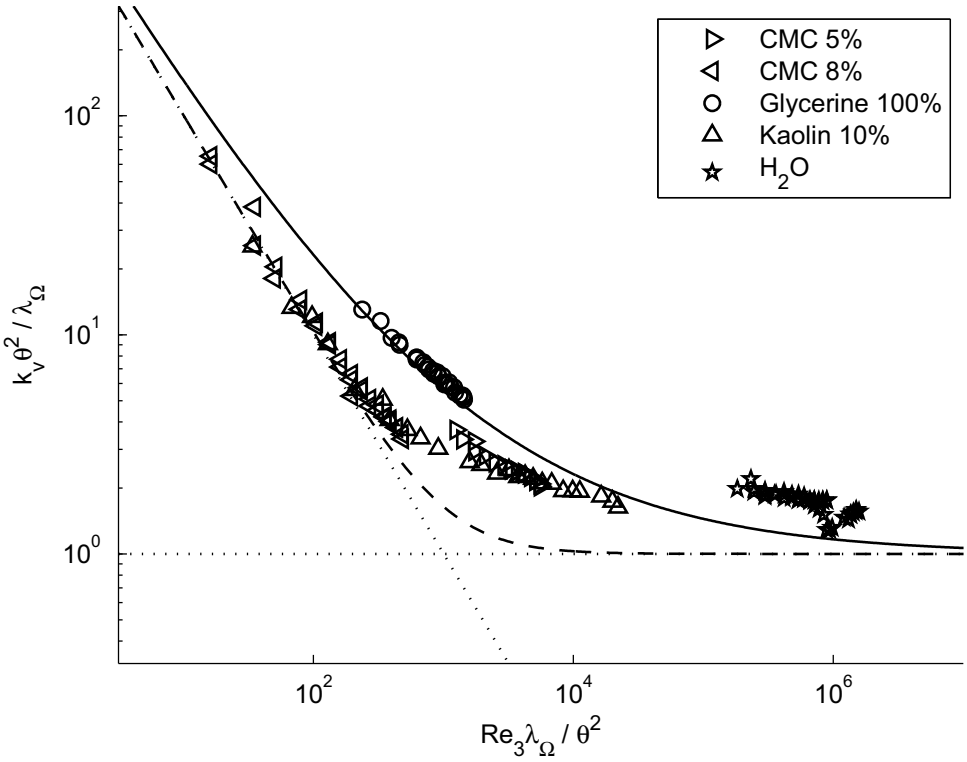

Figure 2.7: Powered addition applied to Mbiya's [9] data sets for a pipe with internal diameter of 50mm and a valve opening of 50%. s-values of 0.4 (solid line) and 1.4 (dashed) are shown for comparison.

[9; 10; 11] notes that λ_Ω is obtained by the minimisation of the overall logarithmic difference between his calculated and experimental k_v-values and cites the lack of dynamic similarity between valves of different sizes as rationalisation for these discrepancies.

An attempt at plotting all the data for a specific valve diameter, regardless of the valve opening, on a single plot afforded no clear visual results. To prevent clutter, data sets were plotted on separate axes according to valve diameter and valve opening (see Appendix C). The plots show a gradual shift towards and beyond (below) the asymptotes with an increase in the valve opening, that is to lower values of both the dependent and independent variables. This observation suggests a dependence upon some parameter that is yet to be considered or identified. To arrive at an accurate prediction of the shifter it is recommended that experiments be tailored so as to specifically investigate the flow parameters in the transitional regime; this was, however, not the focus of Mbiya's [9; 11] study.

Although the graphs obtained through the use of powered addition still leave a lot

to be desired, overall they exhibit, for our particular goal, a qualitatively improved prediction of the process than the model of Mbiya.

Chapter 3

Flow through a packed bed

Packed beds are of significant interest to chemical engineers since they are widely used for mass transfer in industrial plants. A crucial piece of information required for effective design is the difference of piezometric head necessary to ensure steady fluid flow, be it through a pipe, porous medium, etc. See e.g. [16] (*piezo* is derived from the Greek *piezein*, which means to squeeze or press). In the study of porous media this translates into a relation being sought between the pressure gradient and the superficial or discharge velocity.

The two predominant approaches used in the theoretical study of pressure drop through a packed bed differ from one-another in the manner in which the solid and fluid parts of the bed are regarded. The first method regards the pores between the solid phase as a bundle of tangled tubes of irregular and inconsistent cross-section and proceeds to develop a model based on applying, modifying and expanding the well-established results for the flow in single, straight tube. The second method involves the solid phase being seen as an aggregation of individual objects submersed in the fluid phase; the pressure drop being calculated by addition of the resistance of each of the particles, e.g. [17]. The former approximation to reality has enjoyed more publicity and attention in the literature.

In this chapter two methods used in predicting pressure drop over a packed bed or porous medium are discussed: the first, the Ergun equation, is semi-empirical in nature and, surprisingly, one of the very few known example of powered addition with an exponent of unity; the other method, the RUC model, is an analytical approach based on pore-scale modelling of the microstructure of the porous medium and forms a key concept in the discussion following in Chapter 4.

3.1 Ergun equation

One of the pioneers in experimental fluid mechanics was the French engineer, Henry Darcy (1803 - 1858) of Dijon. Involvement in the design of municipal water supply systems led to his research into the flow of water through sand bed filters [18; 19] (i.e. flow through porous media) and the eventual publication in 1856 of *Les Fontaines Publiques de la Ville de Dijon*. The empirical law that he proposed, and that consequently carries his name, states that the rate of flow through a bed of packed particles is proportional to the pressure drop (hydraulic gradient) over the bed [18; 20] – specific discharge is proportional to the fluid pressure gradient in the direction of flow. In one dimension this linear relation is expressed as

$$-\frac{dp}{dx} = \frac{\mu}{\kappa} q, \tag{3.1}$$

where $-dp/dx$ is the streamwise pressure drop, μ the viscosity of the traversing fluid and q the superficial velocity or specific discharge. The coefficient of proportionality, κ, is referred to as the hydrodynamic permeability and is generally determined experimentally (a great deal of work has gone into determining an analytical expression and will be discussed in Section 3.2).

In practice, however, results obtained from experiments tend to deviate from the linear relation predicted by equation (3.1) and become nonlinear at higher velocities, despite the fact that the Reynolds number, Re, may still be fairly small [17]. Hence, wide application of Darcy's law is impeded by its limitation to a fairly narrow range of Reynolds numbers.

Throughout history various attempts have been made to more accurately relate the pressure gradient and superficial velocity. In 1901 Forchheimer proposed [21] (referenced in [22]) the introduction of a quadratic term to take this nonlinear behaviour into account, leading to an empirical generalized form of the Darcy equation, namely

$$-\frac{dp}{dx} = Mq + Nq^2, \tag{3.2}$$

with the coefficients M and N empirical constants that depend on the structural and geometric properties of the porous medium and fluid viscosity [23; 24]. In the case of a superficial velocity, q, less than unity the second term in equation (3.2) becomes negligible and it effectively reduces to the Darcy law, equation (3.1). Conversely, for a high superficial velocity the quadratic term in equation (3.2) predominates. Between these two flow regimes a transitional area exists.

The Ergun equation – a capillary tube model widely used for the prediction of pressure drop of flow through a packed bed – is in essence based upon a combination of

specific asymptotic solutions for the Darcy and Forchheimer regimes and is therefore semi-empirical in nature. In it's derivation the assumption is made that the bed consists of smooth, uniformly sized, spherical particles; that the particles are packed in a statistically uniform random manner; and, that the diameter of the containing column is orders of magnitude larger than that of the particles. Ergun simply added the equation proposed by Blake and Kozeny for laminar flow (Darcy regime)

$$\Phi = 150 Re_s, \tag{3.3}$$

to the Burke-Plummer equation for turbulent flow (Forchheimer regime) [1; 17; 25],

$$\Phi = 1.75 Re_s^2, \tag{3.4}$$

to obtain

$$\Phi = 150 Re_s + 1.75 Re_s^2, \tag{3.5}$$

an expression for the pressure drop across a packed bed for Reynolds numbers rang-

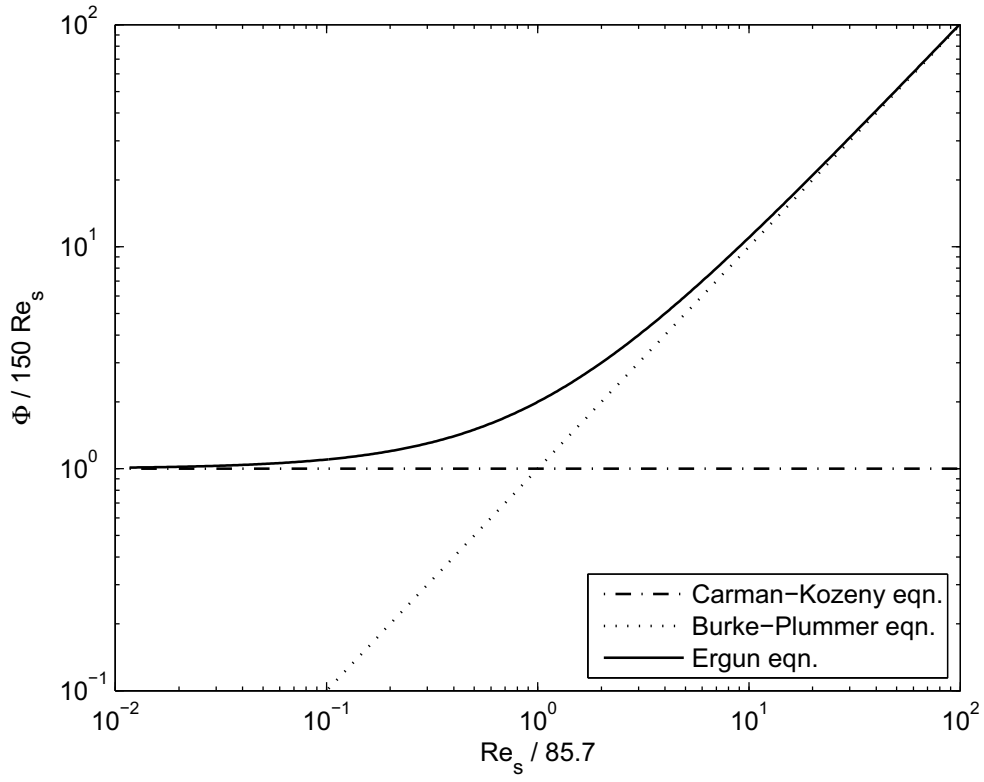

Figure 3.1: Logarithmic correlation for the pressure drop through a packed bed of spheres – the Ergun equation is an instance of powered addition with $s = 1$ (the equation of Carman and Kozeny was added to the Burke-Plummer equation).

ing from the laminar to the turbulent flow regimes. It should be noted that the non-linear effects, represented by the second term on the righthand side of equation (3.5),

are already noticeable at Reynolds numbers well below that of the region which is normally associated with turbulence.

His result mostly yields satisfactory agreement with experimental data for $\varepsilon < 0.5$. In equations (3.3) to (3.5) the variable Φ has been used for simplicity and is defined as

$$\Phi = \frac{\rho_f \varepsilon^3 D_s^3}{\mu^2 (1-\varepsilon)^3} \left(-\frac{dp}{dL} \right), \tag{3.6}$$

with the Reynolds number for a packed bed of spheres, Re_s, given by [1]

$$Re_s = \frac{\rho_f q D_s}{\mu (1-\varepsilon)}. \tag{3.7}$$

In equations (3.6) and (3.7), ρ_f denotes the density of the traversing fluid, ε the bed porosity or void fraction, D_s the diameter of a perfectly spherical particle and L the length of the straight channel (or height of bed).

Ergun had thus, in effect, applied the matching technique proposed by Churchill & Usagi [1; 2; 5; 6; 25] as discussed in Chapter 1 to produce a combined result,

$$\Phi = [(150 Re_s)^s + (1.75 Re_s^2)^s]^{1/s}, \tag{3.8}$$

with equation (3.8) reverting to equation (3.5) by choosing the shifting exponent, $s = 1$; his result is shown in Figure 3.1. The value of the exponent was however not known a priori. Utilizing the generic form suggested by equation (1.39) with

$$Y = \frac{\Phi}{150 Re_s}, \tag{3.9}$$

and

$$Z = \frac{1.75 Re_s}{150} = \frac{Re_s}{85.7}, \tag{3.10}$$

the value of the critical point, as considered in Section 1.4, is obtained at $Z = 1$, that is at $Re_s = 85.7$. Churchill [1] notes that this process happens to be the only one thus far examined in which the best choice of exponent turned out to be unity.

The Ergun equation, expressed in its more well-known form

$$-\frac{\Delta p}{L} = 150 \frac{(1-\varepsilon)^2}{\varepsilon^3} \frac{\mu q}{\phi_p^2 d_p^2} + 1.75 \frac{(1-\varepsilon)}{\varepsilon^3} \frac{\rho q^2}{\phi_p d_p}, \tag{3.11}$$

takes into account cases in which the bed consists of non-spherical particles. In equation (3.11) d_p denotes the mean particle diameter and ϕ_p the particle shape factor (sphericity). The mean particle diameter, d_p, is defined in terms of the specific surface, a_v of the particle,

$$d_p = \frac{6}{a_v}, \tag{3.12}$$

with the specific surface being defined as

$$a_v = \frac{\text{total particle surface}}{\text{volume of the particles}}. \tag{3.13}$$

The reason for the above definitions becomes apparent when regarding a bed consisting of N perfectly spherical particles. Since the surface area of a sphere is given by $4\pi r^2$ and its volume by $\frac{4}{3}\pi r^3$, substitution into equation (3.13) will yield

$$a_v = \frac{4N\pi r^2}{4/3N\pi r^3} = \frac{3}{r} = \frac{6}{D_s}, \tag{3.14}$$

and plugging this result into equation (3.12) sets $d_p = D_s$ (here r and D_s respectively denote the radius and diameter of the sphere) [17].

More often than not the bed does not consist of perfectly spherical particles, in which case it is customary to construct a hypothetical equivalent-volume sphere, $\phi_p d_p$, with

$$d_p = \frac{6V_p}{A_p\phi_p} = \frac{6V_p}{A_{sp}}, \tag{3.15}$$

as used in equation (3.11). Here V_p is the volume of a single, non-spherical particle, A_p its surface area and A_{sp} the surface area of an equivalent volume sphere. Equation (3.15) thus relates the surface area of the particle to the surface area of a sphere of equal volume [24]; cf equation (3.13). Thus, $\phi_p = 1$ and $\phi_s < 1$ for spherical and non-spherical particles respectively.

According to Geldart [26] the most appropriate parameter for use in flow through packed beds is the external surface area of the powder per unit particle volume. Hence, the diameter of a sphere with the same external surface area to volume ratio as that of the particle, d_{sv}, is the most relevant diameter. The Waddell sphericity factor, Ψ, defined as

$$\Psi = \frac{\text{surface area of equivalent volume sphere}}{\text{surface area of particle}}, \tag{3.16}$$

can be shown to link d_{sv} and d_v, , by

$$\Psi = \frac{d_{sv}}{d_v}, \tag{3.17}$$

with d_v the volume diameter, i.e. the diameter of a sphere having the same volume as the particle.

3.2 RUC model

The analytical approach to flow through porous media is based on modelling the microstructure of the porous media on pore-scale level and aims to provide a theoretical

derivation of the empirical Ergun equation. In dealing with porous media that is assumed to have a regular pattern, the idea of constructing a repetitive unit or cell, holds the advantage that flow around each and every solid particle in the medium need not be analyzed. It would thus be possible to 'reconstruct' the particular porous medium under regard from such a building block or unit cell, provided that these cells are both volume-conserving and space-filling.

The actual interstitial pore space, especially in cases where the media under regard is isotropic, and the solid material is thus randomly positioned within the volume, is very seldom open to precise analysis. To circumvent this obstacle, a hypothetical representative unit cell (RUC) was introduced [27; 28] which theoretically approximates the porous material in that it contains the average geometric properties of the material. The RUC model is thus a generalised geometric approximation of the actual geometric properties of the medium in such a manner as to preserve the physical attributes of flow through such a medium; an abstraction of the porous medium rendering it amenable to physical analysis.

The pore-scale geometric relation between the solid and fluid phases of porous media allows for classification into three fundamental classes: granular, spongelike and unidirectional two-dimensional fibre-bed. Analytical expressions for the hydrodynamic permeability, k, and stream-wise pressure drop,$-dp/dx$, of the different RUCs are known [27; 28; 29; 30; 31; 32].

For the remainder of this section the particle Reynolds number, Re_p – an indicator of the ratio between the inertial and viscous forces of the fluid with d_p used as characteristic length – has been defined as

$$Re_p = \frac{\rho q d_p}{\mu}, \tag{3.18}$$

where ρ and μ denote the density and viscosity of the traversing fluid respectively, q the magnitude of the superficial velocity or specific discharge and d the linear RUC dimension. The practical use of the Reynolds number is to distinguish among flow regimes, for example laminar or turbulent flow in pipes or around immersed objects, its value depending upon the situation.

3.2.1 Granular porous media

In media that fall into this class, the solid phase is present in the form of isolated to semi-connected units that are submerged in the surrounding fluid phase. Some examples of granular porous media would be the glass spheres used in packed bed chemical reactors and a pipe filled with sand or marbles. A schematic representation

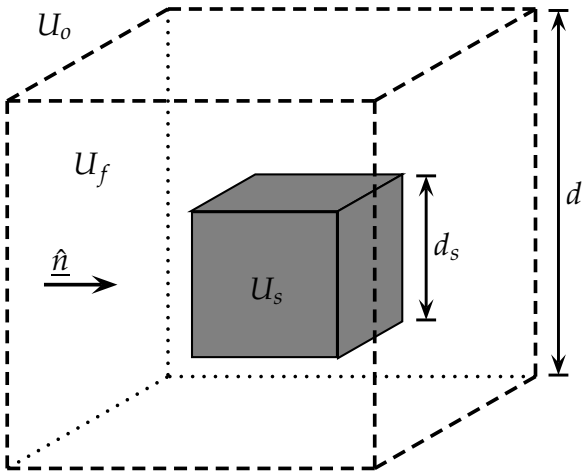

Figure 3.2: Cubic geometry of the RUC model for modelling fluid flow through granular media. The streamwise direction is indicated by $\hat{n}$. The shaded volume represents the solid phase.

of the isotropic granular RUC model [29; 31; 32] is shown in Figure 3.2. U_s denotes the volume of the solid phase, U_f the volume of the fluid phase and U_o the total volume of the RUC.

The relation between the linear dimensions d and d_s of the granular RUC, with ε denoting the porosity, is given by

$$d_s = (1-\varepsilon)^{1/3} d, \tag{3.19}$$

and the stream-wise pressure drop, $-dp/dx$, by

$$-\frac{dp}{dx} = \frac{25.4(1-\varepsilon)^{4/3}}{(1-(1-\varepsilon)^{1/3})(1-(1-\varepsilon)^{2/3})^2} \cdot \frac{\mu q}{d_s^2} + \frac{c_d(1-\varepsilon)}{2\varepsilon(1-(1-\varepsilon)^{2/3})^2} \cdot \frac{\rho q^2}{d_s}, \tag{3.20}$$

where c_d denotes the drag coefficient and Re is the Reynolds number as defined in equation (3.18).

3.2.2 Spongelike porous media

Spongelike or consolidated porous media are distinguished from granular porous media by the fact that the solid and fluid phases are interconnected. In other words, one would be able to move from any point in a given phase to any other point in the same phase, without ever having to leave it. Examples would be plastic and metallic foams, such as those used in electronics, or any substance containing interlinking ducts.

Foamlike media is further differentiated into three sub-models depending on the number of stagnant pore-sections assumed to be present within the foam model [29; 33; 34]. For porous media of this type, the stream-wise pressure drop, $-dp/dx$ is given by

$$-\frac{dp}{dx} = \frac{36\psi^2(\psi-1)}{\varepsilon^2}\cdot\frac{\mu q}{d^2} + \frac{c_d(\psi-1)\psi^2(\psi-3)^2}{4\varepsilon^3}\cdot\frac{\rho q^2}{d}, \tag{3.21}$$

with ψ a geometric factor, defined in this case as

$$\psi = 2 + 2\cos\left(\frac{4\pi}{3} + \frac{1}{3}\cos^{-1}(2\varepsilon - 1)\right), \tag{3.22}$$

subject to the condition that $\psi = 1$ when $\varepsilon = 1$.

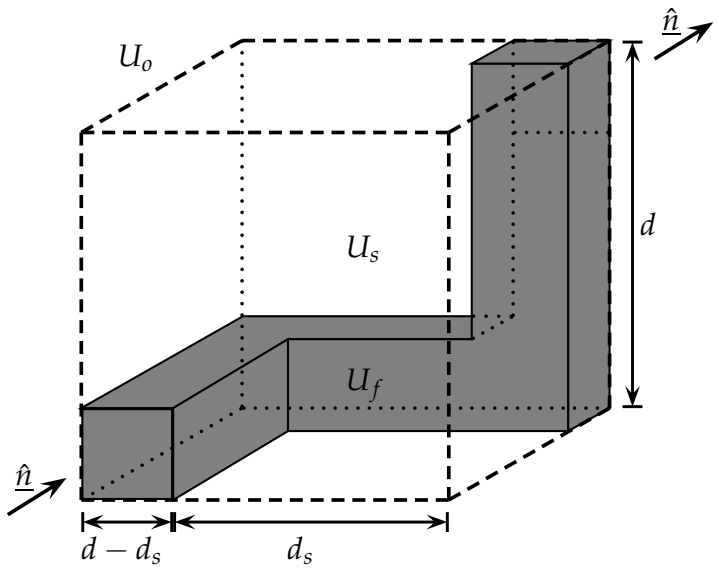

Figure 3.3: Cubic geometry of the RUC model for modelling fluid flow through foam-like media. The streamwise direction is indicated by $\underline{\hat{n}}$. Note that here the shaded volume is representative of the fluid phase.

In Figure 3.3 a schematic representation is given of the isotropic foamlike RUC model. It is important to note that in this figure, as opposed to the other figures, the shaded volume is representative of the fluid phase, U_f. Fluid traversing such a theoretically constructed medium would thus enter through the façade facing the reader, move along the side of the cube and then turn Eastwards to move along the middle channel. It will travel a distance d_s along the side of the cube, before turning in a Northerly direction, to finally exit the model at the backward facing plane.

Expressing the relation between the linear dimensions d and d_s of the foamlike RUC in terms of the porosity, ε, yields a polynomial of the third order,

$$\varepsilon = 1 - 3\left(\frac{d_s}{d}\right)^2 + 2\left(\frac{d_s}{d}\right)^3, \tag{3.23}$$

which may be rewritten in terms of the geometric factor, ψ, as [29]

$$\frac{\psi}{\varepsilon} = \frac{4}{(3-\psi)^2}. \tag{3.24}$$

3.2.3 Unidirectional two-dimensional fibre-bed porous media

Should the solid phase of the medium consist of aligned, disjoint fibre strands surrounded by an interconnected fluid phase, it is classified as a two-dimensional prismatic or unidirectional fibre-bed porous medium. Air flowing through a stack in a timber-drying kiln would be an example of porous media of this kind. Figure 3.4 shows a schematic representation of porous media of this type. It should be noted that the dimension L should be of sufficient length so as to clearly distinguish it from the granular RUC model illustrated in Figure 3.2. The relation between d and d_s for the

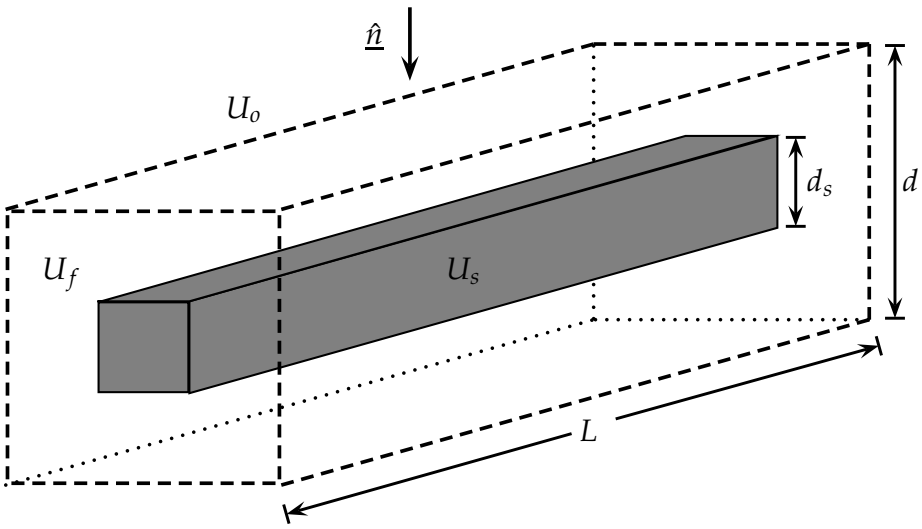

Figure 3.4: RUC model for modelling fluid flow through fibre beds. The streamwise direction is indicated by $\hat{n}$. The shaded volume represents the solid phase.

fibre-bed RUC may be expressed as

$$d_s = d\sqrt{1-\varepsilon}, \tag{3.25}$$

while the stream-wise pressure drop, $-dp/dx$, for the isotropic fibre-bed model is given by [29; 30]

$$-\frac{dp}{dx} = \frac{13.5\sqrt{1-\varepsilon}}{(1-\sqrt{1-\varepsilon})^3} \cdot \frac{\mu q}{d^2} + \frac{c_d\sqrt{1-\varepsilon}}{2\varepsilon(1-\sqrt{1-\varepsilon})} \cdot \frac{\rho q^2}{d}. \tag{3.26}$$

Whereas the Ergun equation was limited to a fairly narrow range of porosities, the fact that the RUC model is based on physical principles (and doesn't contain empirical coefficients) ensures that the latter is applicable over the entire range of porosities from zero through unity. The geometries of the different fundamental classes have also been designed as such that it is physically adaptable to predict the pressure drop in beds consisting of non-spherical particles.

Chapter 4

Fluidised bed

A fluidised bed is formed when a fluid, usually a gas, is forced upwards through a bed of particles. The packed bed of particles, supported on some kind of distributor, is converted into an expanded, suspended bed and in the process takes on many liquid-like properties: the bed has zero angle of repose, pressure increases linearly with distance below the surface, wave motion is observed, denser objects sink and lighter objects may be floated on its surface, their movement almost unhindered [35]. This only happens once the pressure drop across the bed, created by the flow, becomes sufficient enough to support the weight of the constituent particles and is referred to as *incipient fluidisation*. The superficial velocity at which the aforementioned phenomenon occurs is know as the minimum fluidisation velocity, q_{mf}. Additional increase in the fluid flow rate leads to a further expansion of the bed and eventually the formation of bubbles. This is commonly known as *aggregative fluidisation* and leads to agitation of the solid constituents and a consequent fluctuation in the height of the bed [35].

A fluidised system has a number of highly useful properties that may be utilised in industrial applications. Foremost among them is the agitation caused by the bubbles – the already large specific area of a fine powder is further exploited as the stirring action continually moves the particles around, exposing it to the gas. The good mixing of the solids is responsible for a high heat transfer rate from the gas to the particles, causing dispersion of localised temperature regions and leading to radial and axial isothermal conditions. The large contact area between the solid and fluid phases also enhances chemical reaction rate, making fluidisation a technique well suited for catalytic reactions. Thus, although the mechanism may be both physical and chemical in nature, the dominating attribute utilised in a specific industrial process, will determine its application. A broad classification of fluid bed applications is given by [36], from which it is evident that fluidisation is an interdisciplinary field of inquiry.

Despite many attractive features, fluidised beds are not suited to all fluid-solid pro-

cesses and some of the disadvantages may overshadow the potential benefits. Both chemical and mechanical difficulties arise with scale-up in size from laboratory equipment to industrial plant – some of the gas in the bubbles may by-pass particles completely, lowering efficiency; erosion of the containing vessel will inevitably occur in areas of high gas velocity. To optimally reap the benefits of this promising and still incompletely understood process there thus exists a particular need for the development of predictive models; holding challenges for both fundamental and applied research.

Upon analysis of sets of collected data of flow through a porous medium, it is evident that asymptotes exist for some variable dependencies in the transition from packed- to fluidised bed. The transition between such asymptotes is governed, amongst others, by parameters such as particle size, particle size distribution, superficial gas velocity and bed height. Powered addition to a power, s, of such asymptotes f_0 and f_∞, leads to a single correlating equation that is applicable over the whole range of flow rates.

4.1 Newtonian fluid

Experimental data was obtained from measurements performed by the author on laboratory-scale fluidized beds at Telemark University College, Porsgrunn, Norway. The aforementioned method of powered addition is applied to the experimental data and the outcomes discussed; the underlying motivation being an aspiration towards establishing a sound modelling framework for analytical and computational predictive measures. The results of this section were presented at the 5th International Conference on Computational & Experimental Methods in Multiphase and Complex Flow (Multiphase Flow V), New Forest, UK, 15 - 17 June 2009 [4].

4.1.1 Experimental procedure

The bed was contained in a cylindrical perspex tube with an inner diameter of $72mm$. Since the investigation was only concerned with the pressure drop across a specified section of the bed (i.e. between two pressure sensors), the porosity of the plate on which the bed was supported was irrelevant. It was only required not to allow particles to drop through into the antechamber and to function as a uniform gas distributor. To prevent particle entrainment the uppermost end of the containing perspex tube was covered with a porous paper cap and the bed illuminated from behind to allow easy visual detection of the onset of fluidisation.

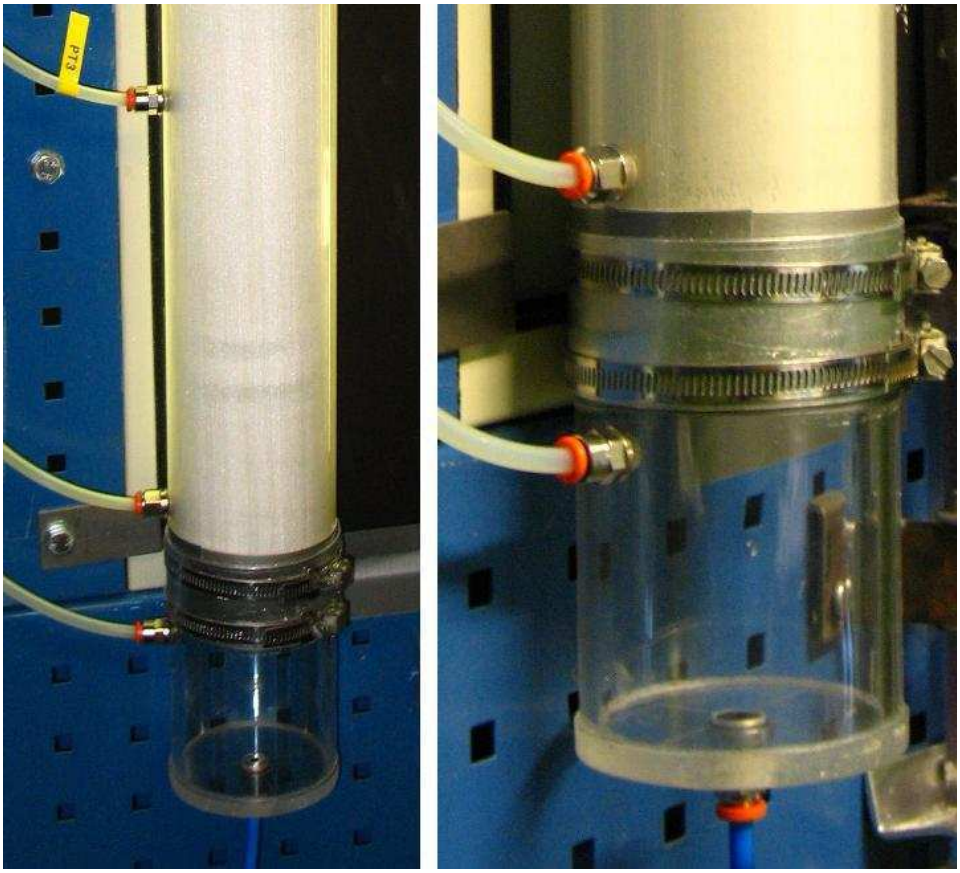

Figure 4.1: Experimental setup

The beds comprised of glass powders, consisting of spherical glass particles, with a density of $2485 kg/m^3$ and available in three different diameter-ranges: $100\mu m - 200\mu m$; $400\mu m - 600\mu m$; and $750\mu m - 1000\mu m$. These particles all fall into Group B and D according to the Geldart powder classification [37]. Since the particles are manufactured they were assumed, for the sake of simplicity, to be perfectly spherical in shape and thus have a Waddell sphericity factor – see equation (3.16) – of $\Psi = 1$ [26] .

In all of the experiments performed the fluid used to fluidise the bed was air at ambient conditions, with a density of $1,2 kg/m^3$ and viscosity of $1.78 \times 10^{-5} N \cdot s/m^2$. Air was pumped into the bed by a compressor and flow into the antechamber was controlled via a manual valve. A digital flow meter, situated between the valve and the antechamber, registered the fluid velocity. By using different gas velocities and only one particle diameter-range or a mixture of the particle diameter-ranges, the parameters of the experiment could be varied. Eight equidistantly spaced pressure tubes were placed along the height of the bed and were connected to digital pressure sensors (Honeywell, model 142PC02G) that measured the pressure (in $mbar$) at these fixed

intervals within the bed. An experiment-specific software program was written with the aid of the LABVIEW package with which the data from each sensor were recorded and written to file; the program was calibrated and allowed for the interval between consecutive readings to be varied. Figure 4.1 shows the bed, antechamber, fluid inlet from below and some of the silicone pressure tubes (leading off to the digital sensors).

A minimum of three runs were performed for each of the three different diameter-ranges mentioned above. A run consisted of a gradual increase until and beyond fluidisation, followed by a gradual and controlled decrease to zero fluid flow. It was noted that hysteresis only became apparent if the bed was allowed a period of rest between consecutive fluidisations. Consequently, runs for a particular diameter-range were conducted in succession allowing the obtained pressure-values to be averaged. It is to this averaged data that the curve-fitting technique was applied.

4.1.1.1 Determining the superficial velocity of the traversing fluid

A digital flow meter, connected to a compressor, measured the flow rate of the air entering the bed. The meter registered rates in liters per minute, $[\ell/min]$, and these readings were recorded with the mentioned software program. To convert ℓ/min, the inner diameter ($72mm$) of the cylindrical perspex tube containing the bed was used, i.e. readings from the meter were multiplied by a factor,

$$\frac{\ell/min}{A_c} = \frac{\frac{(0.1m)^3}{60s}}{\pi r^2} = 4.09 \times 10^{-3} m/s, \tag{4.1}$$

to obtain the superficial velocity. Here A_c is the cross-sectional area of bed and r the radius of the containing cylinder.

4.1.1.2 Determining the porosity of the packed bed

For each of the diameter-ranges an amount of powder was weighed out and poured into the cylindrical perspex tube comprising the fluidised bed. Once inside the tube, the powders were briefly allowed to settle before commencing experimentation. By measuring the distance between the supporting porous plate at the base of the bed and the bed surface, the bulk volume, U_0, occupied by the powder (and hence that of the bed) could be calculated by

$$U_0 = \pi r^2 H, \tag{4.2}$$

where r is the radius of the containing cylinder and H the height of the packed bed.

Porosity or bed voidage, ε, is defined as the ratio between the fluid volume, U_f and

the bulk volume, U_0, i.e.

$$\varepsilon \equiv \frac{U_f}{U_0}, \tag{4.3}$$

and density, ρ, as the mass, m, per unit volume, U

$$\rho_i \equiv \frac{m_i}{U_i}, \tag{4.4}$$

with the subscript denoting the phase under consideration.

It follows naturally that the total or bulk volume, U_0, is merely the sum of the volumes occupied by the solids, U_s, and the fluid, U_f, i.e.

$$U_0 = U_s + U_f, \tag{4.5}$$

with the same being true of the total or bulk mass, m_0

$$m_0 = m_s + m_f, \tag{4.6}$$

where m_s and m_f are the masses of the solids and fluid respectively.

From definition (4.4) and equations (4.5) and (4.6) it follows that

$$U_0 = \frac{m_s}{\rho_s} + \frac{m_f}{\rho_f} = \frac{m_0 - m_f}{\rho_s} + \frac{m_f}{\rho_f}. \tag{4.7}$$

Some further simple algebraic manipulation, utilisation of definition (4.4), substitution with equation (4.6) and rearrangement to make m_f the subject of the formula, yields

$$m_f = U_0 \rho_f \left(\frac{\rho_s - \rho_0}{\rho_s - \rho_f} \right). \tag{4.8}$$

Division of equation (4.8) by ρ_f yields

$$U_f = U_0 \left(\frac{\rho_s - \rho_0}{\rho_s - \rho_f} \right), \tag{4.9}$$

whence follows, by definition (4.3)

$$\varepsilon = \frac{\rho_s - \rho_0}{\rho_s - \rho_f}, \tag{4.10}$$

an expression for the porosity in terms of known or easily measurable quantities.

In an idealised situation of infinite size the diameter of spherical particles would have no influence on the porosity of the bed. However, in the constrained bed found in practical applications, the cross-sectional area of the bed will influence the packing of the particles. Taking this into account and regarding equation (4.10) it now becomes evident that the diameter of particles impacts indirectly on the porosity of the bed by having an influence on the bulk volume, and thus the bulk density thereof. The porosity for each of the diameter ranges were calculated with the aid of equation (4.10) and are listed in Table 4.1.

Particle diameter	Porosity, ε
$100 - 200\mu m$	0.391
$400 - 600\mu m$	0.368
$750 - 1000\mu m$	0.362

Table 4.1: Porosity or bed voidage for the different diameter-ranges.

4.1.2 Asymptotic dependencies

Three regimes are to be identified, namely the two regimes corresponding respectively to the physical conditions related to the two asymptotes f_0 and f_∞ and the change-over regime connecting the two. This latter regime surrounds the critical point, x_c, where the asymptotes meet. Of particular interest is the relation between the extent of the change-over regime surrounding the critical point and the shifting exponent s; in the present case of onset of fluidization the change-over between a packed bed condition and a fluidized state is fairly abrupt leading to a relatively high value of s. These effects will be discussed in the following subsections.

4.1.2.1 The lower asymptote

Before the onset of fluidisation, the bed may be regarded as a packed bed or porous medium consisting of spherical particles. To describe the pressure drop of Newtonian flow through such a structure, the Ergun equation has proven to be satisfactory in most applications as is evident from its extensive utilisation in chemical engineering. In their paper [32], Du Plessis & Woudberg compare the RUC (Representative Unit Cell) model to the Ergun equation for the description of Newtonian flow through a packed bed of uniformly sized spherical granules and find the agreement to be satisfactory. The choice, in this paper, of the RUC model to describe the asymptotic relation at small values of the independent variable is due to the fact that it is adaptable to different physical situations, whereas the Ergun equation is empirically based and will thus vary according to the situation to which it is applied. Furthermore the RUC model allows the usage of the average bed porosity and is applicable over both the entire porosity and laminar Reynolds number ranges.

In the original Ergun equation, which is already a special case of powered addition with shifter, $s = 1$ as discussed in Section 3.1,

$$\frac{\Delta p}{H} = M\frac{(1-\varepsilon)^2}{\varepsilon^3}\frac{\mu q}{D_h^2} + N\frac{1-\varepsilon}{\varepsilon^3}\frac{\rho_f q^2}{D_h}, \tag{4.11}$$

the values of coefficients M and N were acquired experimentally and are given as 150

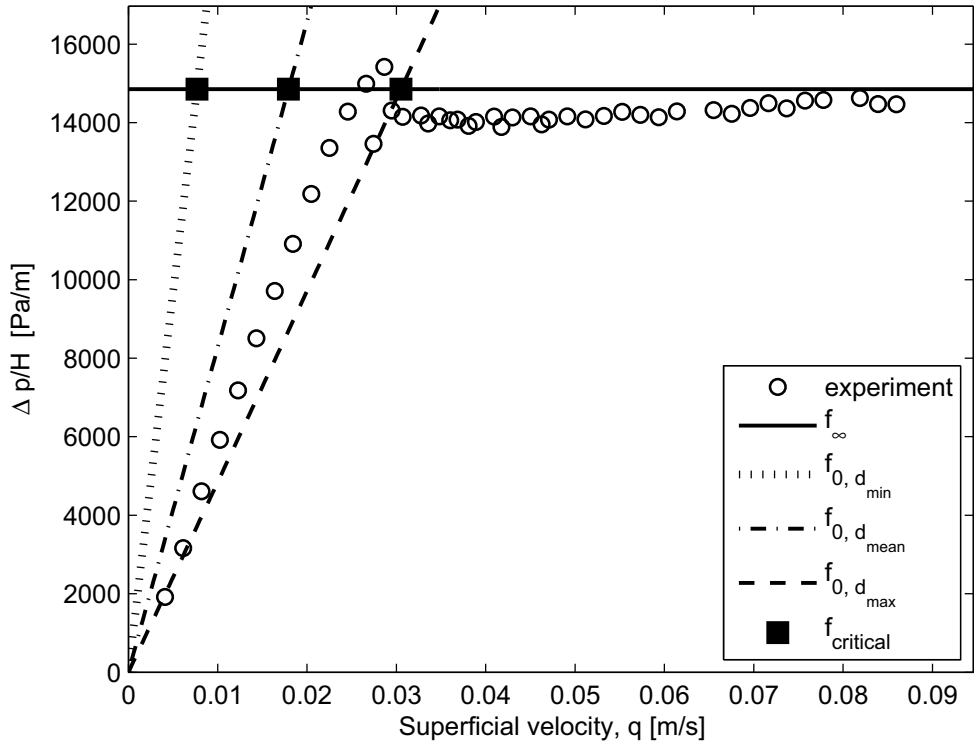

Figure 4.2: Particle diameter-range $100\mu m - 200\mu m$. Influence of chosen particle diameter on the positioning of the lower asymptote, f_0, and the position of the critical point, f_c. The RUC model is used to describe the lower asymptote.

and 1.75 respectively. Here Δp denotes the finite pressure difference (measured in the streamwise direction of fluid flow), H the bed height, ε the porosity or bed voidage, μ the fluid viscosity, ρ_f the fluid density, q the superficial velocity of the traversing fluid and D_h the hydraulic diameter (which is equal to the diameter of the spherical particles).

The work of Du Plessis & Woudberg, as briefly discussed in Section 3.2, allows one to purge equation (4.11) of its empirical elements. Pore-scale analysis of interstitial flow conditions lead to the following expression of coefficients

$$M = \frac{25.4\varepsilon^3}{(1-\varepsilon)^{2/3}(1-(1-\varepsilon)^{1/3})(1-(1-\varepsilon)^{2/3})^2}, \tag{4.12}$$

and

$$N = \frac{\varepsilon^2 c_d}{2(1-(1-\varepsilon)^{2/3})^2}. \tag{4.13}$$

They thus succeed in rewriting (4.11) such that it is independent of, and not limited

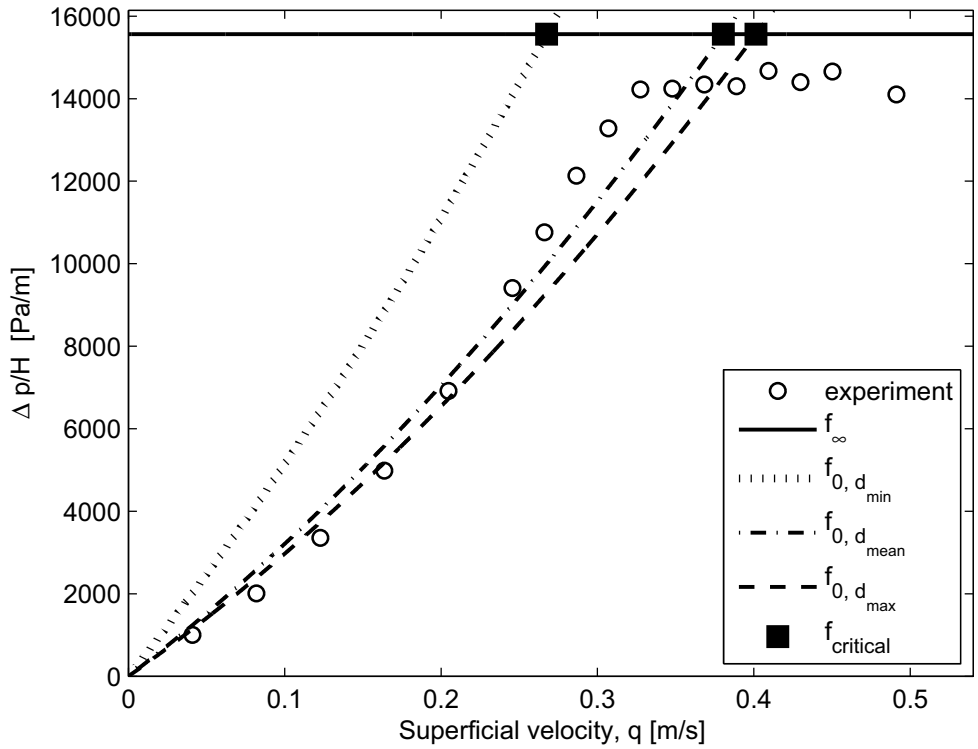

Figure 4.3: Particle diameter-range $750\mu m - 1000\mu m$. The choice of particle diameter determines orientation of the lower asymptote, f_0, and critical point, f_c. Note that the asymptotes need not be straight lines – slight curvature of f_0 due to the quadratic nature of equation (4.11) is evident.

by, the range of porosities used. Here the particle Reynolds number, Re_p, is defined as

$$Re_p \equiv \frac{\rho_f q D_h}{\mu}, \tag{4.14}$$

and as in [32] the value of the form drag coefficient, c_d in (4.13), was taken to be 1.9, presenting the most empirical aspect of the procedure.

4.1.2.2 The upper asymptote

As noted by Geldart [26], the pressure drop across a fluidised bed, given by

$$\Delta p = \frac{m_0 g}{A_c} = \frac{\rho_0 U_0 g}{A_c} = \rho_0 g H, \tag{4.15}$$

is the only parameter that can be predicted with accuracy, since at all times during fluidisation the downward force, i.e. the weight of the bed, $m_0 g$, is balanced by the

upward force, $\Delta p A_c$. Division of equation (4.15) by the bed height, yields

$$\frac{\Delta p}{H} = \frac{m_0 g}{A_c H} = \frac{\rho_0 U_0 g}{A_c H} = \rho_0 g, \tag{4.16}$$

which forms the upper limiting asymptote. Here m_0 denotes the bulk mass, ρ_0 the bulk density, U_0 the bulk volume, g acceleration due to gravity (taken as 9.81 m/s^2) and A_c the cross-sectional area of the bed.

4.1.3 Powered addition of the asymptotes

The original Ergun equation, (4.11), was obtained through simple addition of the Blake-Kozeny and Burke-Plummer equations, the former being a Darcy-type equation predominating in the regime where $Re_p \to 0$ and the latter dominating in the Forchheimer regime (refer to Section 3.1). If powered addition, as discussed in Chapter 1, is used to match the asymptotic conditions – i.e. equations (4.11) and (4.16) are combined – a single correlative measure,

$$\frac{\Delta p}{H} = \left[\left(M \frac{(1-\varepsilon)^2}{\varepsilon^3} \frac{\mu q}{D_h^2} + N \frac{1-\varepsilon}{\varepsilon^3} \frac{\rho_f q^2}{D_h} \right)^s + (\rho_0 g)^s \right]^{1/s}, \tag{4.17}$$

is obtained for the pressure drop over the bed. Here coefficients M and N are as expressed in equations (4.12) and (4.13).

4.1.3.1 Critical point and shifting-exponent

As discussed in Section 1.4 the *critical point* of the matching curve is the value of the independent variable at which the asymptotes meet. To determine this value for the case of the fluidised bed, we set

$$M \frac{(1-\varepsilon)^2}{\varepsilon^3} \frac{\mu q}{D_h^2} + N \frac{1-\varepsilon}{\varepsilon^3} \frac{\rho_f q^2}{D_h} = \rho_0 g, \tag{4.18}$$

which yields a quadratic equation in q. Let q_c be the value of the independent variable at which the asymptotes meet, i.e. the critical point. Solving $q = q_c$ in equation (4.18) yields

$$q_c = \frac{M}{N} \frac{\mu}{2\rho_f D_h} (1-\varepsilon) \left[-1 \pm \sqrt{\left(1 + \frac{N}{M^2} \frac{\varepsilon^3}{(1-\varepsilon)^3} \frac{4\rho_0 \rho_f g D_h^3}{\mu^2} \right)} \right]. \tag{4.19}$$

Since $\frac{N}{M^2} \frac{\varepsilon^3}{(1-\varepsilon)^3} \frac{4\rho_0 \rho_f g D_h^3}{\mu^2} \geq 0$ in equation (4.19) and $q_c \geq 0$, it follows that we may disregard the negative root. Substitution of this q_c value into equation (4.17) will yield the

function value at the intersection of the asymptotes. It is also worth noting that once the pressure drop created by the fluid flow becomes sufficient to support the weight of the bed, fluidisation will take an onset. In the general introductory discussion on fluidised beds at the beginning of this chapter it was remarked that this is referred to as the point of *incipient fluidisation* and the corresponding superficial velocity of the fluid as the minimum fluidisation velocity, q_{mf}. Seeing as the upper limiting asymptote predominates in the composition of the matched solution beyond the critical point, this point of intersection is the threshold value of the superficial velocity at which fluidisation will occur. The value found by equation (4.19) will thus be a theoretical prediction of the minimum velocity required to fluidise the bed, i.e. $q_{mf} = q_c$.

Once the experimental value of $f_c = f\{q_c\}$ for each of the diameter ranges has been determined by the method discussed above, we may proceed to calculate the value of the shifter by equation (1.45). As an alternative we may manually adjust the predictive curve until satisfactory visual correlation with the data is achieved and then assign a value to s.

4.1.3.2 Crossing of the upper asymptote

In Section 1.2.4 a method was outlined to construct a (postulated) dependence should the collected data cross the upper limiting asymptote. Referring to Figure 4.2 it is evident that this is the case for particles within the diameter range $100\mu m - 200\mu m$. This phenomenon is, according to Geldard [26] and Davidson & Harrison [35], caused by the wedging action within the bed and cohesion between the particles and is prevalent in beds composed of Group B particles (into which this diameter range resorts).

Letting $\zeta\{\infty\} = \rho_0 g$, and making use of the functional form suggested by equation (1.35), the dependence

$$\frac{\Delta p}{H} = \rho_0 g \left[1 + \left(\frac{q_A}{q}\right)^{\alpha}\right], \tag{4.20}$$

was postulated to represent behaviour of the bed in the upper limits of the superficial velocity. Here q_A is equivalent to the arbitrary constant of equation (1.35) and α an arbitrary exponent (see Section 1.2.4). The values of both these variables were chosen by trial and error; selecting the former to be equal to the value of the critical point, calculated in equation (4.19), that is $q_A = q_c$, and the latter as $\alpha = 12$, yielded encouraging results. The RUC model, as per equations (4.11), (4.12) and (4.13) was kept as representative of the lower asymptote. After applying the powered addition method used when an asymptote is crossed (outlined in Section 1.2.4) to the constituent terms in the functional expression and some rearrangement, the pressure drop across the

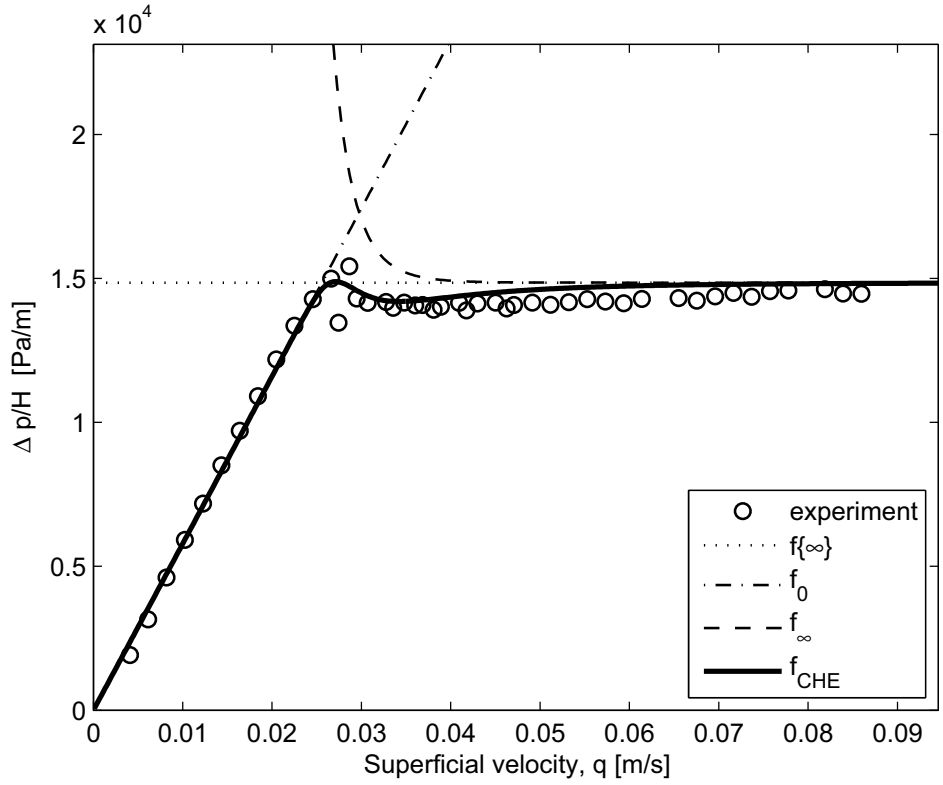

Figure 4.4: Curve-fitting by powered addition with a postulated function for the upper limiting dependency to enable crossing of the upper extremal value. Particles in diameter-range $100\mu m - 200\mu m$. The functional relation is given by equation (4.21), with $x_A = 0.026$, $\alpha = 12$ and $s = 4$ having been used.

bed may now be expressed as

$$\frac{\Delta p}{H} = \frac{\zeta_0\{q\}\zeta_\infty\{q\}}{(\zeta_0\{q\}^s + \zeta_\infty\{q\}^s)^{1/s}}. \tag{4.21}$$

Here $\zeta_0\{q\}$ is the functional dependence in the lower limit of the pressure drop on the superficial velocity as given by equation (4.11) and $\zeta_\infty\{q\}$ as per equation (4.20). In Figure 4.4 the matched curve yielded after plotting equation (4.21) against the collected data is shown; the degree of agreement between the two being a satisfactory result. Here, and in subsequent figures, f_{CHE} refers to the Churchill-Usagi-equation, or matched solution, as per equation (1.6).

4.1.4 Correlation of experimental results

The pressure drop was plotted against the superficial velocity for each of the diameter ranges. Figures 4.2 and 4.3 serve to illustrate the influence of the use of the mini-

mum (d_{min}), average (d_{mean}) and maximum (d_{max}) particle diameters on the orientation of the lower asymptote. A similar plot may be drawn for particle diameter-range

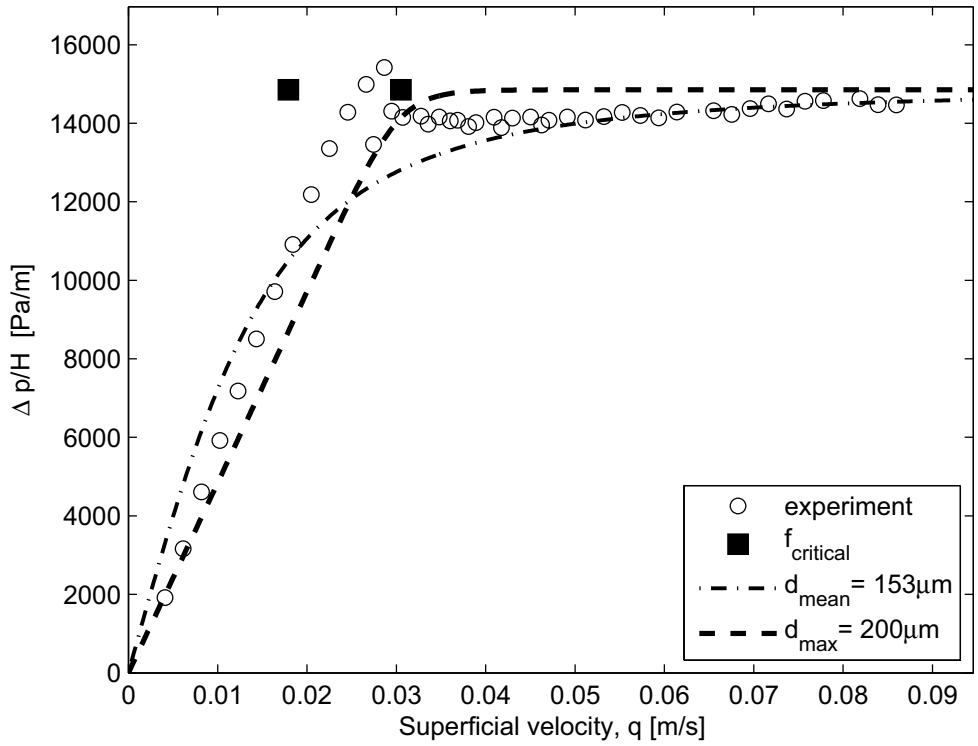

Figure 4.5: Curve-fitting by powered addition to experimental readings for particles in diameter-range $100\mu m - 200\mu m$. The functional relation is given by equation (4.17). An s-value of -2 was used for d_{mean}; an s-value of -14 for d_{max} (as per Table 4.2).

$400\mu m - 600\mu m$. It is important to note that the asymptotes need not be straight lines; this is apparent in Figure 4.3 where the quadratic nature of the RUC model – equation (4.11) with coefficients M and N as expressed in equations (4.12) and (4.13) – starts to dominate due to an increase in the superficial velocity before the onset of fluidisation.

Diameter	$100 - 200\mu m$	$400 - 600\mu m$	$750 - 1000\mu m$
d_{min}	-0.593	-0.825	-1.878
d_{mean}	-2.248	-3.155	-8.193
d_{max}	-14.280	-9.567	-11.786

Table 4.2: Calculated values of shifter-exponent, s, for the different particle diameter possibilities

From these graphical results the particle-diameter yielding the best correlation with

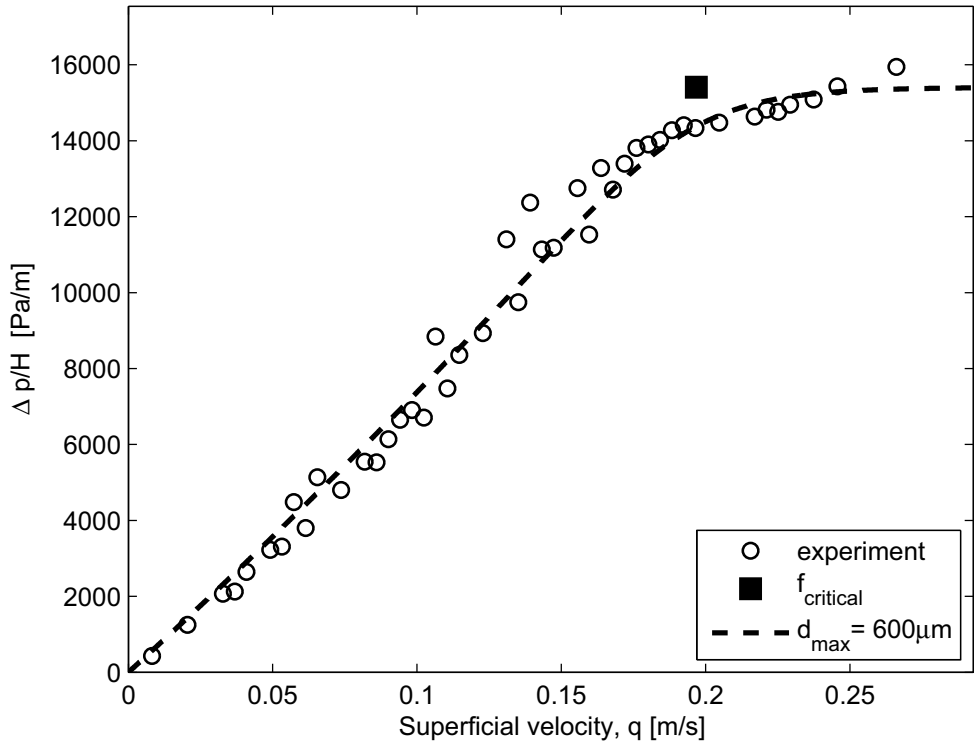

Figure 4.6: Powered addition-curve fitted to data for particles in diameter-range $400\mu m - 600\mu m$. The functional relation is once again given by equation (4.17); s-value of -10 was used.

the experimental data was chosen to be used in the fitting of a predictive curve. In the case where the data points were not noticeably favouring a specific particle diameter, the experimental data was traversed in search of the q_c-value matching the theoretically predicted value of the critical point, as expressed by equation (4.19), most closely. This value was then used to determine an s-value. Calculated values of s are shown in Table 4.2. The corresponding curves were plotted and the best match was chosen by visual inspection. From equation (4.19) it is clear that the diameter of the particle impacts on the value of q_c, and thus on $f_c = f\{q_c\}$. The latter in turn has a direct influence on the value of s, as calculated by equation (1.45). In the format of equation (4.17), with $\Delta p/H$ the dependent and q the independent variable, the relation shows a decreasing dependence as the superficial velocity grows. Furthermore, both the functions at the extremal values are presumed to form upper bounds on the value that the pressure drop may take. Hence, it is expected that the plot should be qualitatively analogous to the case outlined in Section 1.2.2.2 and a negative value of the shifting exponent is to be expected. Indeed, this turns out to be the case.

It should however be noted that the datum point chosen upon traversal of the ex-

perimental data may be a poor choice (an outlier, the result of a poor reading, etc.) Establishing the s-value purely based on this principle may lead to erroneous results; the value of visual inspection should never be underestimated (besides, the method is empirical). The false 'accuracy' portrayed by the values listed in Table 4.2 is merely the result of the algorithm used to traverse the original data sets; as Churchill and Usagi [1; 2; 5; 6] notes the solution is relatively insensitive to changes in s and hence these values were rounded in each of the corresponding figures.

For diameter-range $100\mu m - 200\mu m$, shown in Figure 4.2, the experimental values lie between the average, d_{mean}, and maximum, d_{max}, particle diameters. Curves for the matched solution were plotted for a particle diameter of both $153\mu m$ and $200\mu m$ – the former yielding results that closer match the trend of the data; illustrated by Figure 4.5.

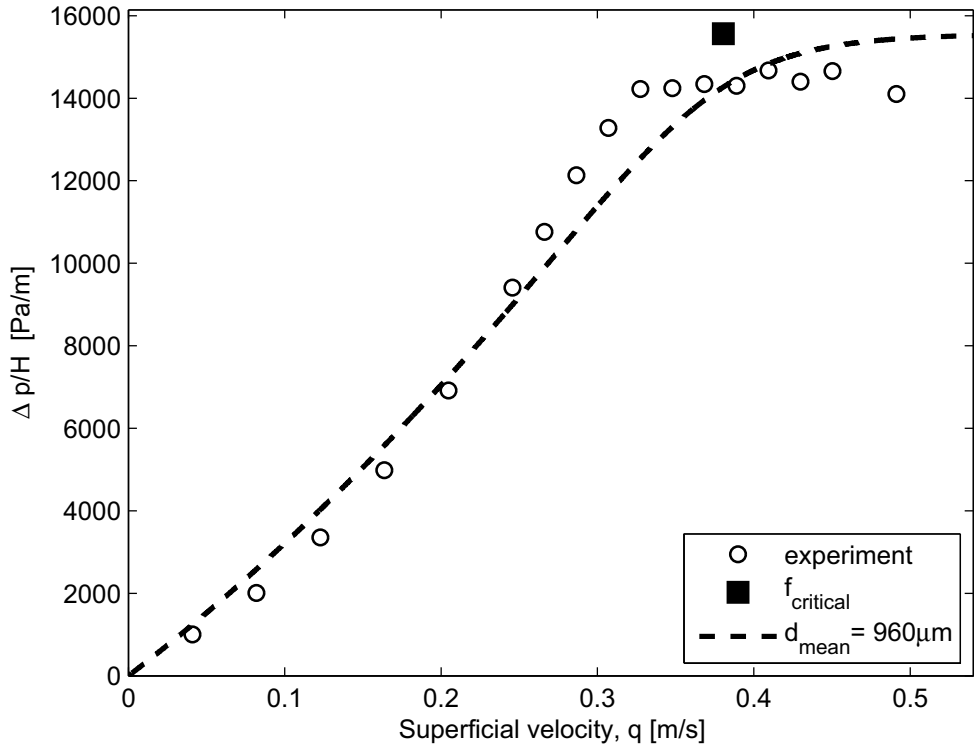

Figure 4.7: Curve-fitting by the method of powered addition of asymptotic solutions as applied to particles in diameter-range $750\mu m - 1000\mu m$. Equation (4.17) represents the functional relation with an s-value of -8 having been used.

In the case of diameter-range $400\mu m - 600\mu m$, the data points were distributed around the asymptote predicted by the upper limit of the range, d_{max}. Use of a particle diameter of $600\mu m$ yields the best graphical results, as shown in Figure 4.6. Examining diameter-range $750\mu m - 1000\mu m$, it was once again difficult to discern the particle di-

ameter to be used by merely regarding data point distribution about the asymptotes. Figure 4.3 shows experimental points crossing the asymptotes for both d_{max} and d_{mean}. Curves were plotted for both solutions; the average diameter of $960\mu m$ more closely followed the trend exhibited by the experimental data. The graphical result of a plot with this diameter is shown in Figure 4.7.

4.2 Non-Newtonian fluid

Digitised data was obtained from the work of Sabiri [38; 39] and Ciceron [40] for the flow of the non-Newtonian fluids glycerol (glycerine) and carboxymethyl cellulose (CMC), a cellulose derivative , through a bed of spherical particles. As in the case of Newtonian flow discussed above in Section 4.1, the bed was contained in a PMMA (poly methyl methacrylate) or perspex cylinder, the interior diameter of which was $90mm$. Two particle sizes were used, the diameters being $2.92mm$ and $5.00mm$ respectively, with the corresponding bed porosities at incipient fluidisation taken as 0.42 and 0.437. The CMC solution of $6g/\ell$ was said to have a consistency index, $K = 0.624Pa.s^n$, behaviour index, $n = 0.7662$, and density of $\rho = 1020.3kg/m^3$. The corresponding parameters for the 75% glycerine solution was taken as $K = 0.025Pa.s^n$, $n = 1$ and $\rho = 1192.5kg/m^3$. These authors consider the latter solution to be an example of non-Newtonian fluid flow, though strictly speaking the use of a behaviour index value, $n = 1$ reverts the power law model for non-Newtonian fluids back to the model for Newtonian fluids.

4.2.1 Asymptotic dependencies

From plots of the digitised data an abrupt transition between the packed- and fluidised bed regimes is evident and hence a shifting exponent larger than unity is expected.

4.2.1.1 The lower asymptote

The assumption is made, as in Section 4.1.2.1, that the unfluidised or packed bed may be viewed as a porous medium consisting of spherical particles. The RUC model of Du Plessis & Woudberg [29; 22; 32] was extended [31] to include non-Newtonian fluids, with the stream-wise pressure gradient expressed as

$$-\frac{dp}{dx} = KF_n q^n, \tag{4.22}$$

where

$$F_n = \frac{2^n(4.47)(1-\varepsilon)^{2/3}}{d_s^{n+1}\left(1-(1-\varepsilon)^{1/3}\right)^n\left(1-(1-\varepsilon)^{2/3}\right)^{n+1}}\left(\frac{2n+1}{n}\right)^n \times\left[1+\frac{(1-(1-\varepsilon)^{2/3})}{12(4.47)\varepsilon}Re_{p_n}\right], \tag{4.23}$$

and

$$Re_{p_n} = \frac{12\rho d^n q^{2-n}}{K}\frac{(1-(1-\varepsilon)^{1/3})}{(1-(1-\varepsilon)^{2/3})^{2-n}}\left(\frac{n}{2(2n+1)}\right)^n. \tag{4.24}$$

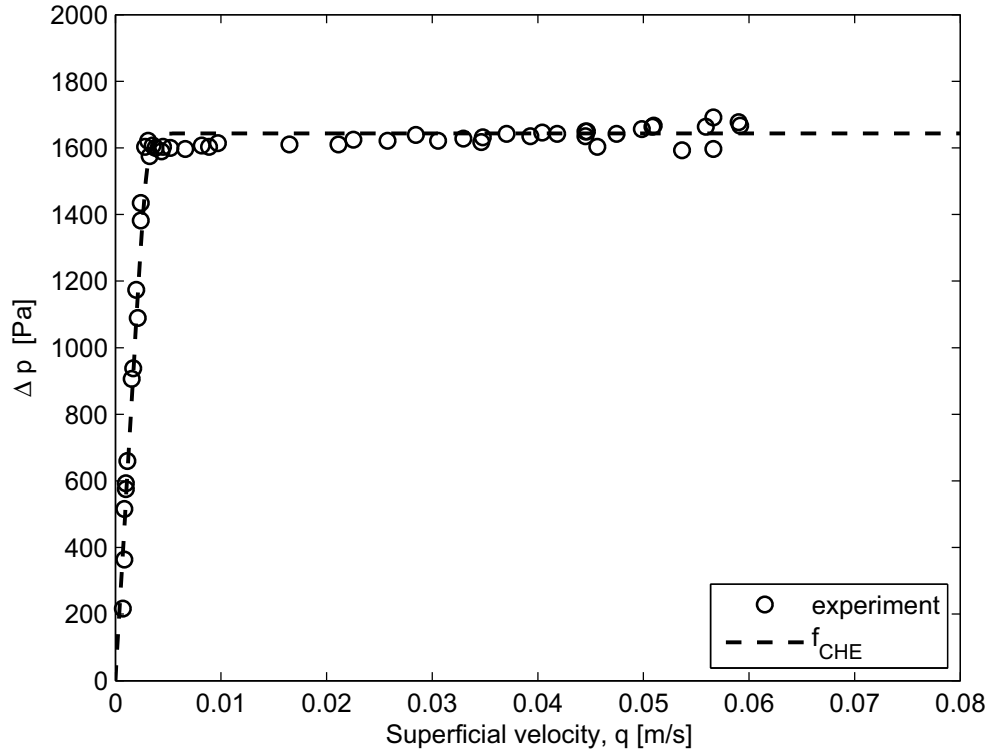

Figure 4.8: Fitting of the matched solution to Sabiri [38; 39] and Ciceron [40]'s data. The bed consisted of particles with diameter 2.92mm and was fluidised with glycerine. An s-value of -10 was used to obtain the fitted curve.

The rational behind the choice of this model to represent the functional dependence of the lower asymptote is similar to that outlined in Section 4.1.2.1.

4.2.1.2 The upper asymptote

As mentioned in Section 4.1.2.2, the pressure drop at incipient fluidisation is sufficient to support the weight of the particles [35; 41], and hence

$$\frac{\Delta p}{H} = (1 - \varepsilon_0)(\rho_s - \rho_f)g. \tag{4.25}$$

with ε_0 the porosity at incipient fluidisation. The relation given by equation (4.25) above will be taken to represent functional dependence at the upper extreme.

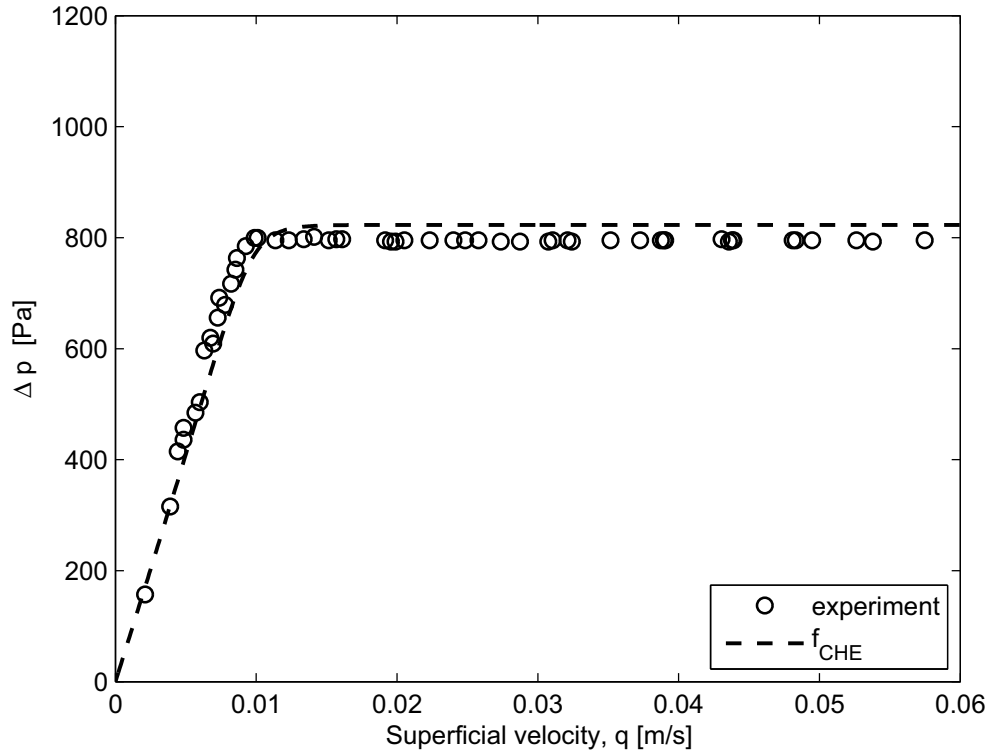

Figure 4.9: Curve-fitting by the method of powered addition of asymptotic solutions as applied to non-Newtonian flow. Equation (4.26) represents the functional relation with an s-value of -10 having been used. The fluid used to fluidise the bed was glycerine; particle diameter $4.99mm$.

4.2.2 Powered addition of the asymptotes

Application of Churchill & Usagi's method of powered addition, outlined in Chapter 1, to the results obtained for the respective dependencies at the extremal values – that

is, combing equations (4.22) and (4.25) and taking the s^{th} order sum of the solutions – produces the desired single measure,

$$\frac{\Delta p}{H} = [[KF_n q^n]^s + [(1-\varepsilon_0)(\rho_s - \rho_f)g]^s]^{1/s}, \tag{4.26}$$

applicable over the entire range of q-values.

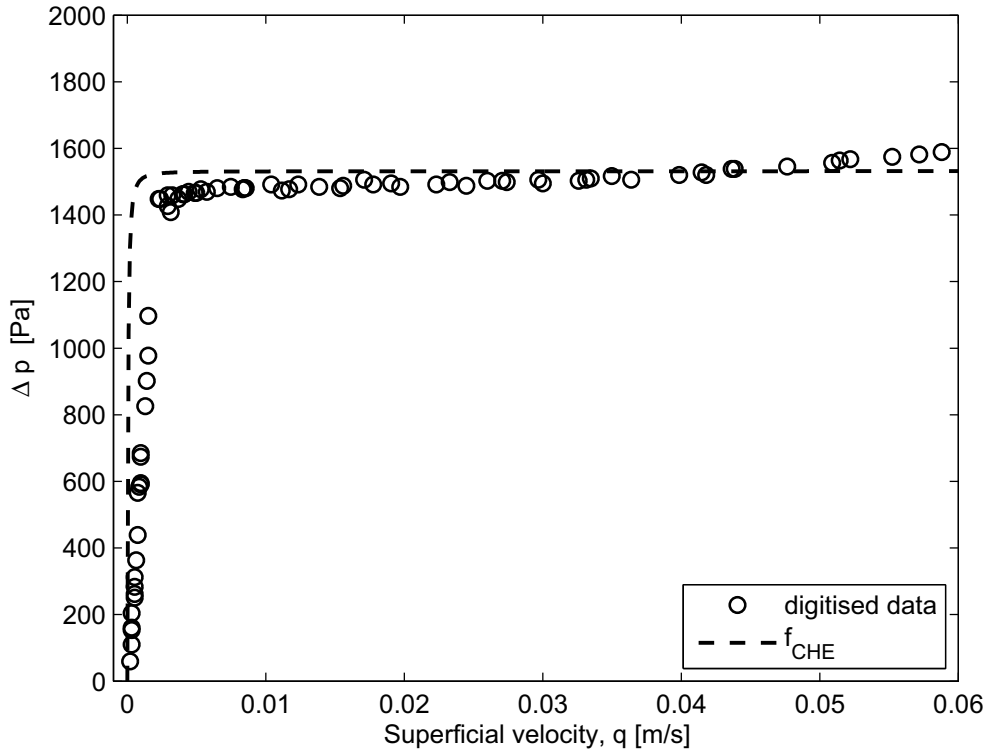

Figure 4.10: Curve-fitting by the method of powered addition of asymptotic solutions as applied to non-Newtonian flow through a bed consisting of spherical particles, diameter 2.92mm. Equation (4.26) represents the functional relation with an s-value of -2 having been used.

4.2.2.1 Critical point and shifting-exponent

Analogous to Section 4.1.3.1, by equating

$$KF_n q^n = (1-\varepsilon_0)(\rho_s - \rho_f)g, \tag{4.27}$$

and isolating the independent variable as,

$$q_c = \left[\frac{(1-\varepsilon_0)(\rho_s - \rho_f)g}{KF_n}\right]^{1/n}, \tag{4.28}$$

the *critical point*, $f\{q_c\}$, of the matching curve where the asymptotic solutions intersect, is obtained. The dependency of this value is thus closely linked to the behaviour index of the particular non-Newtonian fluid under regard.

4.2.3 Correlation of experimental results

For the digitised data of Sabiri [38] and Ciceron [40] the pressure loss over the bed versus the superficial velocity of the traversing non-Newtonian fluid was plotted. The value of the shifting exponent, s, was adjusted by trial-and-error visual evaluation to obtain the graphical representations shown in Figures 4.8 to and 4.11. Figures 4.8 and 4.9 show the results obtained for a bed fluidised with a 75% glycerine solution. The

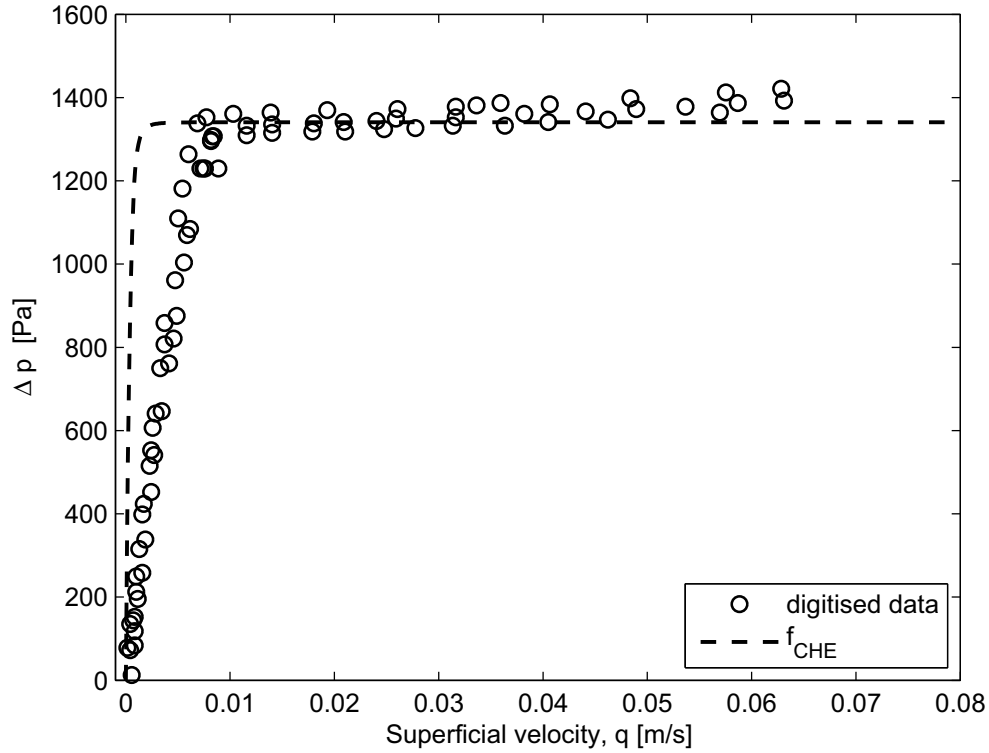

Figure 4.11: Application of the Churchill-Usagi equation to data for a bed of spherical particles, diameter $4.99mm$, fluidised with the non-Newtonian fluid CMC. An s-value of -4 was used in equation (4.26).

expansion of the RUC model to encompass non-Newtonian flow [31] was based on the power law model (or Ostwald de Waele model). The power law model for time-independent, non-Newtonian flow (see Appendix A), given by

$$\tau_{xy} = -K|\dot{\gamma}|^n, \tag{4.29}$$

reverts to the mathematical model for Newtonian flow when $n = 1$. Hence, since a value of unity is assigned to the behaviour index of glycerine, this fluid is strictly speaking not an example of a non-Newtonian substance.

In the work of Sabiri [38] no mention was made of the bed height in the cases where CMC was used as fluidising liquid. Consequently, the uppermost limiting value had to be adjusted accordingly to fit the experimental data. Since the pressure drop in equation (4.25) is linearly related to the height, an incorrect choice of value would only cause a parallel offset and not influence the curvature of the resultant match. In both the cases of glycerine and CMC the data show an abrupt changeover in the transitional areas, which corresponds to the relatively high values obtained for the shifter. As with the Newtonian fluidised bed, studied in Section 4.1, equation (4.26) exhibits a decrease in the dependence of the pressure drop as the superficial velocity increases (for constant n). As anticipated from the discussion in Section 1.2, a negative shifting exponent ensures a satisfactory match.

Chapter 5

Conclusion / Closure

The straightforward addition of the solutions at extremal values to obtain a single relation that holds over the domain of the independent variable, is a practice that has been in use for some time, especially in engineering applications. The method of powered addition, formalised by Churchill & Usagi [1], succeeds, through simple exponentiation of the constituent terms, in adjusting the solution so as to more closely trace the experimental or computational data. The procedure should not be regarded as a trick; rather linear addition of asymptotic models should be regarded as a special case of powered addition when $s = 1$. Prior knowledge of the functional behaviour in at least one of the limits makes the direct application of the proposed method possible. Should, however, only the limiting values be known, but not the functional dependence at either of the extremities, an empirical expression for one or the other limit may be postulated. In cases such as these, a power function is pertinent; its uncomplicated form making it a satisfactory choice in tune with the underlying philosophy of simplicity.

Although the routine has not yet been proven to accurately describe the relative behaviour of the different parameters during a transfer process, it may be argued to be more appropriate, since the rate of change between the two asymptotes can be adjusted to fit experimental readings. For instance, the higher the (absolute) value of the shifter-exponent, s, the more abrupt the changeover between the two asymptotic processes. Furthermore, irrespective of the rate at which the changeover occurs, it will be a smooth transition as is expected for the crossover from one continuum process to another. In the examined cases in this study, and the various examples listed in the literature by Churchill et al. [1; 2; 5; 6; 25; 42; 43], powered addition appears to be favoured over the introduction of *ad hoc* curve-fitting or bridging functions which might introduce unwanted jumps. Thus, although primarily a curve-fitting exercise, this procedure leads to better physical modelling since the only 'tuneable' parameter is

the shifter-exponent, s. Adjusting its value does not change the value of the asymptotic conditions and leaves the double-asymptote character of the transfer process intact.

The main advantages of the method is that a singular functional dependence of the independent variable upon the dependent variable is established over the entire range of the latter. The inherent simplicity of the method suggests that in such a curve-fitting exercise the greater deal of effort should be exerted in determination of the asymptotes, the value of the exponent, s, and possible relation of the latter to some quantifiable parameter.

The sensitivity of the matched curve to changes in the shifter, s, in the vicinity of intersection of the asymptotes, suggests that experiments should be designed so as to focus on this area. More specifically, in performing an experiment it is advantageous to arrange the physical conditions in such a manner that the independent variable is in close proximity of the critical point, x_c. Should the experimental values of the dependent variable at the critical point, $f\{x_c\}$, be known, a good indication of the value of the shifting exponent may be obtained by the logarithmic expression of equation (1.45). It is however important to keep in mind that, since the method is empirical in nature, an exact solution is not obtained and therefore the potential benefit of visual inspection and evaluation on the result should not be disregarded (visual inspection by trial and error adjustment of the correlation between the predictive curve and data points often lead to a better assignment of a value to s). As noted by Churchill & Usagi [1] the matched curve is relatively insensitive to variations in s; the required accuracy being determined by considerations such as the process involved, tunability of other parameters and allowable error-margin.

Appendix A

Fluid classification

In the classification of fluids two different approaches are followed. Hence, the category into which a fluid will fall depends on the criterion being used: either the fluid's reaction to an externally applied pressure, or the response of the fluid due to the application of a shearing force or shear stress, being used as distinguishing factor. The former approach differentiates between *compressible* and *incompressible* fluids, depending on the relation between the pressure and volume of the fluid; the latter is contingent upon the relationship between shear stress and shear rate and leads to the distinction between *Newtonian* (linear relation) and *non-Newtonian* (non-linear relation) fluids [44; 45]. In other words classification is either based on the compressibility or viscosity. Most liquids may be regarded as incompressible [44] (whereas this is not the case for gasses) and accordingly the second approach will be discussed in this section.

Viscosity can be regarded as a fluid's resistance to a shearing force when the fluid is in motion; the nature of the relation between the shear stress and the velocity gradient of the fluid determining into which category the fluid is classified.

A.1 Newtonian flow

For Newtonian fluids the velocity gradient in the direction of flow, dv_x/dy is linearly related to the shear stress, τ_{yx}, by

$$\tau_{yx} = \mu\left(-\frac{dv_x}{dy}\right) = \mu\dot{\gamma}_{yx}, \tag{A.1}$$

where μ denotes the viscosity, a proportionality constant linking the former two factors. In rheology the symbol $\dot{\gamma}$ is frequently used to represent the shear rate of the fluid, with the first subscript referring to the surface on which the stress is acting and

the second to the direction in which it acts, i.e $\dot{\gamma}_{yx}$ is the shear rate of the stress acting on a surface defined by a normal vector in the y-direction and with component in the x-direction (the direction of flow) [44; 45]. The negative sign in equation (A.1) serves to indicate that τ_{yx} opposes the motion of the fluid.

Alternatively, for the case of an incompressible fluid (i.e. ρ constant), equation (A.1) may be written as

$$\tau_{yx} = -\frac{\mu}{\rho}\frac{d}{dy}(\rho v_x) = -\nu\frac{d}{dy}(\rho v_x), \tag{A.2}$$

where ρ represents the fluid's mass density. Now the quantity ρv_x may be thought of as the linear momentum in the x-direction per unit volume of fluid, with τ_{yx} the flux of momentum in the direction of flow, the x-direction [44]. The ratio between viscosity, μ, and mass density, ρ is referred to as the kinematic viscosity and represented by the Greek letter *nu*, ν, in equation (A.2), i.e

$$\nu = \frac{\mu}{\rho}. \tag{A.3}$$

By definition the Newtonian viscosity, μ, is independent of both the shear rate, $\dot{\gamma}_{yx}$, and the shear stress, τ_{yx}, and is dependent only upon the properties of the material, its temperature and pressure. This single constant therefore serves to completely characterize the flow behaviour of the fluid at a given pressure and temperature.

It is important to note that equation (A.1) is for the simple case of unidirectional flow, the velocity vector having only one component directed in the x-direction and being dependent only on the y-coordinate for its magnitude. In the case of three-dimensional flow, the appropriate partial differential equations for each of the nine entries in the shear stress tensor need to be evaluated. This more general case, for the x-plane, of an incompressible fluid is expressed as [17; 44]

$$\tau_{xx} = -2\mu\frac{\partial v_x}{\partial x} + \frac{2}{3}\mu\left(\frac{\partial v_x}{\partial x} + \frac{\partial v_y}{\partial y} + \frac{\partial v_z}{\partial z}\right), \tag{A.4}$$

$$\tau_{xy} = -\mu\left(\frac{\partial v_x}{\partial y} + \frac{\partial v_y}{\partial x}\right), \tag{A.5}$$

$$\tau_{xz} = -\mu\left(\frac{\partial v_x}{\partial z} + \frac{\partial v_z}{\partial x}\right). \tag{A.6}$$

Similar expressions to those of equations (A.4) to (A.6) may be set up for each of the y- and z-planes; as above there will be two shearing components (in the plane being regarded) and one component normal to the plane in each of the cases. Furthermore, it holds for a Newtonian fluid that [17; 44]

$$\tau_{xx} = \tau_{yy} = \tau_{zz} = 0. \tag{A.7}$$

Therefore, the complete definition of a fluid that falls into this category is not only that it has a constant viscosity, but also that the fluid obeys equation (A.7).

A.2 Non-Newtonian flow

A fairly large category of fluids does not obey the Newtonian law of viscosity, in other word the viscosity is not independent of the shear rate and the relation between the shear stress and shear rate is not a linear one. These fluids are classified as non-Newtonian and require, besides viscosity, the measurement of additional parameters (normal stresses, etc.). Broadly these fluids are classified into three general classes as (a) time independent or purely viscous; (b) time dependent; and (c) viscoelastic, though most real materials exhibit a combination of features. Each of these categories may be further subdivided [44; 45]: time independent fluids into shear-thinning or pseudo-plastic fluids, viscoplastic fluids and shear-thickening or dilatant fluids; and time dependent fluids into thixotropic and rheopectic fluids. The classification is by no means sharply defined and merely serves to aid in the mathematical modelling of the fluids. Indeed, rheology – from the Greek word *rheos* meaning stream – is the branch of physics concerned exclusively with the study of the flow of matter and the quantitative and qualitative relationships between deformations and stresses and their derivatives.

The extension of the RUC model to incorporate non-Newtonian fluids [31], used in Section 4.2.1.1, is based on the power law (or Ostwald de Waele) model and will thus be the only model outlined here. In this model, which is effectively a generalised expression used to model Newtonian as well as non-Newtonian fluids, the non-linear relation between the shear stress and shear rate is given by

$$\tau_{yx} = K(\dot{\gamma}_{yx})^n, \tag{A.8}$$

where K, the fluid consistency index, and n, the flow behaviour index, are empirical curve fitting parameters used to characterise the fluid and are constant at a fixed temperature and pressure. The exponent, n, is a measure of how much the fluid deviates from a Newtonian fluid and hence for $n = 1$ equation (A.1) will revert to equation (A.8) with $K = \mu$. Division of the shear stress by the shear rate,

$$\eta = \frac{\tau_{yx}}{\dot{\gamma}_{yx}}, \tag{A.9}$$

gives the so-called apparent viscosity, η, a parameter frequently used in the literature. For values of $n < 1$ the fluid exhibits shear-thinning properties, meaning that the apparent viscosity of the fluid decreases as with an increase in shear rate. The opposite behaviour is observed when $n > 1$ and hence these fluid are known as shear-thickening.

Criticism against the power law is that for zero shear rate the apparent viscosity in equation takes on an infinite value and that for real fluids the exponent, n, is not

constant over the entire range of flow. Another objection is that the consistency index, K, is dependent upon the behaviour index, n, and may thus not be compared unless the latter values are similar. Despite all the critique, the power law model has the advantage of simplicity and is therefore, according to Chhabra [44], one of the models used most widely in literature dealing with process engineering.

Appendix B

Derivation of Slatter Reynolds number

In its most general form, without any simplifications, the Navier-Stokes equation is a complicated, nonlinear partial differential equation used to describe the motion of a fluid substance (as yet, no general solution has been obtained) [14]. During the last part of the 19^{th} century Osborne Reynolds studied these equations governing flow in an attempt to determine when two different flow situations may be deemed similar.

Two instances of flow are said to be dynamically similar if (a) their corresponding linear dimensions have a constant ratio (that is, they are geometrically similar); and (b) pressures at corresponding points have a constant ratio (geometrically similar streamlines)[14]. Reynolds considered geometrically similar flow situations and came to the conclusion that these flows would be dynamically similar, providing the differential equations describing them were identical. He found that if the dimensionless group $\rho vl/\mu$ was the same, this criterion was met (here, ρ is the mass density, v is a characteristic velocity, l a characteristic length, and μ the viscosity). Thus, the parameter

$$Re = \frac{\rho v l}{\mu} \quad , \tag{B.1}$$

has taken his name, Reynolds number, and may be viewed as the ratio of the inertial forces to viscous forces [14; 46; 16], i.e.

$$Re \quad \propto \quad \frac{\text{inertial forces}}{\text{viscous forces}} \quad . \tag{B.2}$$

Many variations on the above definition of the Reynolds number for straight, round tubes exist; the characteristic quantities being chosen so as to be specific to the case where it is being applied. The Slatter Reynolds number, Re_3, is one such variant based on the yield pseudo-plastic model. It starts from the assumption that, in the presence of a yield stress, the core of the fluid moves as a solid, unsheared plug [47; 15; 10] resulting in annular flow.

The fact that velocity components perpendicular to a surface cannot exist in the region of the surface, accounts for the existence of a laminar sub-layer immediately adjacent to the solid surface. It also implies that solid boundaries suppress turbulence. Slatter [47; 15] notes that the definition of yield stress states by implication that if the shear stresses are insufficient to overcome the former, the material will behave as a solid. Such is the case in the unsheared core of plug flow – a coaxial solid plug existing

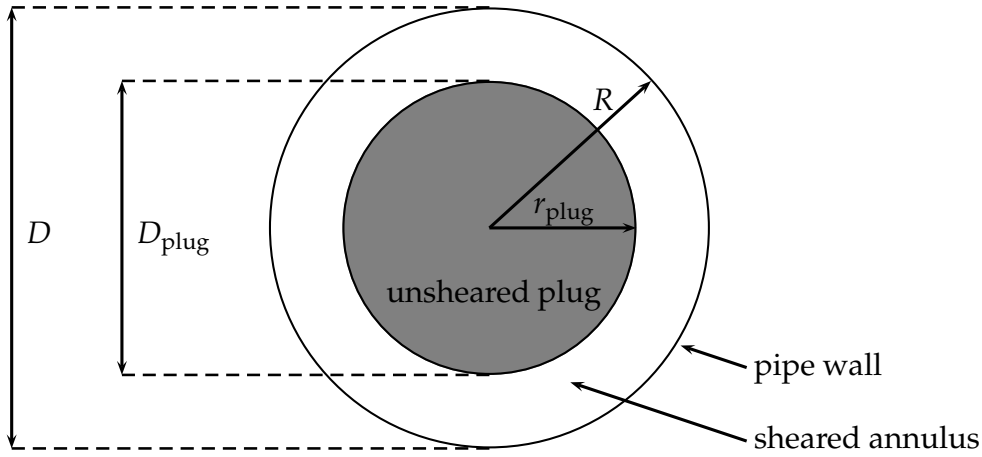

Figure B.1: Schematic cross-section of pipe showing unsheared plug geometry.

in the centre of the pipe with flow in an annular region – a representation of which is shown in Figure B.1. He argues that this plug may be regarded as a solid boundary and that it will affect the stability of the laminar flow in the surrounding annulus [47; 15; 10]. Hence, the flow represented by that of the plug must be subtracted since it is no longer being treated as part of the fluid flow. The velocity profile of annular flow also differs from that of plane Poiseuille flow (the flow of an incompressible Newtonian fluid in a tube), as illustrated in Figure B.2.

The constitutive rheological equation for the yield pseudo-plastic model is formulated as [47; 15]

$$\tau = \tau_y + K\left(-\frac{dv_z}{dr}\right)^n = \tau_y + K(\dot{\gamma}_{rz})^n \quad , \tag{B.3}$$

with τ_y denoting the yield stress, K the fluid consistency index and n the flow behaviour index. The shear rate, $(-dv_z/dr) = \dot{\gamma}_{rz}$, may be expressed as the velocity gradient in the direction perpendicular to that of the shear force (cf. viscous stress dyadic in equation (B.6)). Setting $n = 1$ in equation (B.3) yields the so-called Bingham-plastic model, while $\tau_y = 0$ results in it reverting back to that for power-law fluids.

Cauchy's differential equation for the movement of any continuum, which holds at

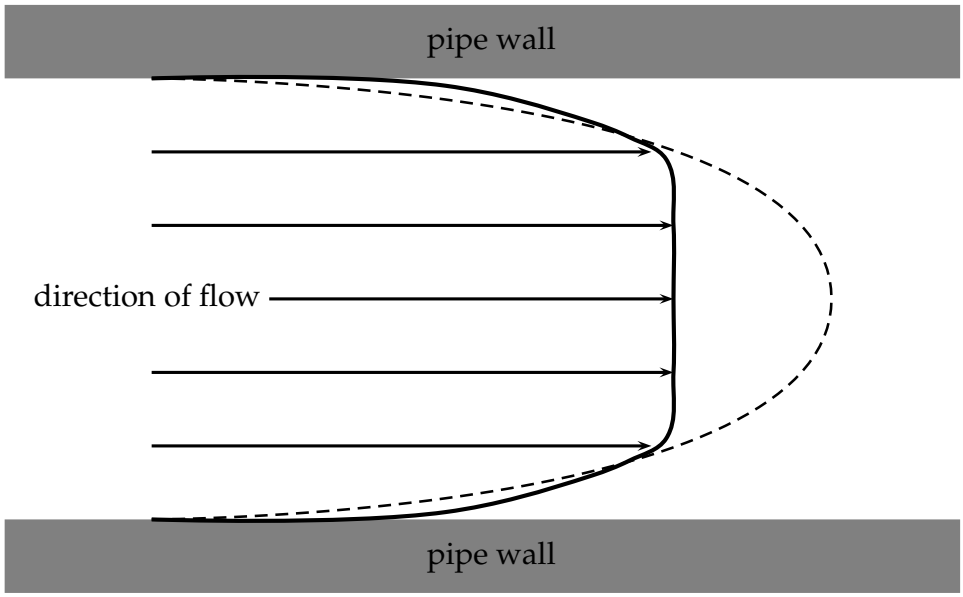

Figure B.2: Schematic representation of velocity profile for plug flow (solid line). The qualitative velocity profile of an incompressible Newtonian fluid is shown in a dashed line for comparison.

any arbitrary point within the continuum, states

$$\rho \frac{D\underline{v}}{Dt} = \rho \underline{f}_b + \nabla \cdot \underline{\underline{\sigma}} \quad , \tag{B.4}$$

where ρ denotes the density, $\underline{v}$ the velocity, $\underline{f}_b$ the body forces and $\underline{\underline{\sigma}}$ the stress tensor. Since the pressure in a continuum with fluid properties is linked to the internal surface forces, there should be a relation between the pressure and the stress tensor. This is indeed the case and the stress tensor may be written as

$$\underline{\underline{\sigma}} = -p\underline{\underline{1}} + \underline{\underline{\tau}}(\underline{v}) \quad , \tag{B.5}$$

with p the pressure and $\underline{\underline{\tau}}$ the so-called viscous stress dyadic, represented in its matrix form for cylindrical coordinates as

$$\underline{\underline{\tau}} = \begin{bmatrix} \tau_{rr} & \tau_{r\theta} & \tau_{rz} \\ \tau_{\theta r} & \tau_{\theta\theta} & \tau_{\theta z} \\ \tau_{zr} & \tau_{z\theta} & \tau_{zz} \end{bmatrix} . \tag{B.6}$$

According to convention the first subscript refers to the face upon which the stress is acting and the second to the direction in which it acts (*first face, second stress*). In other words the entry τ_{rz} corresponds to the stress acting on a surface defined by a normal vector in the r-direction and with component in the z-direction (the direction of flow as per Figure B.3).

Equation (B.4) may now, with the aid of equation (B.5), be rewritten as

$$\rho \frac{D\underline{v}}{Dt} = \rho \underline{f}_b - \nabla p + \nabla \cdot \underline{\underline{\tau}} \quad . \tag{B.7}$$

Once the flow has developed fully, there is no more acceleration of fluid particles. Hence the velocity profile is constant, no longer time dependent and $\underline{v} = v\{r\}\underline{k}$. This being the case, one may then set the left-hand side of equation (B.7) equal to zero, since

$$\frac{D\underline{v}}{Dt} = \frac{\partial \underline{v}}{\partial t} + \underline{v} \cdot \nabla \underline{v} = \frac{\partial \underline{v}}{\partial t} + v_r \frac{\partial \underline{v}}{\partial r} + \frac{v_\theta}{r} \frac{\partial \underline{v}}{\partial \theta} + v_z \frac{\partial \underline{v}}{\partial z} \quad , \tag{B.8}$$

where

$$v_r = \frac{\partial \underline{v}}{\partial \theta} = \frac{\partial \underline{v}}{\partial z} = 0 \quad , \tag{B.9}$$

and $\partial \underline{v}/\partial t = 0$ (no acceleration). If it is further assumed that the influence of gravity upon the flow is negligible (or has reached an equilibrium at fully developed flow) it implies that equation (B.7) reduces to

$$\nabla p = \nabla \cdot \underline{\underline{\tau}} \quad . \tag{B.10}$$

However, a pressure gradient only exists in the direction of flow. Using a cylindrical coordinate system with the z-direction orientated along the axis of the pipe, this means that

$$-\frac{\partial p}{\partial z}\,\underline{k} = -\frac{dp}{dz}\,\underline{k} = \nabla \cdot \underline{\underline{\tau}} \quad , \tag{B.11}$$

but since $\partial p/\partial z$ is a constant for fully developed flow, equation (B.11) may be written as

$$c\,\underline{k} = \nabla \cdot \underline{\underline{\tau}} \quad , \tag{B.12}$$

where c is a constant value.

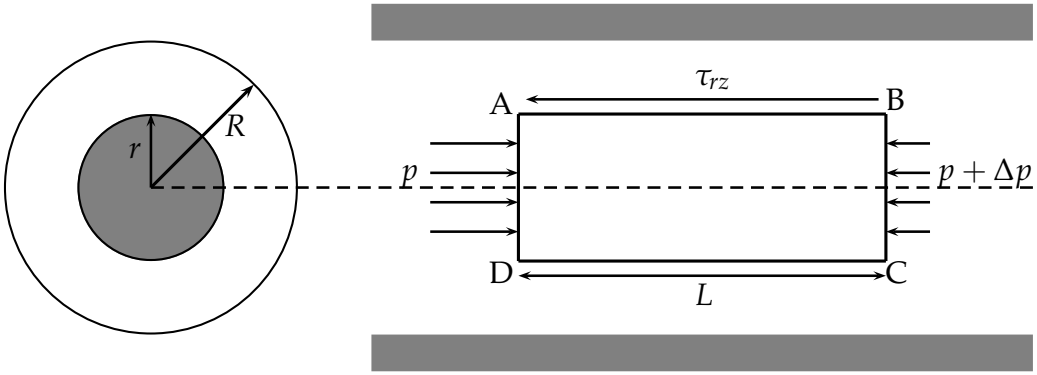

Figure B.3: Schematic representation of flow in a tube to show influence of shear stress. The fluid flow is from left to right.

Flow is caused by a pressure difference across the ends of the pipe. Once the flow has fully developed the radial velocity is zero and the fluid is flowing at a steady rate, in other words a fixed pressure gradient exists between any two reference points of the pipe. (See Figure B.3 illustrating the conditions present during fully developed, steady flow of an incompressible fluid in a pipe of radius R).

Regarding an arbitrary fluid element, $ABCD$, as per Figure B.3, the linear momentum balance (which is in the direction of flow, i.e. the z-direction) may be written as [44]

$$p(\pi r^2) - (p + \Delta p)(\pi r^2) = \tau_{rz}(2\pi r L) \quad , \tag{B.13}$$

with r and L as indicated. Rearranging this yields,

$$\tau_{rz}(r) = \left(-\frac{\Delta p}{L}\right)\frac{r}{2} = \left(-\frac{dp}{dz}\right)\frac{r}{2} = c\,\frac{r}{2} \quad . \tag{B.14}$$

Thus the shear stress varies linearly over the pipe or tube's cross-section, with the maximal value obtained at the wall and no shear stress at the axis [44]. What is important to note is that equation (B.13) is based only on the balancing of forces and that no assumptions have been made regarding fluid type or flow pattern. Hence it is applicable to laminar as well as turbulent flow, providing that the fluid is incompressible and the flow is steady and fully developed [44]. Even in the presence of a yield stress, this statement would still be true since, once the flow has developed fully, the linear momentum balance should still hold. The plug or unsheared core, although regarded as a solid boundary, moves along with the fluid and thus the flow in the annular region surrounding it may be considered as a special instance of plane Couette-Poiseuille flow (the resulting velocity profile, as previously mentioned, is shown in Figure B.2).

Letting τ_0 denote the shear stress at the pipe wall, i.e.

$$\tau_{rz}(R) = \tau_0 \quad , \tag{B.15}$$

equation (B.14) may be re-written as

$$\tau_{rz}(r) = \frac{\tau_0}{R} r \quad , \tag{B.16}$$

Rearranging equation (B.3) as

$$-\left(\frac{\tau_{rz}(r) - \tau_y}{K}\right)^{1/n} = \frac{dv_z}{dr} \quad , \tag{B.17}$$

it may now be integrated as follows

$$\begin{aligned}
\int_{v_z(r)}^{v_z(R)} dv_z &= -\left(\frac{1}{K}\right)^{1/n} \int_r^R [\tau_{rz}(r) - \tau_y]^{1/n} dr \\
\Rightarrow v_z(R) - v_z(r) &= -\left(\frac{1}{K}\right)^{1/n} \int_r^R \left[\frac{\tau_0}{R} r - \tau_y\right]^{1/n} dr \\
0 - v_z(r) &= -\left(\frac{1}{K}\right)^{1/n} \left[\frac{\left(\frac{\tau_0}{R} r - \tau_y\right)^{1+1/n}}{1 + 1/n} \frac{R}{\tau_0}\right]_r^R \\
v_z(r) &= \frac{n}{n+1}\frac{R}{\tau_0}\left(\frac{1}{K}\right)^{1/n} \left[(\tau_0 - \tau_y)^{(n+1)/n} - \left(\frac{\tau_0}{R} r - \tau_y\right)^{(n+1)/n}\right] \\
&= \frac{n}{n+1}\frac{R}{\tau_0}\left(\frac{1}{K}\right)^{1/n} \left[(\tau_0 - \tau_y)^{(n+1)/n} - (\tau_{rz} - \tau_y)^{(n+1)/n}\right]
\end{aligned} \tag{B.18}$$

Since the plug moves along with the fluid, yet does not shear (i.e. behaves as a solid), it implies that by setting $\tau_{rz} = \tau_y$ in equation (B.18) the velocity of the plug may be obtained as

$$v_{\text{plug}} = \frac{n}{n+1}\frac{R}{\tau_0}\left(\frac{1}{K}\right)^{1/n}(\tau_0 - \tau_y)^{(n+1)/n} \quad . \tag{B.19}$$

By the same reasoning as above, it follows from equation (B.16) that for $\tau_{rz} = \tau_y$, the radius of the plug is determined as

$$r_{\text{plug}} = \frac{\tau_y}{\tau_0}R \quad , \tag{B.20}$$

and the area of the annulus by

$$A_{\text{ann}} = \pi(R^2 - r_{\text{plug}}^2) \quad . \tag{B.21}$$

The sheared diameter, D_{shear}, as indicated in Figure B.1, may be calculated from

$$D_{\text{shear}} = D - D_{\text{plug}} \quad , \tag{B.22}$$

and

$$D_{\text{plug}} = 2r_{\text{plug}} \quad . \tag{B.23}$$

As mentioned earlier the flow represented by the plug needs to be subtracted since it is treated as a solid body and doesn't form part of the fluid flow. The flux through the annular part of the pipe is given by

$$Q_{\text{ann}} = Q - Q_{\text{plug}} \quad , \tag{B.24}$$

with

$$Q_{\text{plug}} = v_{\text{plug}}A_{\text{plug}} \quad , \tag{B.25}$$

where Q denotes the flux indicated by the respective subscripts and A the cross-sectional area. The corrected mean velocity in the annulus is thus obtained,

$$\overline{v}_{\text{ann}} = \frac{Q_{\text{ann}}}{A_{\text{ann}}} \quad . \tag{B.26}$$

Returning to the fundamental assumption of equation (B.2) where, according to Massey [16],

$$\text{inertial force} \quad \alpha \quad \rho l^2 v^2 \quad , \tag{B.27}$$

and

$$\text{viscous force} \quad \alpha \quad l^2\tau_{\text{visc}} \quad , \tag{B.28}$$

with τ_{visc} the representative viscous shear stress. The constitutive rheological equation – here, the yield pseudo-plastic model – for the fluid being considered relates the viscous stress to the shear rate. Slatter [47; 15; 48] notes that the so-called bulk shear

rate, $8\overline{v}/D$, has successfully been used in other rheological formulations and proposes its use as representative shear rate. Its use yields

$$\tau_{\text{visc}} = \tau_y + K\left(\frac{8\overline{v}}{D}\right)^n \quad , \tag{B.29}$$

as representative shear rate. Since the shearing of the fluid only takes place in the annular region surrounding the plug, taking the sheared diameter, D_{shear}, as per equation (B.22), as the characteristic length is preferable. The same reasoning leads to the choice of the velocity in the annulus, $\overline{v}_{\text{ann}}$, as characteristic velocity. Substitution of these parameters into equation (B.29) together with relations (B.27) and (B.28) produces

$$Re \quad \propto \quad \frac{\rho\overline{v}_{\text{ann}}^2}{\tau_y + K\left(\frac{8\overline{v}_{\text{ann}}}{D_{\text{shear}}}\right)^n} \quad . \tag{B.30}$$

Only the choice of a proportionality constant remains. The choice should result in the newly defined relation reverting back to standard form under Newtonian conditions. In other words setting $\tau_y = 0$, $K = \mu$ and $n = 1$ in equation (B.30) should reduce it to equation (B.1). This is achieved by selecting the value 8, whence

$$Re_3 = \frac{8\rho\overline{v}_{\text{ann}}^2}{\tau_y + K\left(\frac{8\overline{v}_{\text{ann}}}{D_{\text{shear}}}\right)^n} \quad , \tag{B.31}$$

is obtained; the so-called Slatter Reynolds number.

Appendix C

Plots with Mbiya's data sets

The following plots are based on the data sets generated by Mbiya [9] for pipes with varying diameters and at pre-selected opening values – Figures C.1 to C.4 are for a pipe with internal diameter of 40mm; Figures C.5 to C.8 for 50mm; Figures C.9 to C.12 for 65mm; Figures C.13 to C.16 for 80mm; and Figures C.17 to C.20 for 100mm. In each of the representations (bottom) two matched solutions have been plotted: $s = 0.4$ and $s = 1.4$ in a solid and dashed line respectively.

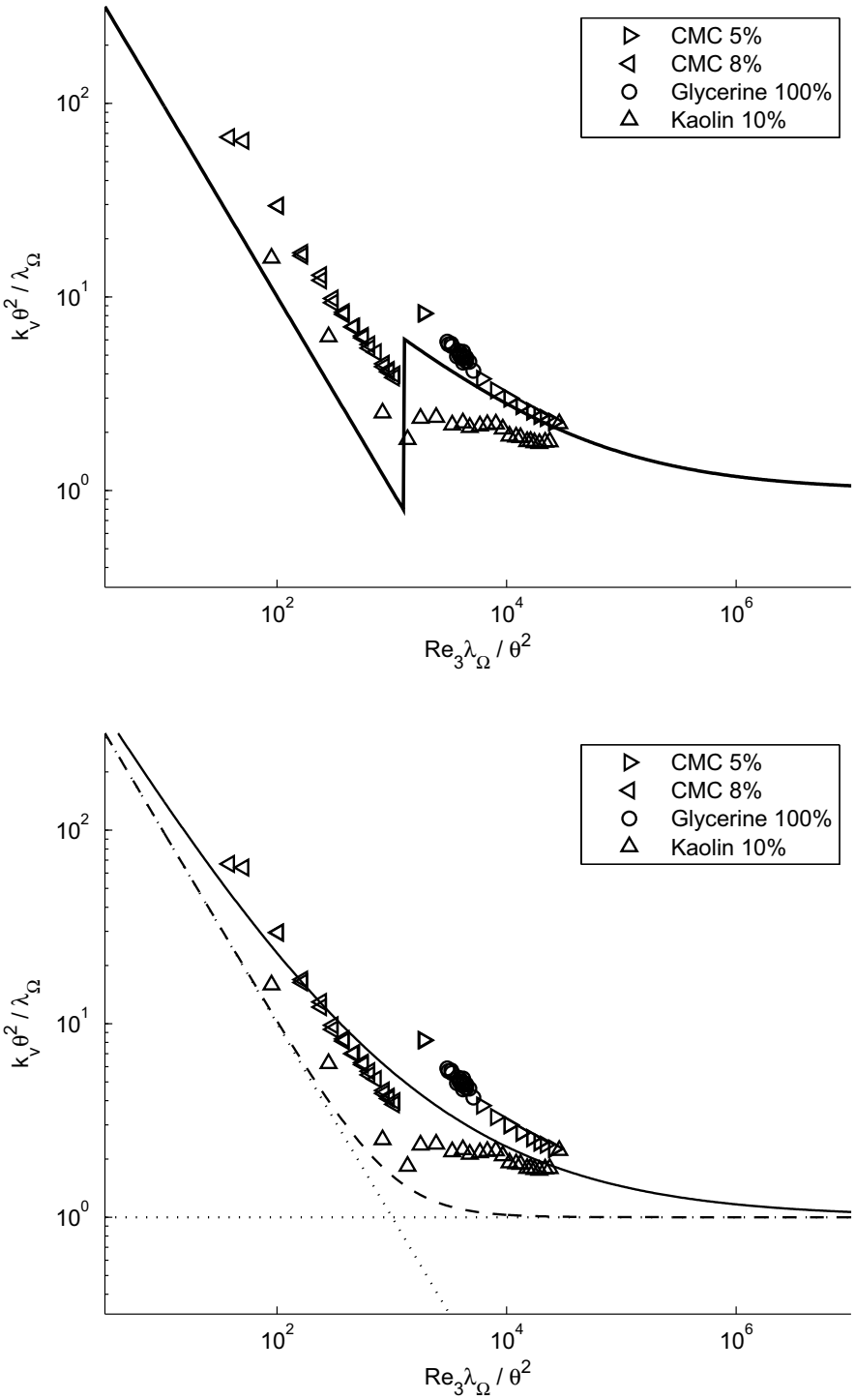

Figure C.1: Internal pipe diameter: 40mm. Valve opening: 25%. Mbiya's two-constant model (top), powered addition (bottom).

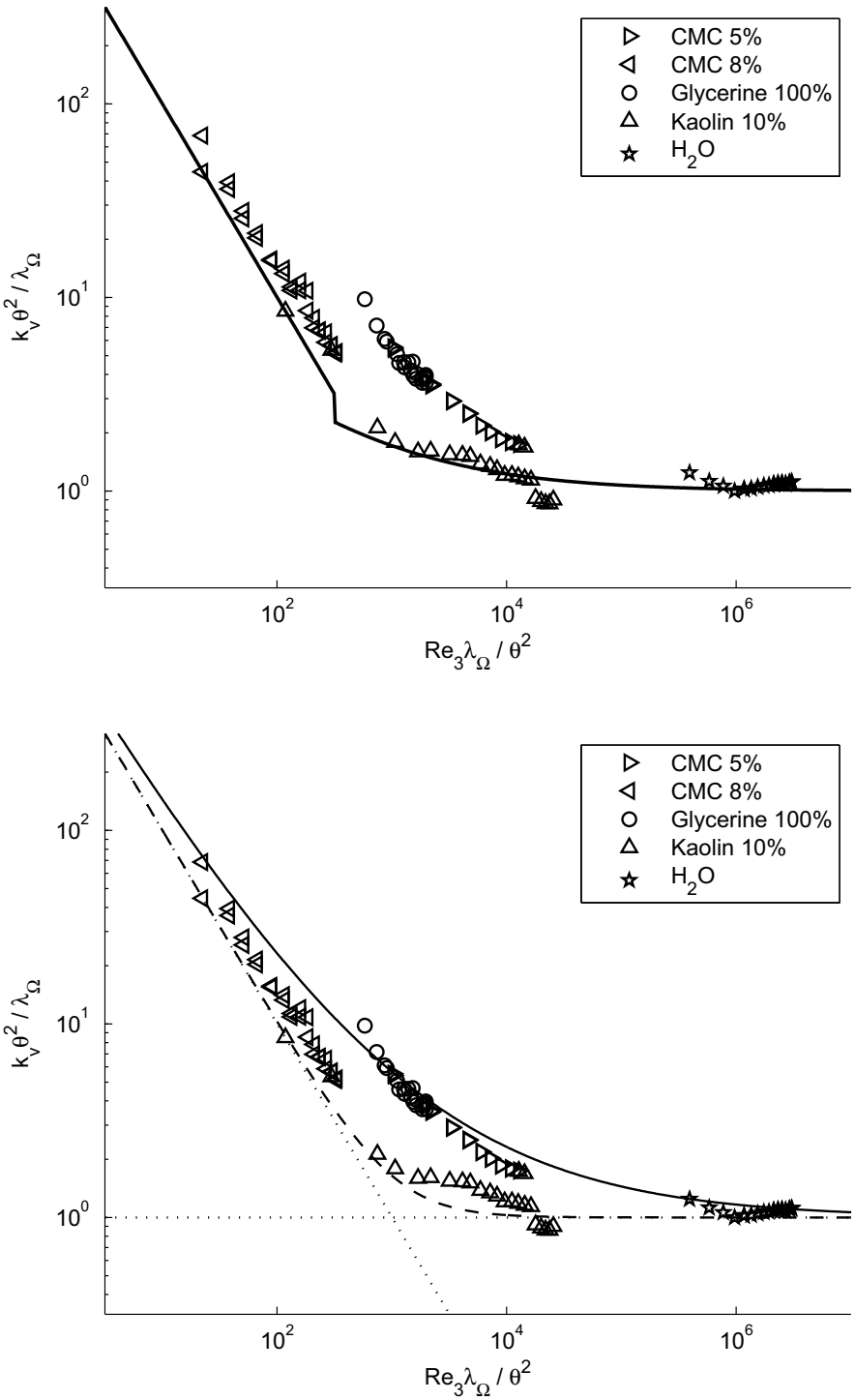

Figure C.2: Internal pipe diameter: 40mm. Valve opening: 50%. Mbiya's two-constant model (top), powered addition (bottom).

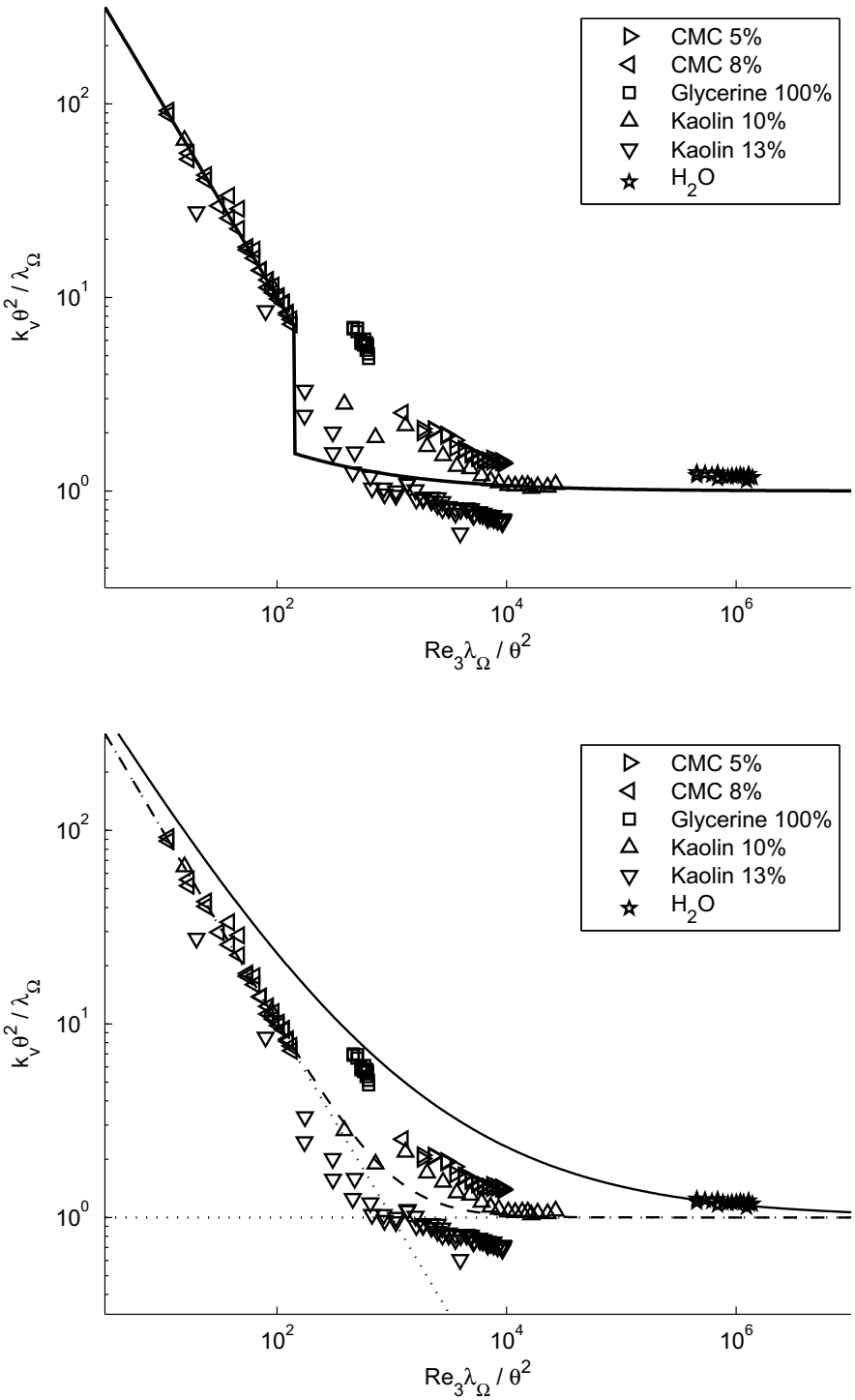

Figure C.3: Internal pipe diameter: 40*mm*. Valve opening: 75%. Mbiya's two-constant model (top), powered addition (bottom).

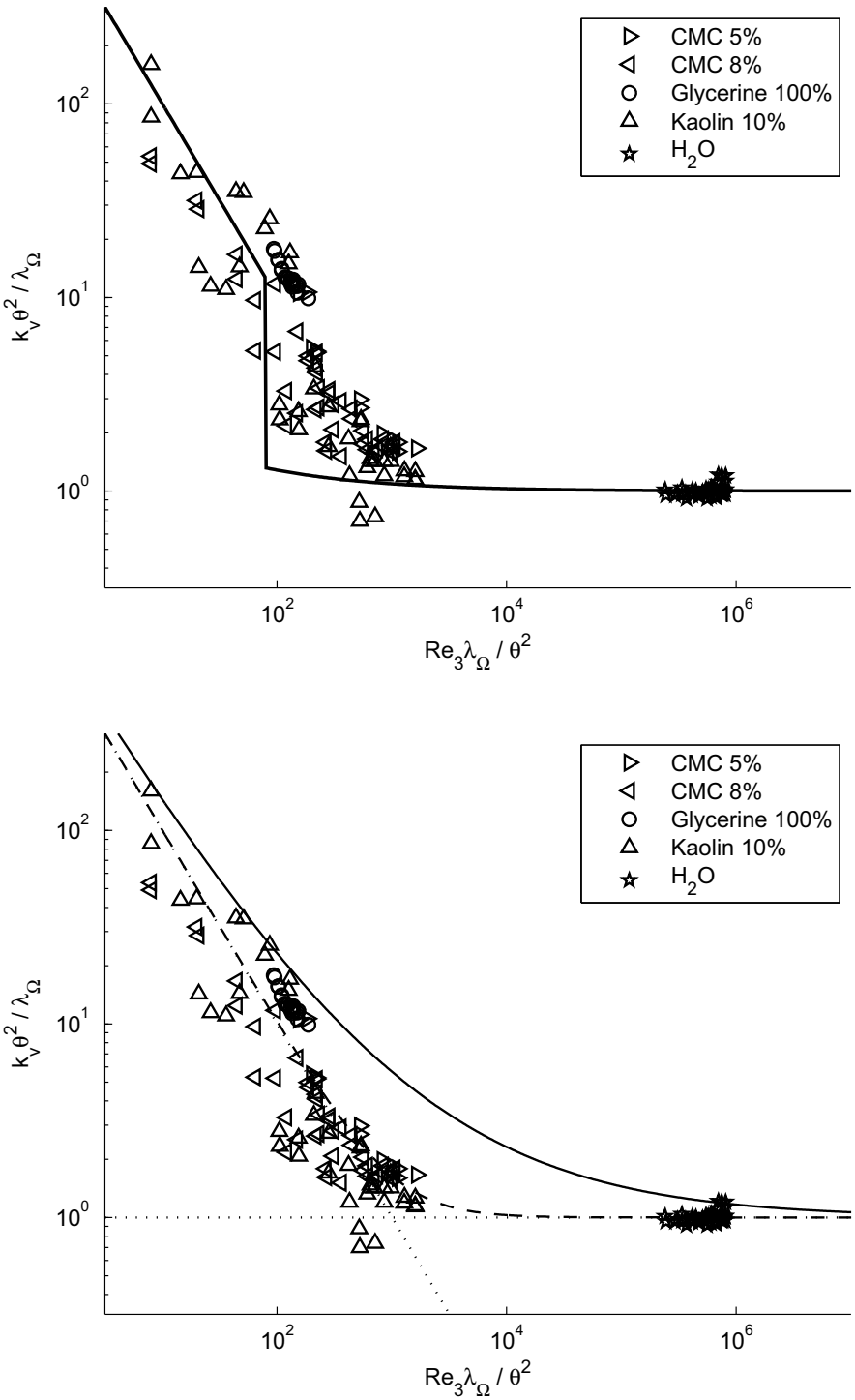

Figure C.4: Internal pipe diameter: 40mm. Valve opening: 100%. Mbiya's two-constant model (top), powered addition (bottom).

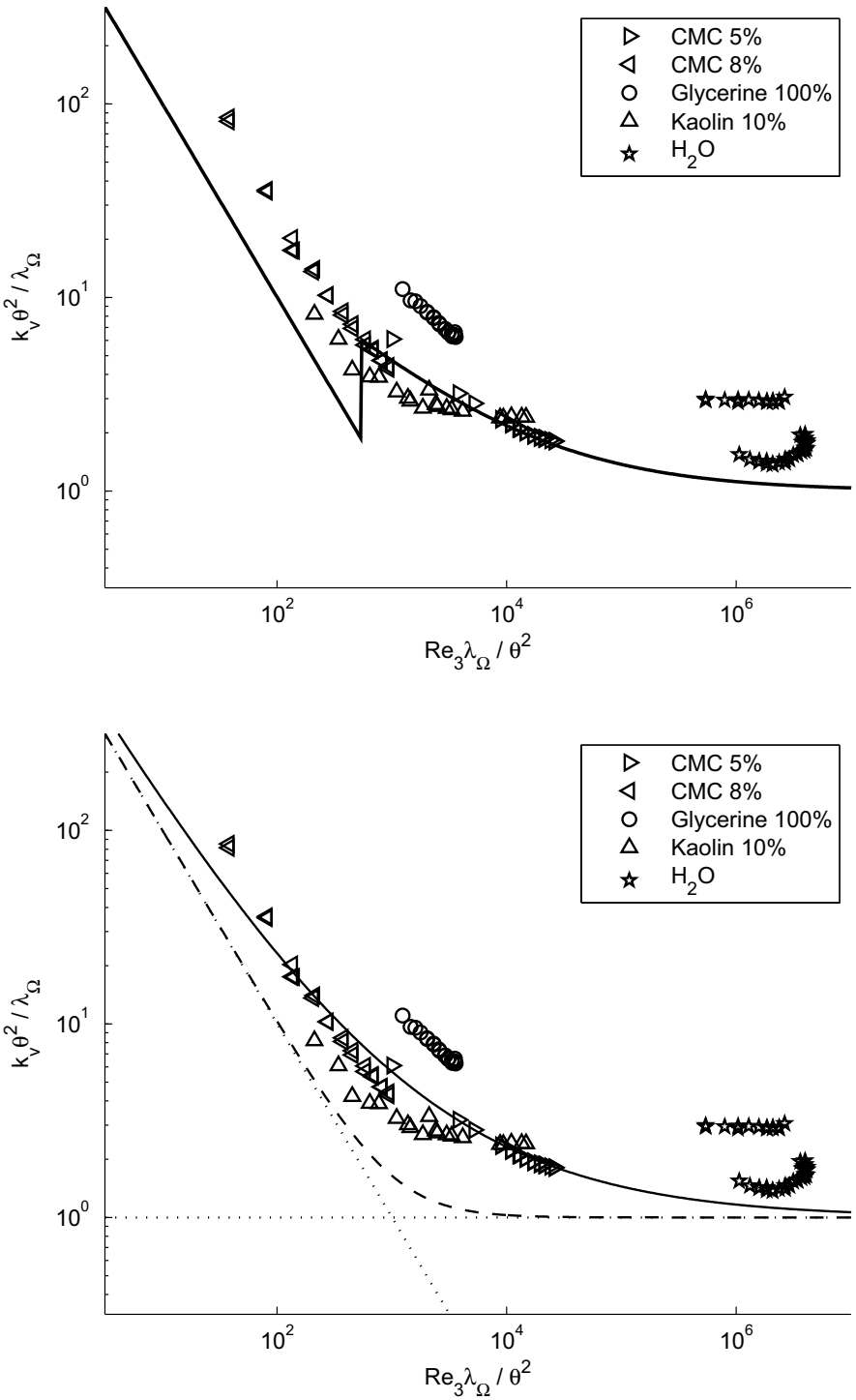

Figure C.5: Internal pipe diameter: 50mm. Valve opening: 25%. Mbiya's two-constant model (top), powered addition (bottom).

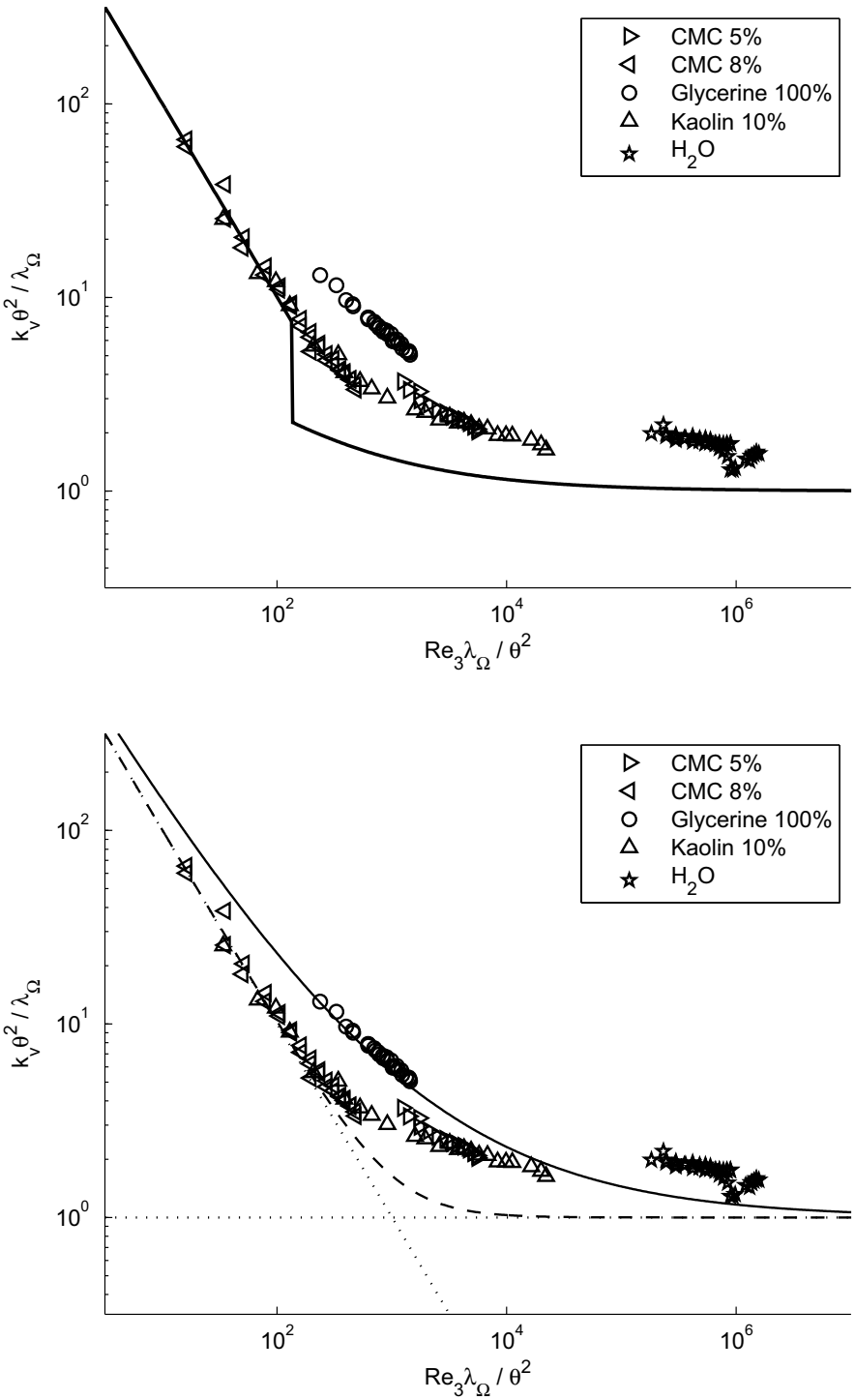

Figure C.6: Internal pipe diameter: 50mm. Valve opening: 50%. Mbiya's two-constant model (top), powered addition (bottom).

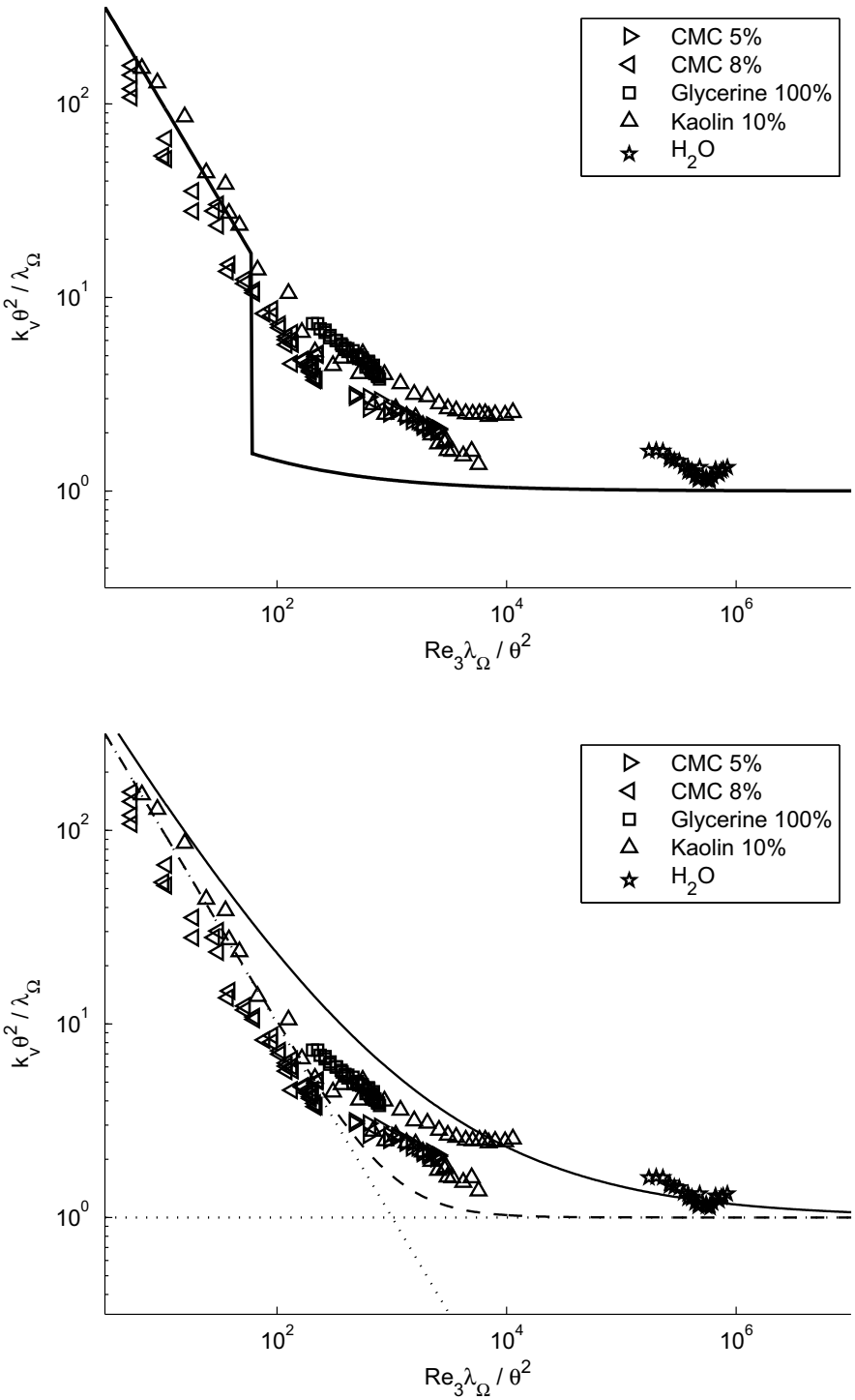

Figure C.7: Internal pipe diameter: 50mm. Valve opening: 75%. Mbiya's two-constant model (top), powered addition (bottom).

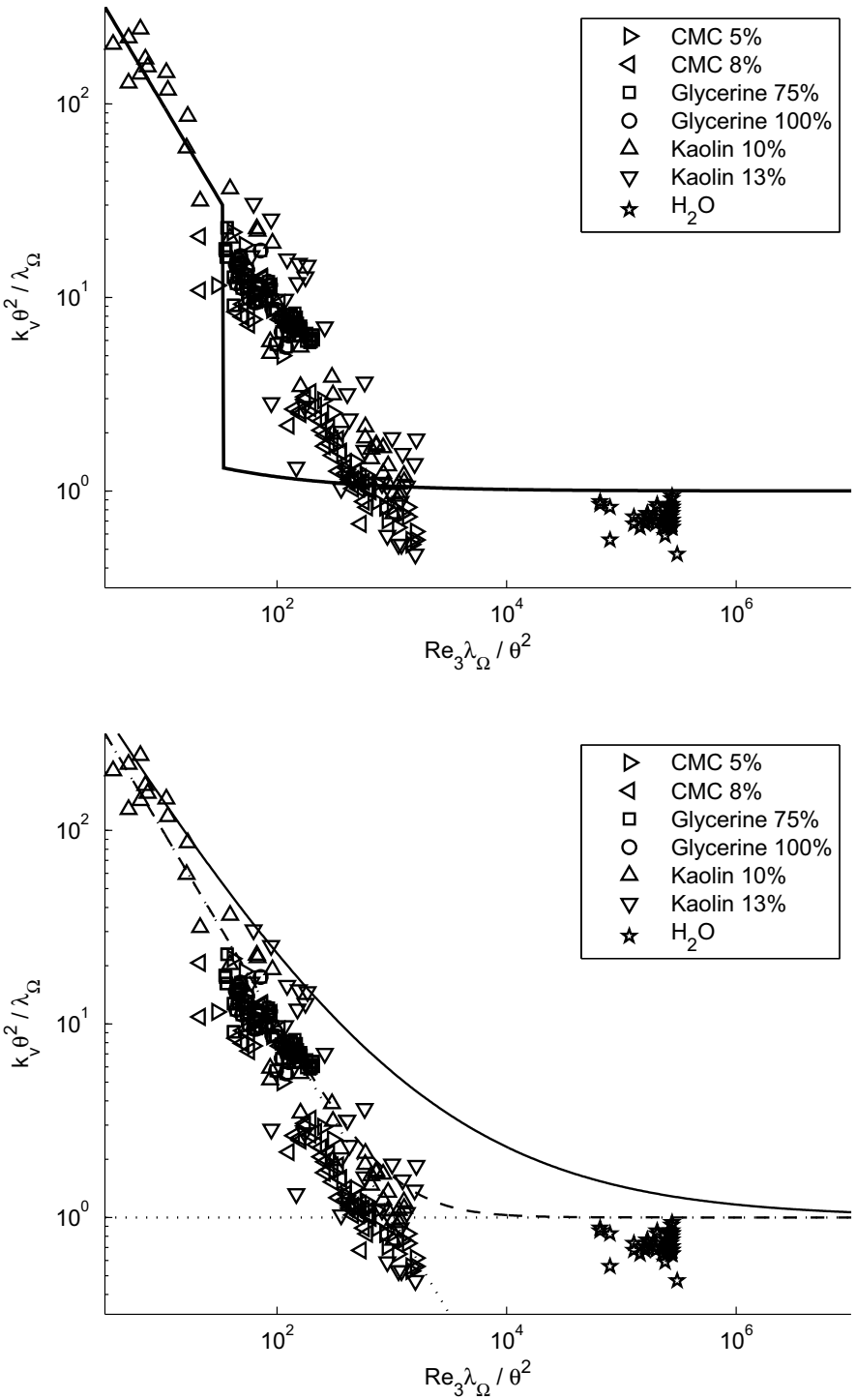

Figure C.8: Internal pipe diameter: 50mm. Valve opening: 100%. Mbiya's two-constant model (top), powered addition (bottom).

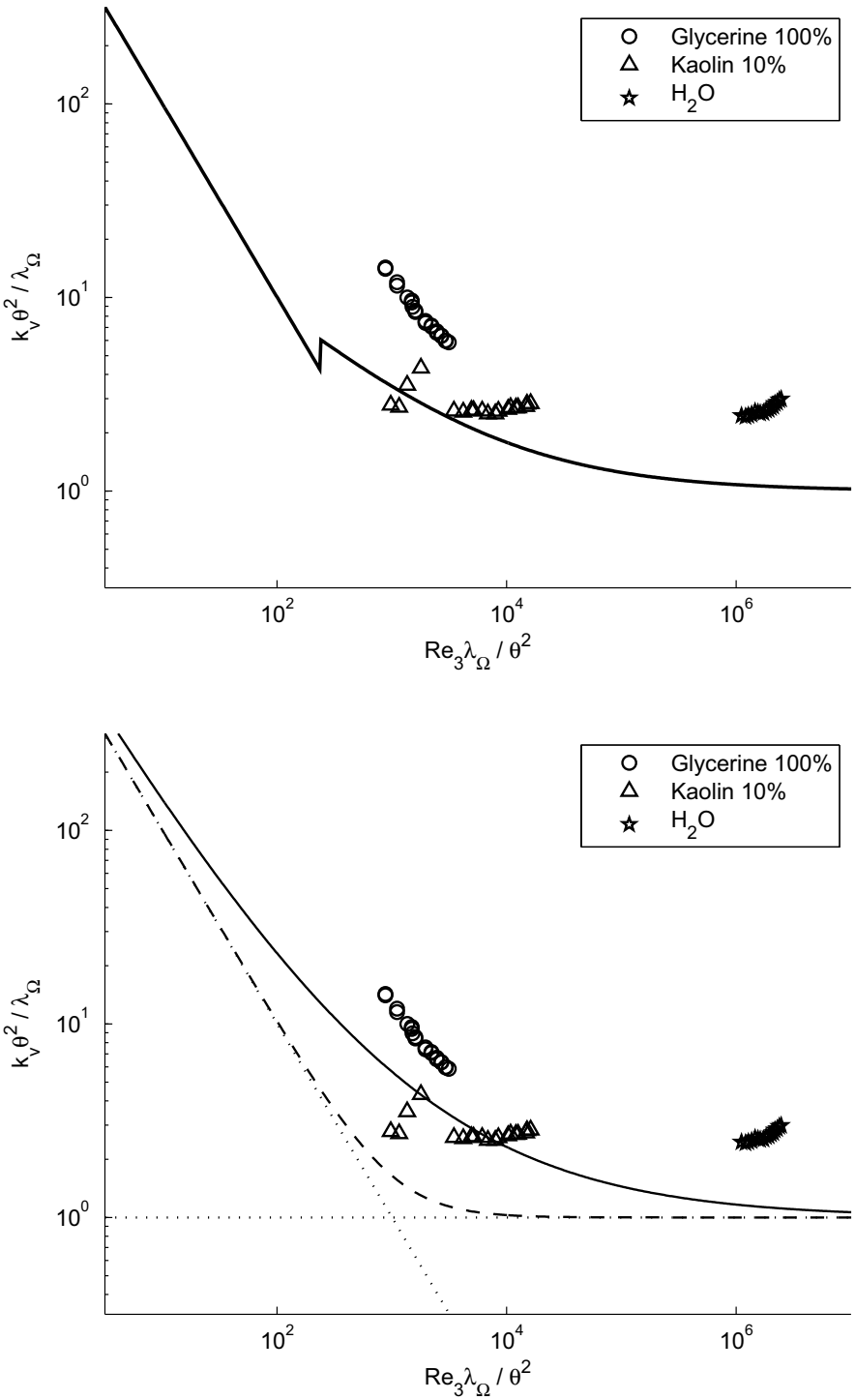

Figure C.9: Internal pipe diameter: 65mm. Valve opening: 25%. Mbiya's two-constant model (top), powered addition (bottom).

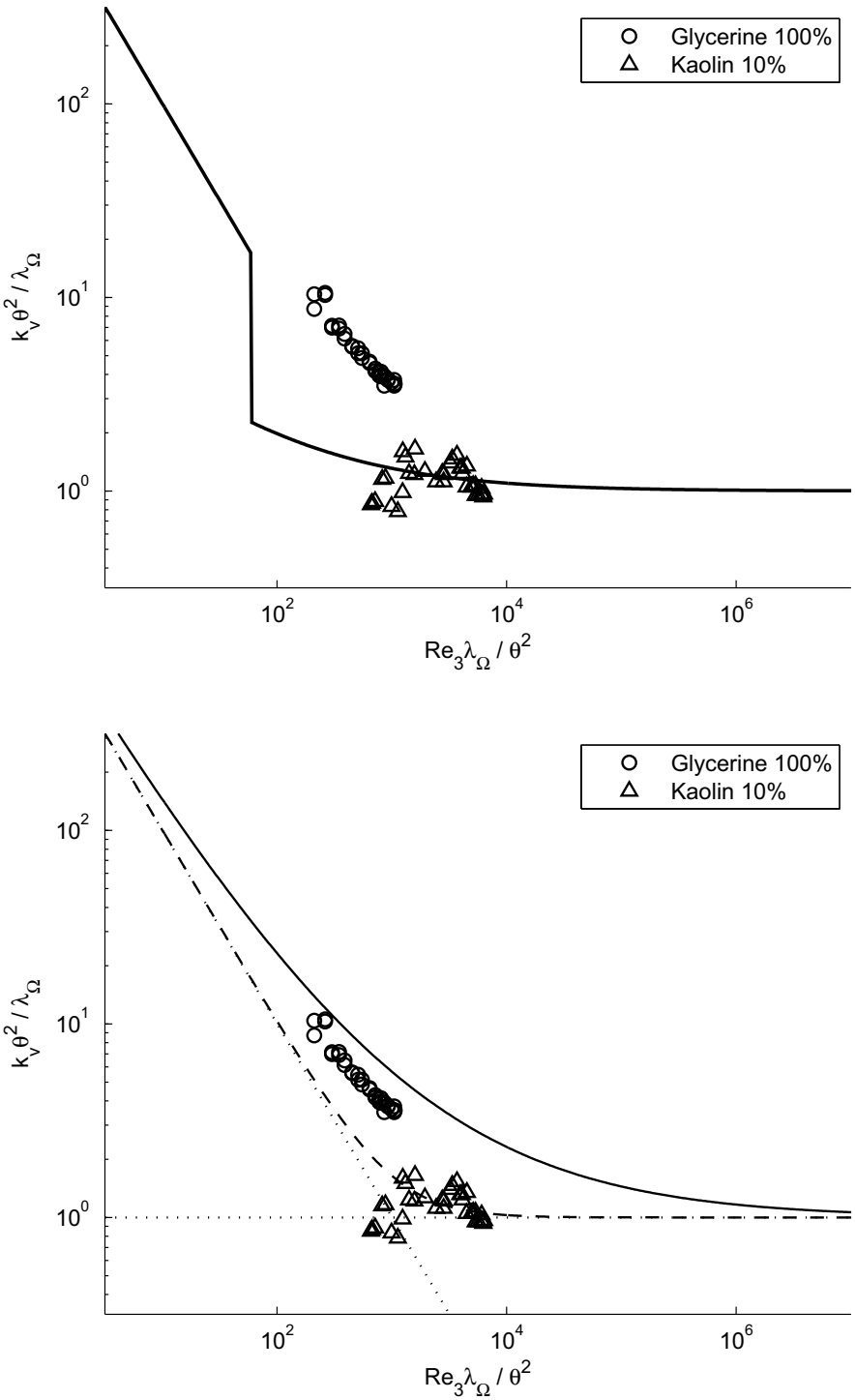

Figure C.10: Internal pipe diameter: 65mm. Valve opening: 50%. Mbiya's two-constant model (top), powered addition (bottom).

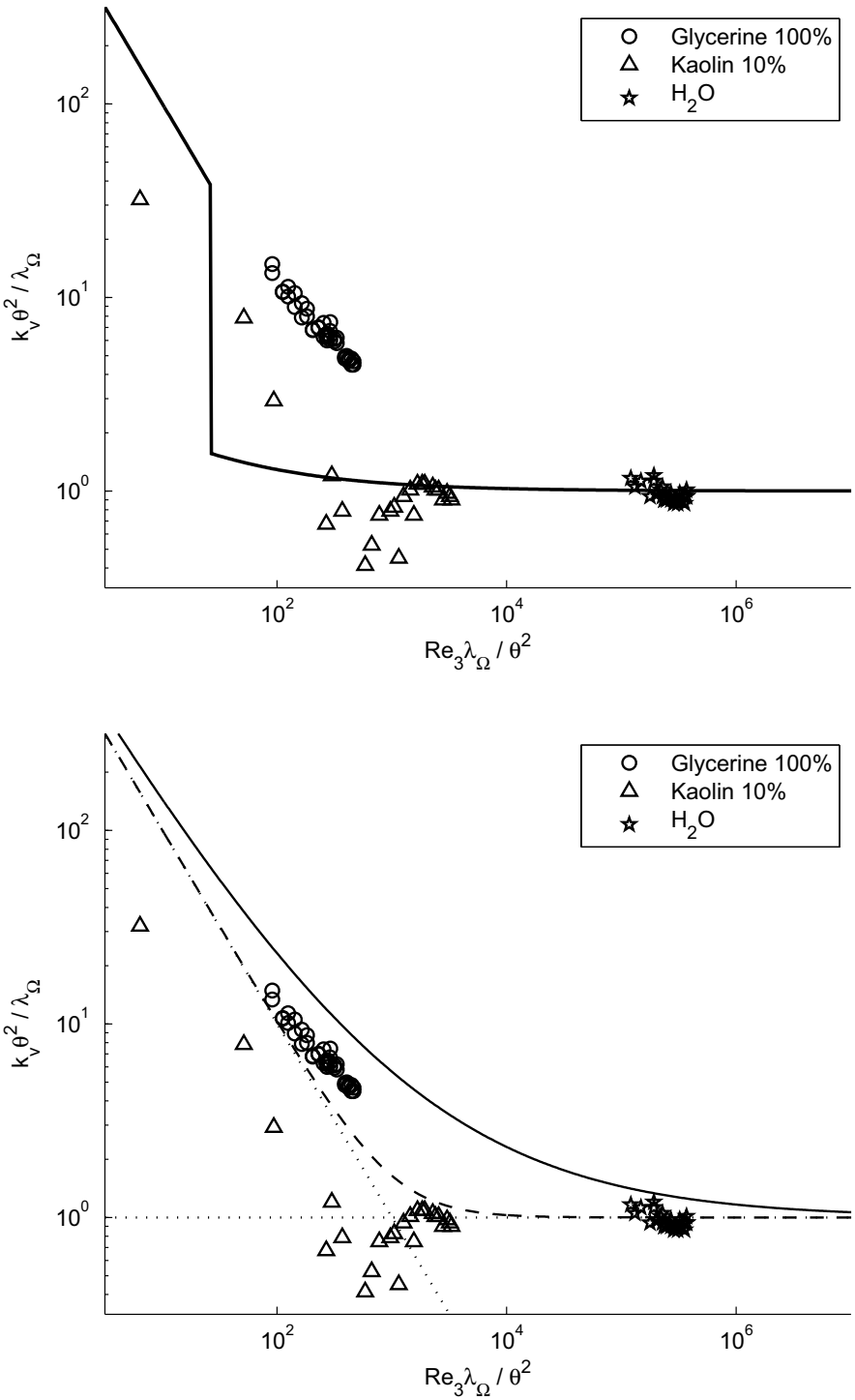

Figure C.11: Internal pipe diameter: 65mm. Valve opening: 75%. Mbiya's two-constant model (top), powered addition (bottom).

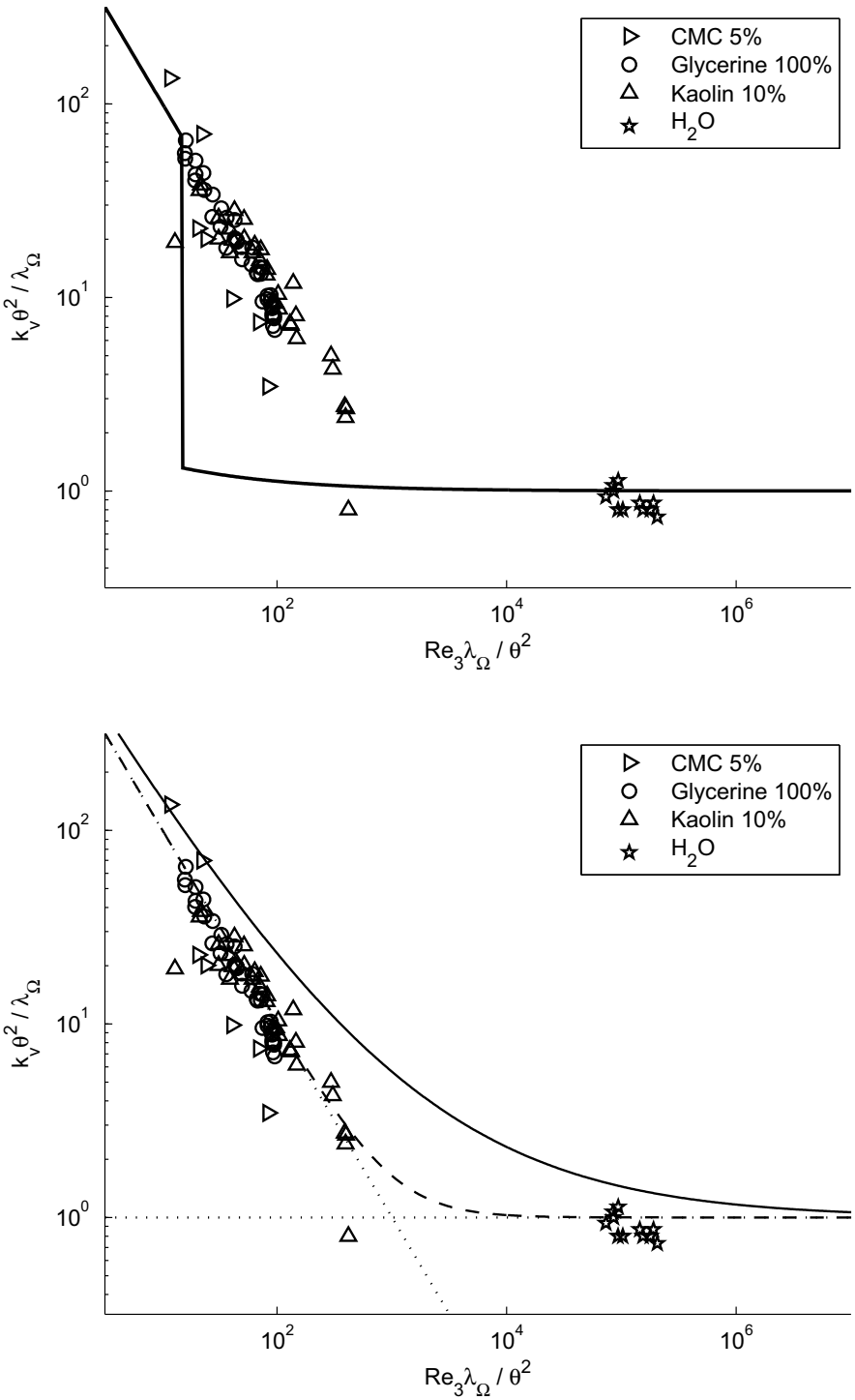

Figure C.12: Internal pipe diameter: $65mm$. Valve opening: 100%. Mbiya's two-constant model (top), powered addition (bottom).

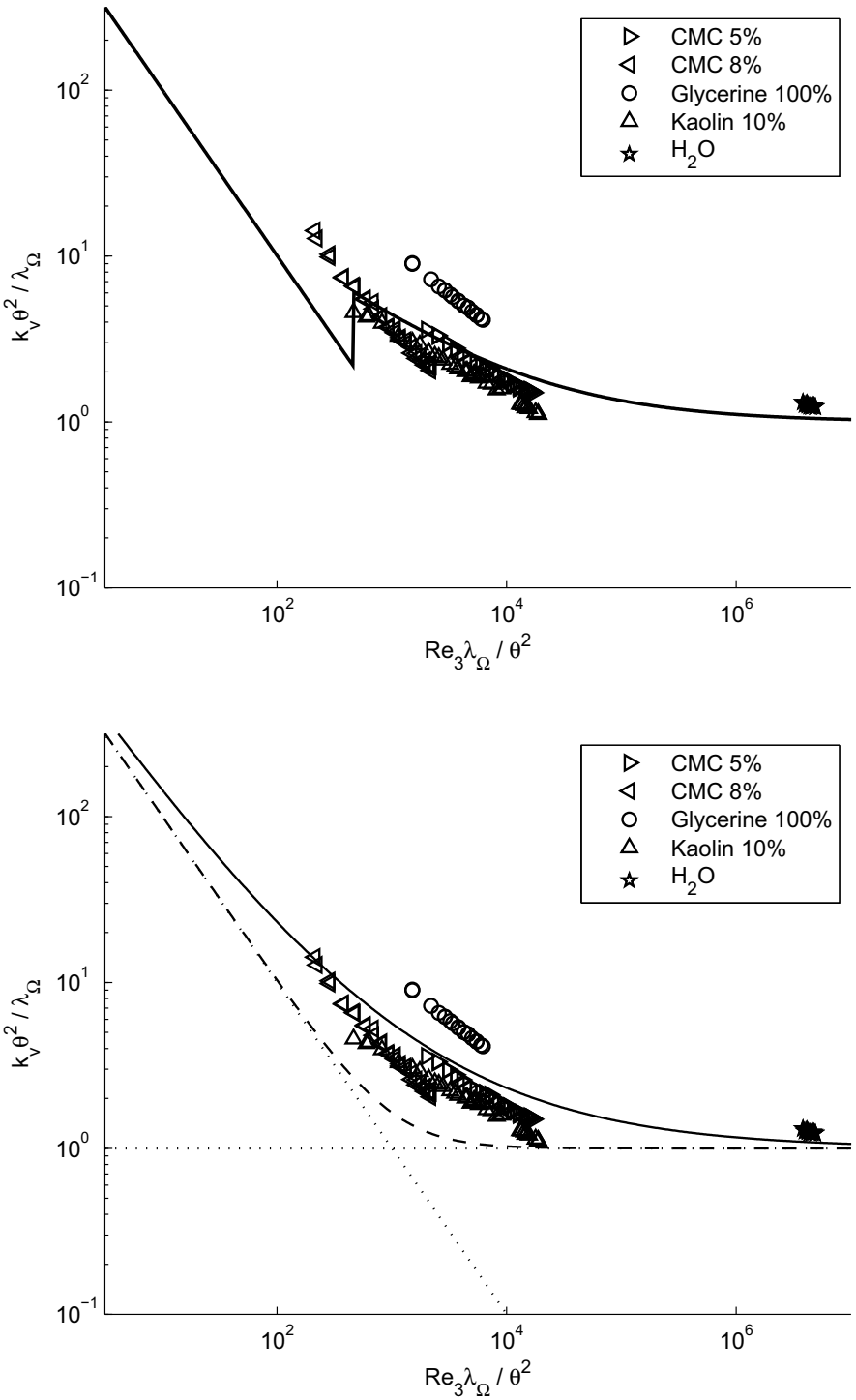

Figure C.13: Internal pipe diameter: 80mm. Valve opening: 25%. Mbiya's two-constant model (top), powered addition (bottom).

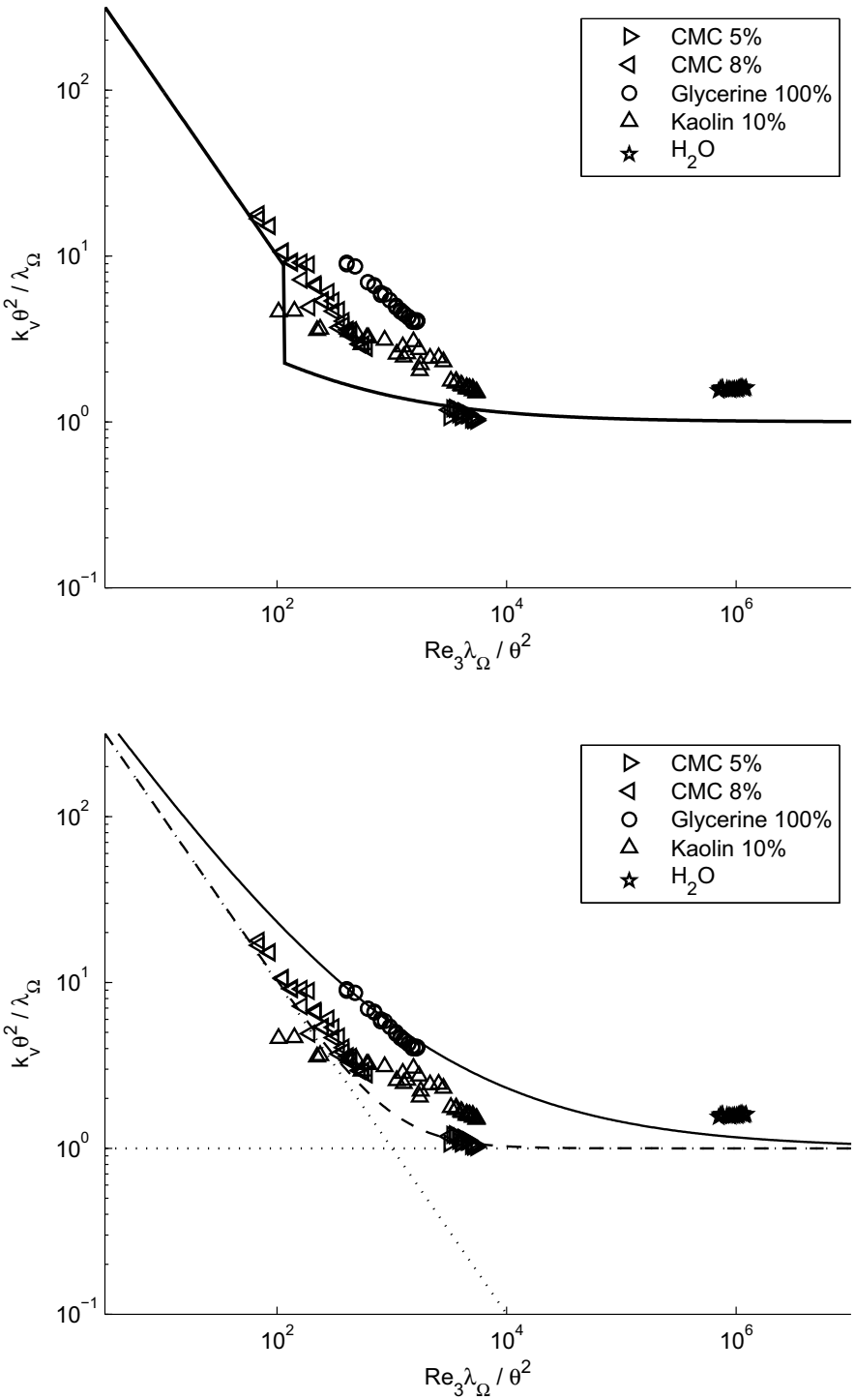

Figure C.14: Internal pipe diameter: 80mm. Valve opening: 50%. Mbiya's two-constant model (top), powered addition (bottom).

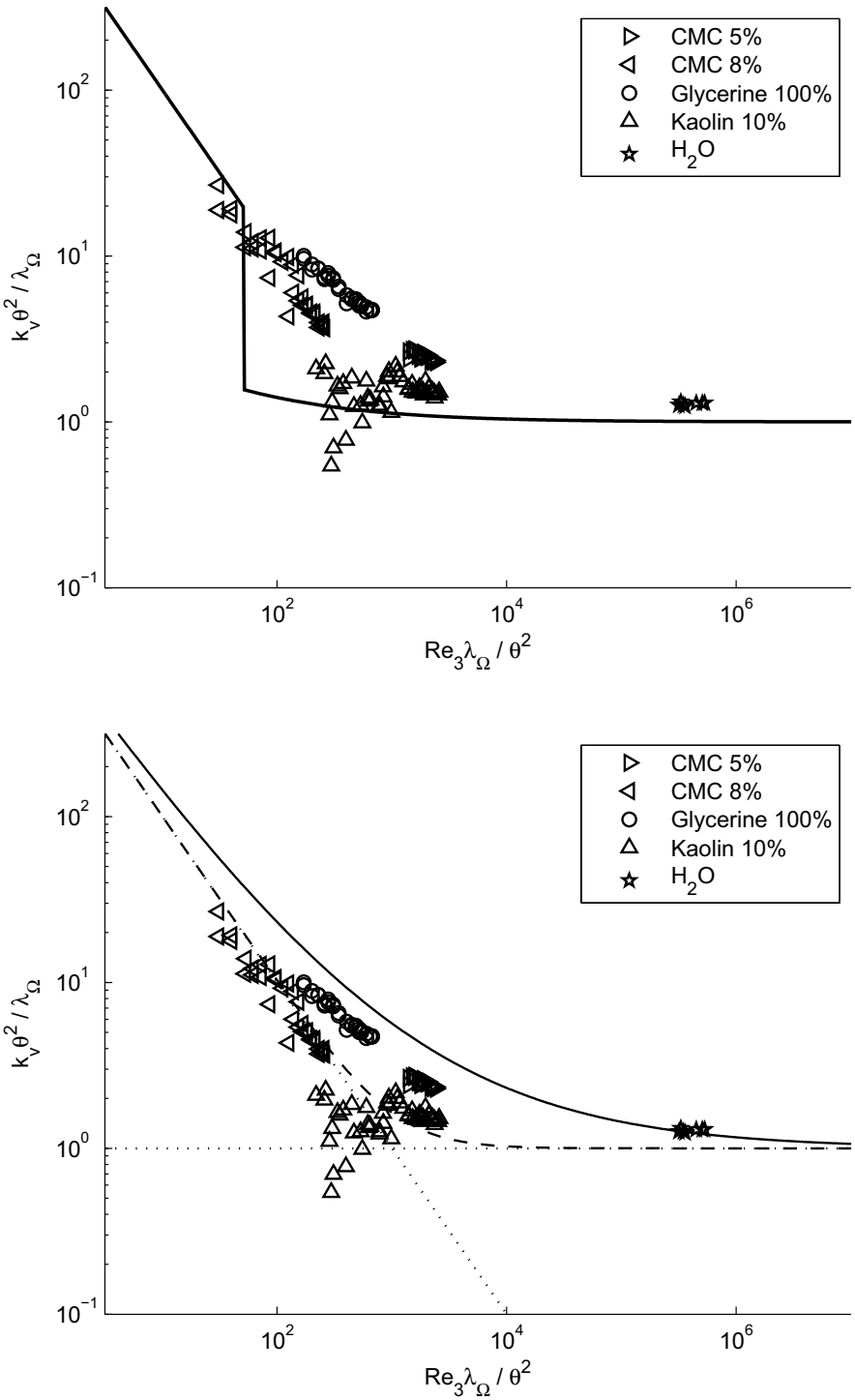

Figure C.15: Internal pipe diameter: 80mm. Valve opening: 75%. Mbiya's two-constant model (top), powered addition (bottom).

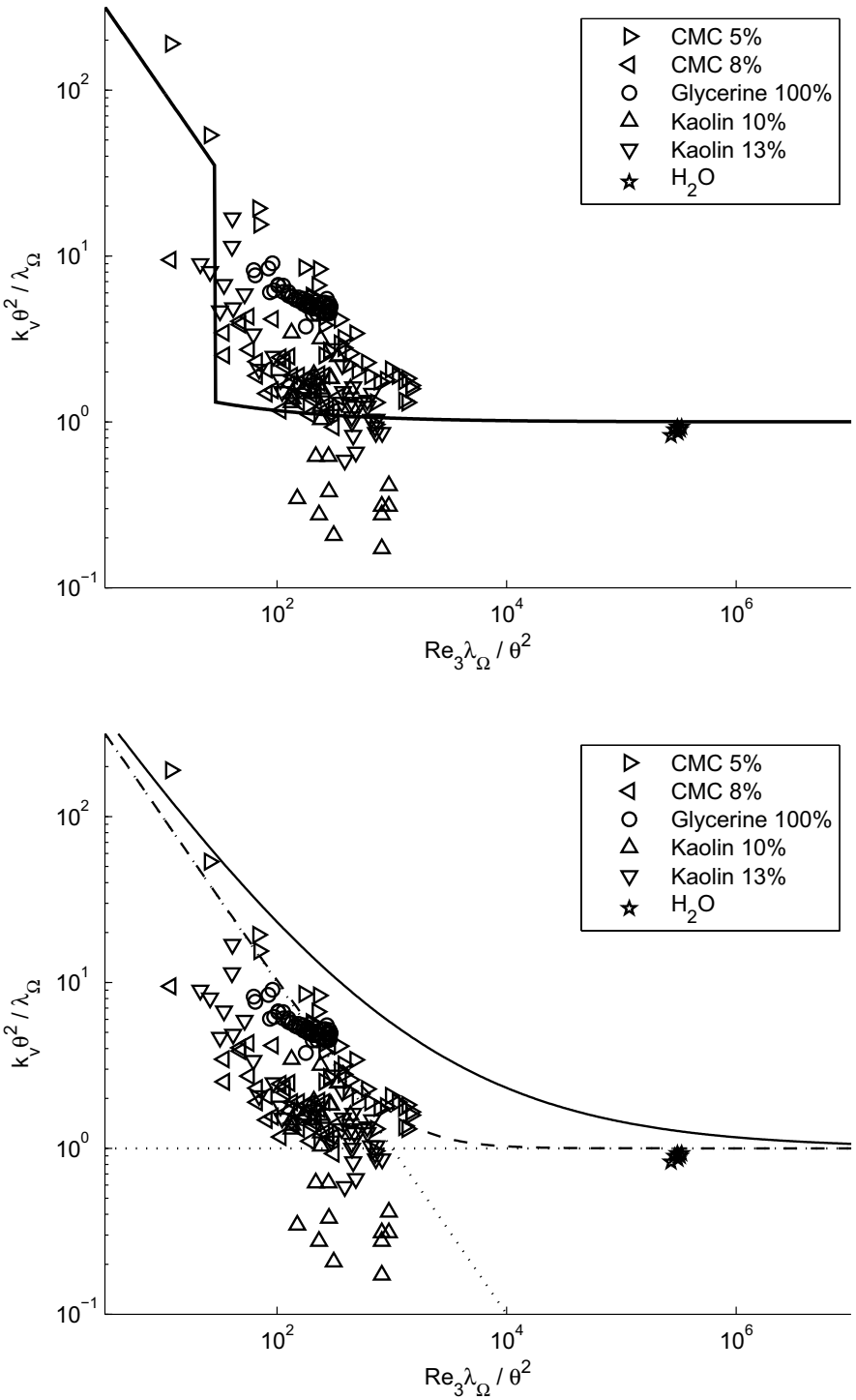

Figure C.16: Internal pipe diameter: $80mm$. Valve opening: 100%. Mbiya's two-constant model (top), powered addition (bottom).

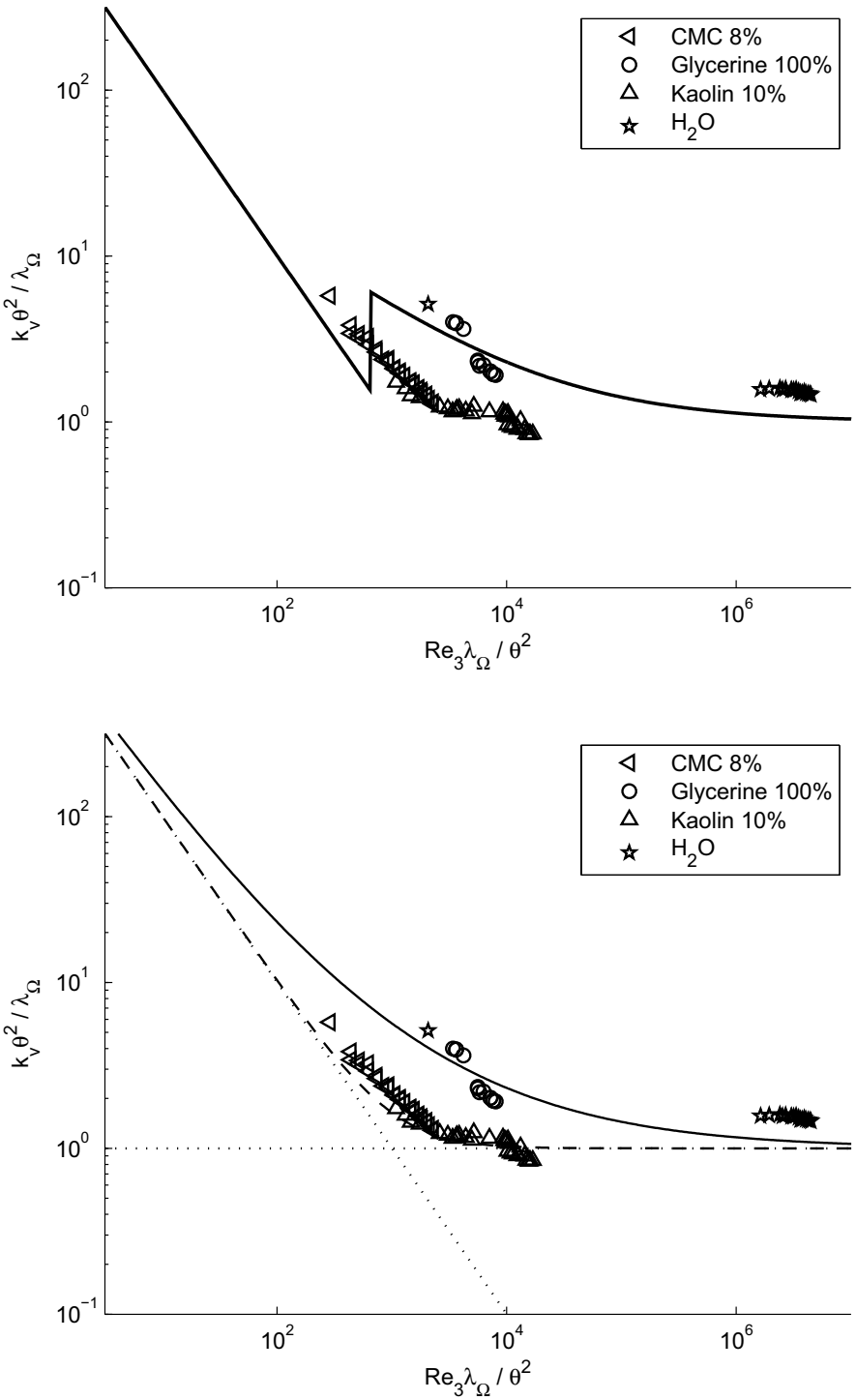

Figure C.17: Internal pipe diameter: 100mm. Valve opening: 25%. Mbiya's two-constant model (top), powered addition (bottom).

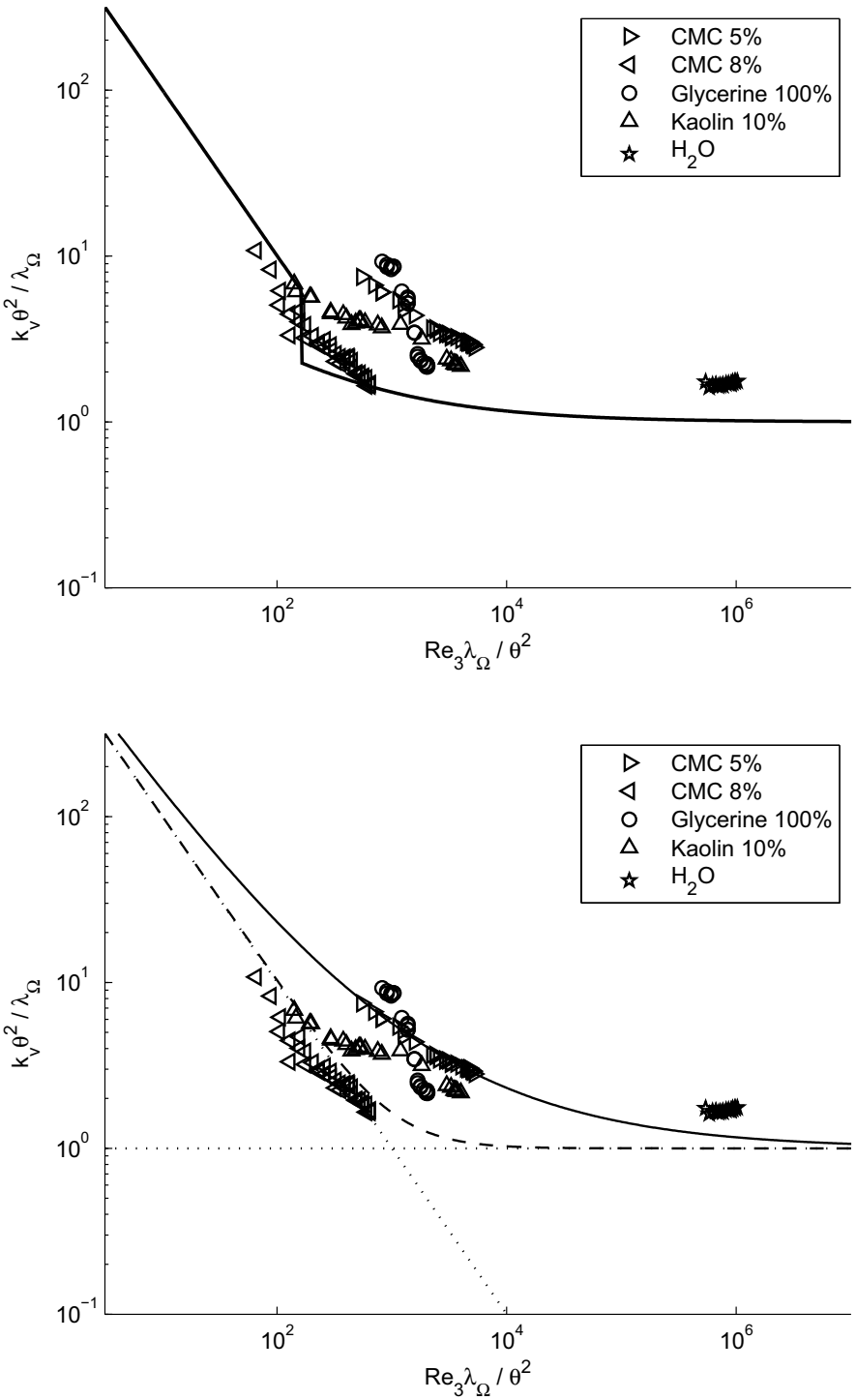

Figure C.18: Internal pipe diameter: 100mm. Valve opening: 50%. Mbiya's two-constant model (top), powered addition (bottom).

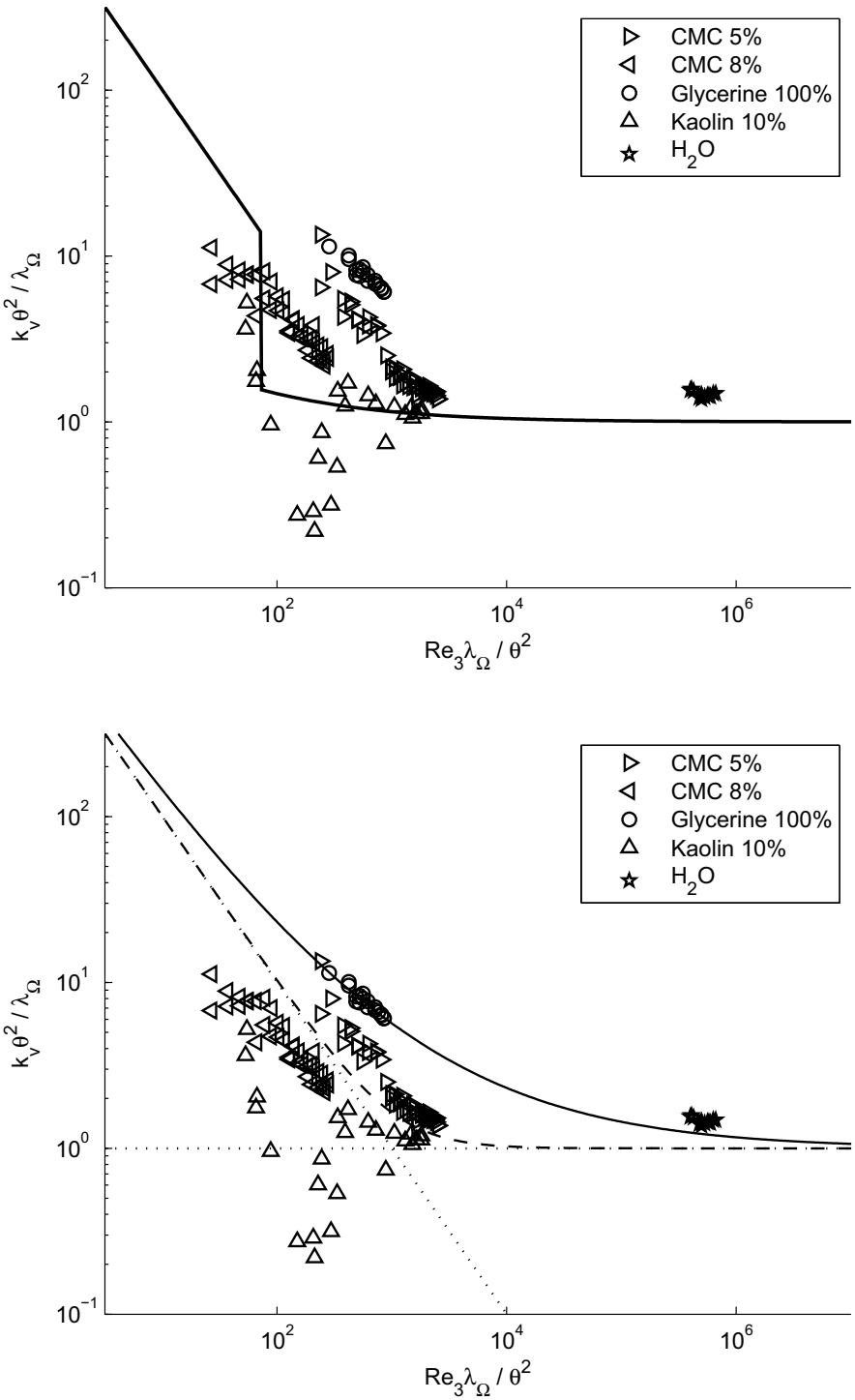

Figure C.19: Internal pipe diameter: 100mm. Valve opening: 75%. Mbiya's two-constant model (top), powered addition (bottom).

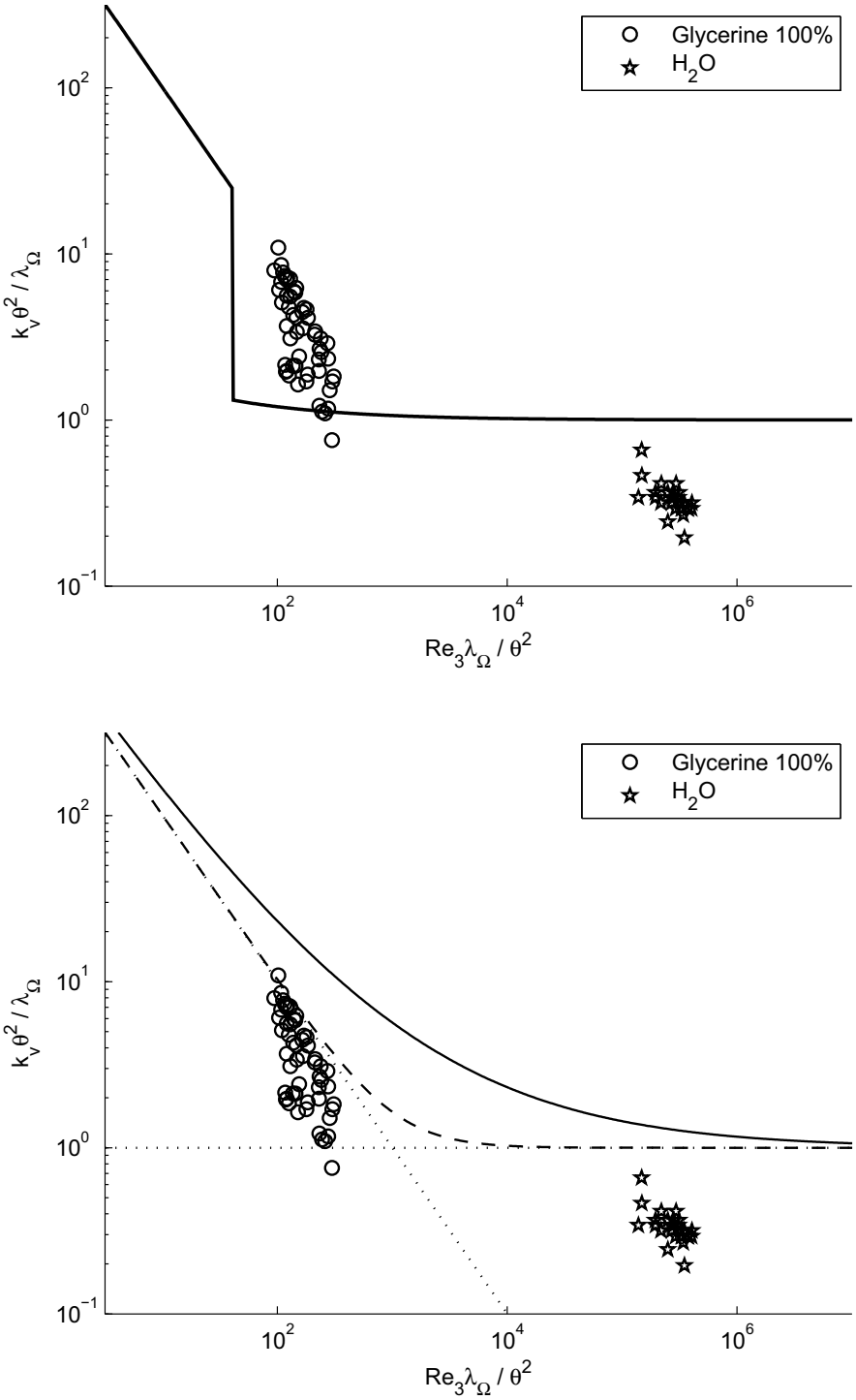

Figure C.20: Internal pipe diameter: 100*mm*. Valve opening: 100%. Mbiya's two-constant model (top), powered addition (bottom).

Appendix D

Høgskolen i Telemark (Telemark University College) data sets

Measurements were performed on a laboratory-scale fluidized beds at Høgskolen i Telemark (Telemark University College), Porsgrunn, Norway between 13 – 20 October 2008. The beds, contained in a cylindrical perspex tube with inner diameter of $72mm$, comprised of glass powders, consisting of spherical glass particles, with a density of $2485kg/m^3$ and available in three different diameter-ranges: $100\mu m - 200\mu m$; $400\mu m - 600\mu m$; and $750\mu m - 1000\mu m$. In all of the experiments performed the fluid used to fluidise the bed was air at ambient conditions, with a density of $1,2kg/m^3$ and viscosity of $1.78 \times 10^{-5} N \cdot s/m^2$. Below are the tables containing the experimental data.

Eight pressure tubes were placed along the height of the bed and were connected to digital pressure sensors (Honeywell, model 142PC02G) that measured the pressure at these fixed intervals within the bed. In Tables D.1 to D.3 these distances are indicated in the heading of each column under the sensor number. The unprocessed pressure data was plotted against distance of the sensor from the porous plate on which the bed was supported; the result of this plot is shown in Figure D.1. Since the pressure drop is a linear function of the height, this plot served to demonstrate possible anomalies in individual sensors (e.g. sensor 3 may be disregarded); for the results discussed in Section 4.1.4 sensors number 2 and 8 were used.

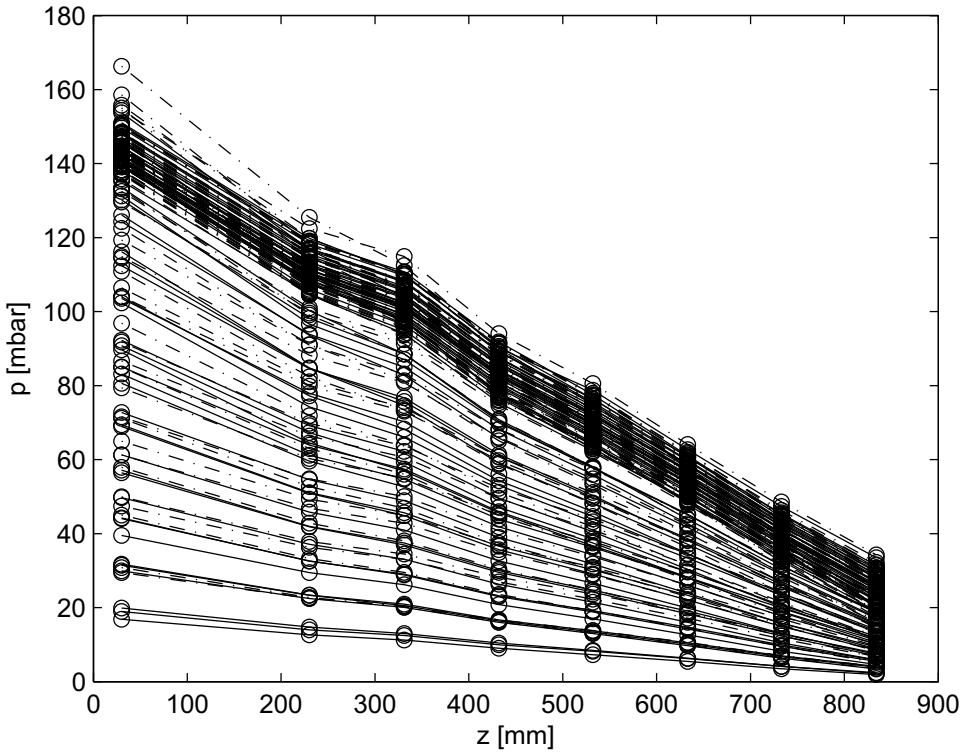

Figure D.1: Plot of raw pressure data, p [$mbar$], against vertical sensor distance from porous plate supporting the bed, z [mm].

Table D.1: **Experimental data:** $100\mu m - 200\mu m$

		Pressure reading [$mbar$]							
Run no.	Fluid velocity [ℓ/min]	Sensor 1 at 30mm	Sensor 2 at 230mm	Sensor 3 at 331mm	Sensor 4 at 432mm	Sensor 5 at 532mm	Sensor 6 at 633mm	Sensor 7 at 733mm	Sensor 8 at 834mm
1	1.0	18.95367	13.97865	12.47998	9.97153	8.19564	6.24307	4.11083	2.44127
1	1.5	29.45802	22.50327	20.46747	16.69936	13.78390	10.58586	7.06468	4.10142
1	1.5	31.71953	23.37373	20.92357	16.69455	13.72598	10.46761	6.98105	4.09170
1	2.0	44.23392	32.58558	29.07701	23.22803	19.18734	14.67983	9.88536	5.80791
1	2.0	47.45059	36.27742	33.05562	26.95077	22.27800	17.12554	11.52700	6.64074
1	2.5	57.16058	41.98516	37.48037	30.00802	24.72962	19.06505	12.90695	7.65287
1	2.5	61.25906	46.86933	42.75256	34.86980	28.84536	22.18569	14.99435	8.61511
1	3.0	69.43926	51.06728	45.65560	36.57947	30.19570	23.31342	15.81362	9.37380
1	3.0	71.57872	54.78347	50.02074	40.80785	33.78059	25.99408	17.59990	10.10408
1	3.5	83.14843	61.17979	54.77007	43.91534	36.27275	27.99853	18.97105	11.18065
1	3.5	86.62369	66.36983	60.66311	49.50889	41.01771	31.59137	21.44899	12.30176
1	4.0	89.69118	64.52500	56.91698	45.58397	36.67933	28.20242	19.88684	11.68692
1	4.0	104.11834	79.87414	73.09329	59.69633	49.51141	38.17544	25.98106	14.90201
1	4.5	102.36348	74.28898	66.06832	53.04520	43.19946	33.35199	23.34626	13.62672
1	4.5	114.92805	88.23026	80.79961	66.01456	54.79415	42.25936	28.80221	16.52285
1	5.0	116.17686	84.75726	75.72347	60.78099	49.78898	38.61803	26.95733	15.74490
1	5.0	129.63451	99.60787	91.32100	74.67666	62.02810	47.88498	32.68384	18.75286
1	5.5	131.27105	96.64048	87.02657	69.93299	57.86981	45.20526	31.39424	18.73062
1	5.5	143.19501	110.11652	101.05768	82.68961	68.73886	53.10092	36.29719	20.83395
1	6.0	140.71135	104.59733	94.08356	75.37287	62.41638	49.10311	34.35508	20.84876

1	6.0	155.77877	119.82464	110.00074	90.00264	74.93903	57.92552	39.72977	22.80072	
1	6.7	137.30826	104.68540	93.68090	76.21013	64.72154	50.55105	35.65335	23.38454	
1	7.2	143.66332	109.60585	97.19038	78.19839	66.01514	49.91619	35.65843	23.20328	
1	7.5	139.24016	107.55382	97.64640	79.33942	65.98832	51.08681	35.84478	21.79643	
1	8.2	138.26897	107.45096	98.18819	80.12238	66.77726	52.26275	36.93814	23.01949	
1	8.8	139.80218	108.44007	99.08177	80.91219	67.63333	52.68154	37.58476	23.50440	
1	9.3	139.09265	108.28225	99.29549	81.22111	67.96525	53.31013	37.87421	24.23955	
1	9.5	141.04250	110.04500	100.91311	82.73708	69.42457	54.52606	39.35610	25.40003	
1	10.2	139.87939	108.97352	100.04982	81.98070	68.73311	53.79404	38.55321	25.07929	
1	10.5	141.47716	110.46737	101.16052	82.81549	69.69395	54.66842	39.48391	25.42576	
1	11.0	142.49261	111.24627	101.84766	83.38153	70.54348	55.24936	40.22767	26.22084	
1	11.3	142.75993	111.88912	103.25492	85.07759	71.68847	56.63545	41.09635	27.60944	
1	12.0	143.44573	112.25759	102.35387	84.17410	71.40622	55.92243	41.02664	27.00476	
1	12.5	142.96052	112.10615	103.44525	85.18065	71.97998	57.21298	41.79914	28.08601	
1	13.0	144.63398	113.35956	104.52047	86.16547	72.49527	57.23472	41.94579	27.93436	
1	14.0	145.64961	114.41792	106.03504	87.40193	73.70032	58.74014	42.90218	28.89478	
1	14.5	146.63855	115.59877	107.19530	88.59874	75.04634	58.99676	43.98648	30.22047	
1	15.0	146.82798	115.58757	106.77035	87.33459	74.56986	58.73262	43.73842	29.85128	
1	16.0	148.26245	117.06430	108.02094	89.00982	76.42204	60.73306	45.33969	31.38724	
1	16.5	147.89646	116.71141	108.20082	89.07898	75.86198	60.28201	44.75427	30.77585	
1	18.0	151.07298	119.83305	110.13862	90.16209	78.75561	62.71305	47.31179	33.51320	
1	18.0	150.09448	118.82371	110.56998	91.42715	77.94969	61.65001	46.27425	32.21510	
1	21.0	154.40616	122.42441	114.89508	94.07749	80.56975	64.10849	48.56672	34.24769	
2	1.0	19.91246	14.74455	13.00390	10.41056	8.46593	6.32458	4.12837	2.26370	
2	1.5	31.46901	23.31639	20.52694	16.38738	13.41072	10.13072	6.76314	3.86675	
2	2.0	44.07534	32.64586	28.81068	22.98897	18.83527	14.24136	9.55657	5.44049	
2	2.0	49.96295	37.89944	34.48134	28.24541	23.69153	18.50824	12.95172	7.34183	

2	2.5	56.43280	41.83302	36.96538	29.50493	24.19337	18.31545	12.32831	7.00286
2	2.5	64.95705	49.32144	44.91410	36.80456	30.90628	24.16738	16.95837	9.60028
2	3.0	68.94417	50.90249	44.86096	35.64332	29.09635	22.03620	14.94192	8.49914
2	3.0	79.38394	60.32102	54.98873	45.08250	37.89271	29.64294	20.85377	11.79799
2	3.5	80.60229	59.59118	52.63005	41.86214	34.23018	25.99541	17.71046	10.14971
2	3.5	91.78604	69.80201	63.69963	52.24970	43.94261	34.40088	24.24143	13.72256
2	4.0	90.80617	67.29338	59.34688	47.10358	38.59949	29.69004	20.65183	12.15332
2	4.0	106.45842	81.05205	74.00585	60.73939	51.13637	40.05744	28.27693	16.00707
2	4.5	103.95869	77.23255	68.26545	54.31246	44.62854	34.40268	23.89899	14.06476
2	4.5	119.36293	90.94339	83.13075	68.26489	57.50979	45.07742	31.85597	18.04746
2	5.0	114.48023	84.69949	74.63738	59.09574	48.27525	37.11917	25.60308	15.14239
2	5.0	132.47156	101.02046	92.42198	75.94336	64.02614	50.21547	35.53490	20.13958
2	5.5	126.13774	93.61950	82.80409	65.78329	53.95129	41.66010	28.91680	17.11203
2	5.5	144.07458	109.93704	100.66474	82.75572	69.81166	54.76697	38.81401	22.02571
2	6.0	133.53266	100.23262	88.56288	70.36369	57.66536	45.09129	31.31094	18.70923
2	6.0	144.78643	107.60966	96.56636	77.33829	62.86056	48.71806	33.61238	20.34326
2	6.5	146.39020	110.17557	97.54777	77.66879	63.78966	50.09816	34.99826	20.81332
2	6.5	155.01642	114.93788	102.92396	82.17852	66.42439	51.26324	35.31367	20.85887
2	7.0	139.38114	106.90805	97.26687	78.90553	65.41615	50.68363	35.60543	21.41209
2	7.0	153.73415	116.79388	103.87230	82.88353	68.21691	53.49968	37.46851	22.16719
2	7.5	139.26822	106.94046	97.50228	79.30229	65.72393	50.86324	35.66534	21.58967
2	8.0	135.26647	104.78936	94.96704	76.72219	63.07773	48.42134	33.21551	19.03779
2	8.0	139.96762	108.09785	98.59973	80.37087	66.84944	51.75903	36.70935	22.50517
2	8.5	138.26575	106.61012	97.01648	78.73832	65.12830	50.40495	35.17106	21.07523
2	9.0	135.86904	104.50213	94.99676	76.90472	63.52455	48.77717	33.97631	19.95810
2	9.0	139.28137	107.62518	98.12986	79.85086	66.30457	51.58593	36.18421	21.96616
2	10.0	140.60183	109.28015	100.08808	81.83816	68.37994	53.62902	38.11935	23.86511

2	10.5	140.07210	108.63031	99.41336	81.07756	67.43890	52.55467	37.15344	22.97271
2	11.0	141.21518	110.41596	101.40096	82.99087	69.42071	54.57213	39.03407	24.86750
2	11.5	141.99720	110.77658	101.86728	83.69061	70.16683	55.14786	39.84526	25.75519
2	12.0	142.40941	111.37948	102.34806	83.93763	70.38646	55.53733	39.90576	25.81822
2	12.5	142.93961	111.65007	102.74339	84.32176	70.63280	55.58618	39.83593	25.53862
2	13.0	143.56165	112.39243	103.62741	85.36852	71.86691	56.85634	41.06499	26.85584
2	13.5	144.22028	112.84497	104.06300	85.49462	71.84296	56.51731	40.88843	26.61891
2	14.0	143.93218	112.74858	104.00270	85.49451	71.92644	56.86727	41.01487	26.79413
2	15.0	145.57501	114.19133	105.43206	86.67028	72.84098	57.69316	41.96749	27.63499
2	15.0	145.70004	114.41449	105.61930	86.87833	73.02095	57.83390	42.11374	27.91896
2	16.0	146.29011	115.02179	106.34576	87.64247	73.71559	58.41319	42.58864	28.33714
2	16.0	147.14760	115.75897	106.98838	88.25085	74.38296	58.91393	42.87117	28.64089
2	17.0	147.45107	115.95524	107.38838	88.39379	74.45723	59.23945	43.35198	29.12633
2	17.5	148.46164	117.09807	108.37056	89.30377	75.55441	59.90274	43.80617	29.55493
2	18.5	149.63964	118.30075	109.71234	90.61882	76.43647	60.70647	44.50068	30.36546
2	19.0	150.22350	118.61215	110.19165	91.24476	77.12572	61.30695	45.06564	30.56619
2	20.0	150.65087	119.13030	110.76587	91.84067	77.52071	61.04941	45.11649	30.79523
2	20.5	150.27862	118.96432	110.62423	91.50373	77.41373	62.00419	45.66405	31.56087
3	1.0	16.84427	12.62445	11.25106	9.00968	7.30037	5.44298	3.49720	1.90923
3	1.5	29.96102	22.43216	20.05485	16.01966	12.99250	9.71781	6.31899	3.40898
3	1.5	30.79923	22.76569	20.15868	16.10808	13.09811	9.81541	6.45706	3.50770
3	2.0	39.48826	29.44061	26.19510	20.79546	16.97804	12.66395	8.21437	4.62265
3	2.0	44.98719	33.26624	29.50803	23.55728	19.18642	14.39765	9.52555	5.15216
3	2.5	49.74815	37.13560	33.10856	26.31464	21.47308	16.04101	10.45758	5.87613
3	2.5	57.90293	42.84704	38.04106	30.38176	24.77129	18.59881	12.34431	6.66376
3	3.0	61.28985	45.84170	40.98080	32.61772	26.58820	19.89710	13.04638	7.30911
3	3.0	71.15631	52.70352	46.85958	37.43455	30.54725	22.94988	15.27651	8.23732

3	3.5	72.74040	54.55345	48.88410	38.99853	31.79462	23.86969	15.77411	8.85639
3	3.5	84.94022	62.96774	56.03969	44.79749	36.58657	27.51678	18.34966	9.89328
3	4.0	85.09059	63.95068	57.46286	45.92757	37.45983	28.19914	18.74906	10.54437
3	4.0	96.84109	71.86130	64.00848	51.19302	41.84386	31.48795	21.02892	11.33134
3	4.5	92.23371	69.15029	62.23768	49.58913	40.49213	30.35307	20.17625	11.46790
3	4.5	110.88897	82.36203	73.45829	58.78820	48.08986	36.22395	24.23178	13.06475
3	5.0	103.60224	77.91233	70.22975	56.11854	45.91198	34.60408	23.19849	13.30382
3	5.0	122.52935	91.08612	81.32051	65.10912	53.29928	40.17296	26.90490	14.50752
3	5.5	112.38854	84.61192	76.70964	61.43827	50.29983	38.18121	26.27689	15.48643
3	5.5	133.16106	99.07050	88.51467	70.92000	58.08743	43.80871	29.37095	15.84294
3	6.0	124.28750	93.88977	84.99829	68.21433	55.98589	42.68254	29.41096	17.35591
3	6.0	146.08920	108.80058	97.30172	78.00791	63.94068	48.25644	32.39463	17.48203
3	6.5	130.12421	98.20525	88.54555	70.83782	58.05055	43.88243	30.38866	18.63796
3	6.5	158.59803	118.21295	105.83019	84.90383	69.64067	52.59066	35.34106	19.08515
3	7.0	140.65024	107.78195	97.33003	78.08029	64.19464	48.75003	33.73483	20.48654
3	7.0	166.31043	125.50837	112.43966	90.24232	74.05578	55.97285	37.64417	20.35110
3	7.5	137.59934	105.40685	95.71284	77.47269	63.97739	49.31108	34.21863	20.14165
3	8.0	137.11140	105.10373	95.45544	77.13630	63.43102	48.72076	33.46370	19.19675
3	8.0	138.13331	106.05061	96.38750	78.11380	64.63298	49.98657	34.77459	20.67317
3	9.0	137.55421	105.69629	96.10111	78.10008	64.70215	50.10192	34.92248	20.82460
3	9.0	139.54503	107.94128	98.54228	80.29305	66.86345	52.16548	36.97141	22.88847
3	10.0	139.57699	108.52177	99.23635	80.89677	67.29424	52.48387	37.06866	22.85139
3	10.0	140.66618	109.32079	100.20578	81.94740	68.52820	53.74163	38.21769	23.97466
3	11.0	140.70446	109.77812	100.69468	82.41134	68.85881	53.95808	38.47130	24.23114
3	11.0	141.27693	110.14729	101.00479	82.73103	69.14132	54.14565	38.46499	24.12873
3	12.0	141.66306	110.59522	101.62458	83.38771	69.86125	54.88727	39.16449	24.87650
3	13.0	142.35165	111.27673	102.43089	84.13912	70.54626	55.62033	39.85654	25.67854

3	13.0	142.92486	111.80618	102.97554	84.57201	70.89130	55.94520	40.23063	25.99207
3	15.0	144.61491	113.37735	104.46328	85.91812	72.20520	57.13543	41.27319	27.07760
3	15.0	144.47785	113.09924	104.29429	85.79490	72.12999	56.88218	40.99619	26.71276
3	18.0	146.08767	114.81142	106.11654	87.57753	73.84228	58.45894	42.57734	28.44945
3	18.0	147.88382	116.61998	107.93253	89.23612	75.04796	59.66874	43.36701	28.96747
3	21.0	148.55597	117.16319	108.53330	89.51039	75.88834	60.64421	44.68205	30.54577

Table D.2: **Experimental data:** $400\mu m - 600\mu m$

		Pressure reading [$mbar$]							
Run no.	Fluid velocity [ℓ/min]	Sensor 1 at 30mm	Sensor 2 at 230mm	Sensor 3 at 331mm	Sensor 4 at 432mm	Sensor 5 at 532mm	Sensor 6 at 633mm	Sensor 7 at 733mm	Sensor 8 at 834mm
1	5.0	12.47307	9.66077	8.62459	6.97451	5.68746	4.39089	3.01765	1.82501
1	5.0	14.86238	11.19224	10.09635	8.28818	6.77191	4.86699	3.20382	1.92120
1	8.0	20.03674	15.45186	13.85388	11.16670	9.11916	7.04298	4.87215	2.93491
1	8.0	24.68648	18.54897	16.78764	13.73811	11.24063	8.09726	5.40752	3.18642
1	10.0	25.76351	19.84229	17.81906	14.34789	11.73083	9.07014	6.28271	3.78260
1	10.0	30.60494	22.99243	20.82058	17.03720	13.93828	10.05256	6.73762	3.95324
1	12.0	31.38214	24.14986	21.71559	17.47413	14.29712	11.06161	7.67032	4.61369
1	12.0	37.07740	27.85626	25.25027	20.65060	16.90550	12.20747	8.20905	4.79460
1	14.0	43.56601	32.73062	29.69981	24.28463	19.88560	14.36910	9.68586	5.64406
1	15.0	39.50100	30.38600	27.36668	22.01353	18.02347	13.95464	9.69544	5.83548

1	16.0	49.90141	37.50068	34.04958	27.84346	22.81291	16.49085	11.14165	6.48276	
1	18.0	47.14571	36.24588	32.67700	26.26940	21.51619	16.66751	11.58932	6.97832	
1	18.0	56.31119	42.33560	38.46462	31.46220	25.78589	18.65425	12.61635	7.33284	
1	20.0	62.73135	47.17904	42.88610	35.08623	28.76922	20.82500	14.10229	8.19072	
1	21.0	55.47809	42.66349	38.50406	30.95203	25.37350	19.67471	13.69391	8.25721	
1	22.0	69.83019	52.53770	47.79128	39.10401	32.08194	23.24487	15.76144	9.14884	
1	24.0	65.40606	50.31900	45.45785	36.54396	29.98828	23.27737	16.22637	9.79572	
1	24.0	78.27064	58.91598	53.62934	43.89968	36.03347	26.12359	17.73757	10.28832	
1	26.0	85.96473	64.73517	58.96917	48.28258	39.65186	28.76241	19.55468	11.33609	
1	27.0	75.60274	58.19565	52.61821	42.32165	34.74545	26.98331	18.84402	11.40993	
1	28.0	94.06170	70.86872	64.59339	52.90951	43.47306	31.54807	21.47119	12.44333	
1	30.0	86.59599	66.67462	60.32805	48.53433	39.85715	30.99183	21.67547	13.17175	
1	30.0	102.62222	77.35580	70.54673	57.80686	47.52231	34.50471	23.50349	13.60322	
1	32.0	110.85267	83.58886	76.27891	62.52000	51.40831	37.33633	25.43776	14.69902	
1	33.0	97.70831	75.25335	68.14546	54.85934	45.09311	35.08511	24.57585	14.96938	
1	34.0	120.14988	90.63561	82.75725	67.84916	55.80136	40.53488	27.60846	15.91864	
1	36.0	108.85495	83.81417	75.96438	61.17650	50.31445	39.18129	27.47096	16.73744	
1	36.0	128.46331	96.93078	88.54703	72.61283	59.72867	43.38018	29.53563	16.97550	
1	38.0	115.47948	88.88727	80.52022	64.82926	53.27228	41.47862	29.03164	17.65904	
1	38.0	136.54043	103.03522	94.16306	77.22303	63.53896	46.10076	31.34993	17.93030	
1	40.0	122.04502	93.95955	85.18373	68.63917	56.47071	44.00321	30.88404	18.87604	
1	40.0	145.00739	109.07331	99.49380	81.34623	67.16307	49.02260	33.13176	18.70521	
1	42.0	129.66120	99.84218	90.66364	73.28454	60.33399	47.11710	33.14908	20.43076	
1	42.0	142.72394	107.84912	97.44880	78.54425	64.44130	50.30743	35.27952	21.03025	
1	44.0	135.71658	104.52799	95.10630	76.93736	63.44021	49.52340	34.79160	21.60873	
1	44.0	142.56012	109.99692	98.98923	79.63777	65.63001	51.55839	36.57591	22.85391	
1	46.0	141.76524	109.23016	99.32104	80.20370	66.40349	51.74544	36.59427	22.75907	

1	46.0	143.20200	110.64218	100.89796	82.20466	67.82450	53.22464	38.26184	24.62993	
1	48.0	144.10181	111.11117	100.74270	81.58687	67.67080	53.00661	38.06414	24.73772	
1	48.0	144.03684	111.46639	101.38260	82.30580	68.71205	54.29577	39.42763	26.23747	
1	50.0	147.52569	114.73452	104.67990	84.94436	70.49199	55.44070	40.30257	27.12829	
1	50.0	147.46080	114.93851	105.10425	85.79560	71.87664	56.93933	41.69095	28.40981	
1	55.0	154.19383	121.69134	111.73694	91.13155	76.03026	60.43981	44.91478	31.85158	
1	60.0	159.49338	131.21941	119.87880	97.06514	81.13404	64.82618	48.95381	36.14123	
1	60.0	159.61222	130.28136	119.63378	97.77522	82.39414	66.46323	50.65368	37.91139	
1	65.0	161.17748	136.63153	125.77380	102.53000	86.45093	70.25459	54.34780	41.60692	
2	2.0	4.00184	3.14559	2.76971	2.28862	1.86352	1.40278	0.84395	0.55511	
2	5.0	11.27150	8.70600	7.77919	6.30914	5.14173	3.89896	2.55149	1.50441	
2	5.0	12.47297	9.64460	8.63398	6.97979	5.70685	4.39488	2.95952	1.83564	
2	8.0	20.93510	16.14124	14.49920	11.68765	9.55755	7.38093	5.04283	3.07878	
2	9.0	20.19048	15.52932	13.93982	11.25894	9.18370	6.97815	4.66504	2.68806	
2	10.0	26.92062	20.73070	18.65096	15.01625	12.29076	9.49541	6.51763	3.96288	
2	12.0	28.76253	22.08426	19.84833	16.00552	13.06255	9.94559	6.69129	3.82374	
2	12.0	32.96856	25.38138	22.85793	18.39149	15.05676	11.64149	8.01267	4.84772	
2	15.0	35.75539	27.45237	24.69584	19.90774	16.25381	12.38829	8.37094	4.76520	
2	15.0	39.36229	30.30813	27.32234	21.98042	17.99770	13.92341	9.60848	5.80075	
2	18.0	43.80603	33.63526	30.28955	24.41329	19.94807	15.21413	10.31755	5.86625	
2	18.0	47.57869	36.63157	33.06220	26.60169	21.79062	16.86814	11.66791	7.03523	
2	20.0	54.58777	42.04637	37.97858	30.56739	25.04995	19.39874	13.44545	8.09480	
2	21.0	51.55605	39.59177	35.69153	28.76785	23.52073	17.94537	12.19523	6.92782	
2	23.0	64.59128	49.77651	45.00922	36.23664	29.72316	23.02963	15.98860	9.62169	
2	24.0	61.25233	47.05651	42.45222	34.22240	28.00480	21.38717	14.57007	8.27181	
2	25.0	71.26277	54.93779	49.71274	40.04402	32.85389	25.46127	17.69480	10.64862	
2	27.0	69.03148	53.05420	47.90260	38.61899	31.63267	24.17079	16.49387	9.36379	

2	28.0	81.40012	62.78441	56.87046	45.82935	37.62666	29.17905	20.30024	12.20950
2	30.0	81.58830	62.73210	56.70198	45.74088	37.50082	28.69976	19.62639	11.14876
2	30.0	89.53073	69.08868	62.63458	50.50183	41.48611	32.17291	22.39676	13.45694
2	33.0	92.60604	71.26185	64.45724	52.04030	42.71480	32.73959	22.44560	12.76614
2	33.0	100.97967	77.98598	70.77343	57.10337	46.94020	36.41610	25.37060	15.23134
2	35.0	108.20658	83.60412	75.92660	61.28717	50.40436	39.10158	27.25006	16.34799
2	36.0	104.25340	80.29892	72.70102	58.74761	48.29691	37.07288	25.45709	14.50867
2	38.0	120.23632	92.96659	84.52233	68.26554	56.18232	43.58769	30.38024	18.19035
2	39.0	115.28421	88.85246	80.54706	65.13069	53.66094	41.25844	28.42687	16.25486
2	40.0	127.26477	98.39666	89.47711	72.25991	59.44680	46.06315	32.02939	19.03103
2	41.0	122.08935	94.10361	85.35134	69.06057	56.98517	43.84981	30.24094	17.33591
2	42.0	134.55232	104.07309	94.65605	76.37560	62.79527	48.19556	33.16498	19.42371
2	44.0	130.58845	100.65033	91.27134	73.89695	61.01685	47.15042	32.32927	18.84326
2	45.0	140.99056	108.16534	98.20147	79.60862	65.87443	51.24222	35.88078	21.71132
2	47.0	139.91225	107.65446	97.27962	78.50397	64.69438	49.80986	34.48300	20.63210
2	48.0	143.24367	110.57988	99.97094	80.75368	66.87601	52.21661	37.19853	23.89245
2	50.0	143.66343	111.33899	100.66576	81.22103	67.04632	52.11376	36.95294	23.66952
2	50.0	145.43289	112.88463	102.26172	82.75032	68.56416	53.58253	38.53997	25.38465
2	53.0	149.28754	116.68948	106.39317	86.39020	71.94616	56.71037	41.36806	28.28784
2	54.0	150.71955	117.61970	107.39017	87.17190	72.36795	56.92587	41.34217	28.12552
2	56.0	154.21454	121.35673	110.89534	90.11633	74.97946	59.51833	43.98456	31.05747
2	58.0	156.27843	123.19471	112.41828	91.66406	76.74096	61.08615	45.22682	32.06106
2	60.0	158.35981	128.07058	116.59086	94.78343	79.07091	63.10953	46.97786	33.96852
2	60.0	158.05377	126.94818	115.29475	93.21163	77.61210	61.82538	46.11662	33.30743
2	65.0	160.58203	135.11372	122.70204	98.90643	82.22012	66.03807	50.22370	37.66949
3	5.0	9.75932	7.49250	6.68745	5.43245	4.41773	3.35694	2.17855	1.30308
3	5.0	10.93890	8.45070	7.55172	6.12880	4.99557	3.78550	2.47839	1.46683

3	8.0	15.91752	12.17714	10.90958	8.82212	7.17750	5.46808	3.61970	2.12463	
3	8.0	18.07666	13.90792	12.47558	10.08202	8.22463	6.24925	4.15939	2.40521	
3	10.0	20.50193	15.65945	14.04888	11.34577	9.23657	7.04063	4.69368	2.72959	
3	10.0	23.77298	18.26928	16.41944	13.24983	10.81075	8.22155	5.51455	3.16949	
3	12.0	25.31131	19.31844	17.34407	14.00201	11.40202	8.69486	5.82812	3.37215	
3	13.0	31.51706	24.20706	21.78477	17.56705	14.34293	10.91756	7.36374	4.20735	
3	15.0	31.87946	24.32072	21.86298	17.63833	14.36743	10.97166	7.38498	4.25182	
3	15.0	36.22178	27.81605	25.04767	20.20019	16.49149	12.55936	8.49340	4.84120	
3	18.0	38.74619	29.55745	26.59716	21.44906	17.48266	13.36006	9.01446	5.17797	
3	18.0	44.14563	33.90580	30.56528	24.65013	20.13753	15.34172	10.41134	5.92603	
3	20.0	43.78044	33.39666	30.07402	24.24978	19.76939	15.11611	10.22152	5.86300	
3	21.0	52.33698	40.20508	36.27914	29.26247	23.91645	18.23446	12.39737	7.04637	
3	22.0	48.87781	37.28808	33.59740	27.09038	22.09687	16.89944	11.44577	6.55911	
3	24.0	61.46230	47.23031	42.66091	34.41861	28.15183	21.47594	14.63190	8.31007	
3	25.0	58.45964	44.61812	40.23992	32.45693	26.49317	20.28047	13.76543	7.88483	
3	27.0	71.06649	54.63662	49.39770	39.86576	32.63427	24.90975	17.00094	9.64702	
3	28.0	67.60859	51.62473	46.59671	37.59868	30.71594	23.53657	16.00310	9.17041	
3	30.0	73.96724	56.48868	51.01900	41.17456	33.65482	25.80396	17.56158	10.06646	
3	30.0	83.59943	64.31426	58.21753	47.01226	38.50932	29.41631	20.11126	11.40484	
3	33.0	84.86699	64.84396	58.61280	47.32654	38.72544	29.71562	20.25836	11.62027	
3	33.0	94.17102	72.49140	65.67967	53.06474	43.49197	33.23368	22.73812	12.88351	
3	36.0	95.19472	72.79876	65.85241	53.20785	43.59625	33.49384	22.87252	13.13710	
3	36.0	103.09433	79.40183	72.00163	58.20090	47.72753	36.48173	24.97972	14.13918	
3	39.0	106.41159	81.42004	73.71523	59.60278	48.88190	37.59311	25.73306	14.77635	
3	40.0	120.18752	92.64140	84.13524	68.06836	55.87748	42.72325	29.28677	16.55220	
3	42.0	116.30383	89.09179	80.74810	65.37108	53.68223	41.38226	28.44563	16.40447	
3	43.0	131.67615	101.55366	92.32181	74.74656	61.35884	46.92768	32.16816	18.13568	

3	45.0	129.55270	99.21452	90.01288	72.94406	59.93467	46.24452	31.85635	18.40151
3	45.0	137.67638	105.79360	95.67742	77.12172	63.22443	48.38765	33.10340	19.01679
3	48.0	136.91345	104.62819	94.84727	76.84671	63.16601	48.63935	33.46887	19.42282
3	48.0	142.83786	110.52200	100.20395	80.94223	66.70872	51.38624	35.52433	21.17729
3	50.0	141.56859	109.23063	98.63936	79.38849	65.30014	50.42647	35.34568	21.90277
3	50.0	143.41260	111.04867	100.24596	80.75000	66.53655	51.60226	36.48179	23.04857
3	55.0	148.32176	115.74693	105.43876	85.65062	71.13303	55.72259	40.20836	26.92806
3	55.0	148.87682	116.26460	105.94905	85.93918	71.36502	55.97836	40.59947	27.42201
3	60.0	155.60770	123.18178	112.91939	91.86608	76.40451	60.42434	44.57548	31.48237
3	60.0	155.54647	123.38450	112.37616	91.06673	75.62759	59.81520	43.98377	30.95980
3	65.0	159.00676	130.13127	118.15746	94.86080	78.64998	62.38601	46.44977	33.64406

Table D.3: **Experimental data:** $750\mu m - 1000\mu m$

		Pressure reading [$mbar$]							
Run no.	Fluid velocity [ℓ/min]	Sensor 1 at 30mm	Sensor 2 at 230mm	Sensor 3 at 331mm	Sensor 4 at 432mm	Sensor 5 at 532mm	Sensor 6 at 633mm	Sensor 7 at 733mm	Sensor 8 at 834mm
1	10.0	9.77829	7.59895	6.86236	5.59822	4.61242	3.57332	2.43170	1.55725
1	10.0	9.02922	7.00768	6.28926	5.18274	4.30057	3.33313	2.19653	1.30954
1	20.0	19.39146	15.01717	13.64963	11.10084	9.18120	7.15512	4.99486	3.18978
1	20.0	18.46015	14.28424	12.87461	10.55536	8.77891	6.82609	4.64388	2.69461
1	30.0	32.41464	25.09598	22.87748	18.59110	15.41785	12.06065	8.51348	5.43105

1	30.0	31.24210	24.16362	21.83511	17.88048	14.89102	11.61576	8.00216	4.61026	
1	40.0	47.92672	37.15278	33.96709	27.61795	22.96277	18.02221	12.81190	8.24704	
1	40.0	46.60605	36.05610	32.64262	26.72250	22.27046	17.39835	12.05993	6.91598	
1	50.0	64.48103	49.99906	45.77099	37.22982	30.97949	24.34375	17.35569	11.14318	
1	50.0	65.27084	50.53424	45.82872	37.52869	31.30494	24.46902	17.02566	9.71970	
1	60.0	87.72582	68.00077	62.34147	50.72111	42.21389	33.17279	23.73166	15.28602	
1	60.0	89.34851	69.25605	62.92726	51.56066	43.05216	33.67578	23.48638	13.32852	
1	65.0	100.27644	77.71582	71.27299	58.01583	48.28382	37.97735	27.19327	17.53144	
1	65.0	103.13024	79.99091	72.75268	59.64028	49.82832	38.98072	27.21011	15.40811	
1	70.0	114.40336	88.58967	81.27594	66.16956	55.05048	43.34823	31.17878	20.23470	
1	70.0	115.72131	89.79516	81.73912	67.01958	56.00007	43.79573	30.53552	17.12569	
1	75.0	125.20633	96.96977	89.06448	72.54645	60.43384	47.77256	34.53194	22.39082	
1	75.0	127.18710	98.48291	89.53778	73.24799	60.96986	47.37618	32.60744	18.31325	
1	80.0	137.06661	105.40219	95.34198	77.40298	63.69349	48.92375	33.73848	19.70655	
1	80.0	140.55830	108.93484	100.22681	81.78028	68.13080	53.93161	38.80769	25.06995	
1	85.0	142.48277	108.81385	98.49233	79.76859	66.50970	51.70298	36.29361	22.25470	
1	85.0	147.35917	113.94777	104.08193	85.21952	71.45493	56.75041	41.68667	28.35765	
1	90.0	144.49449	111.48420	101.60131	82.89069	69.40686	54.76826	39.66504	26.42413	
1	90.0	153.00203	119.03521	109.16840	89.81076	75.90412	61.04509	46.01535	33.40346	
1	95.0	158.21229	124.70373	114.70735	94.60775	80.52460	65.63853	50.55788	38.32575	
1	100.0	157.13965	124.62731	114.88821	94.78839	81.15711	66.60255	51.78054	39.95403	
1	105.0	163.52639	138.52997	130.55266	109.48002	94.98798	79.15806	63.53539	51.54221	
1	110.0	162.85023	138.36161	129.25356	107.92779	93.75011	78.45765	62.84715	51.20585	
1	110.0	164.11721	142.89167	135.69581	114.38118	99.93651	84.22050	68.13877	55.95756	
1	120.0	163.83682	148.23504	145.76618	124.89255	108.75464	91.42036	74.65948	63.05205	
2	10.0	9.52192	7.22726	6.40016	5.14772	4.07093	3.03589	1.90244	0.96457	
2	10.0	9.56803	7.37443	6.60403	5.29302	4.25849	3.16662	1.96947	0.95207	

2	20.0	19.17324	14.44983	12.88567	10.29101	8.16733	6.09636	3.88914	1.92683
2	20.0	19.26746	14.80344	13.28955	10.62789	8.54724	6.36409	4.06970	1.90010
2	30.0	31.98915	24.06422	21.52979	17.17591	13.64739	10.20704	6.57866	3.25862
2	30.0	32.38947	24.85073	22.36863	17.84572	14.37584	10.71241	6.91567	3.18255
2	40.0	46.92932	35.28275	31.66052	25.22868	20.09657	15.04509	9.74394	4.81186
2	40.0	48.73125	37.38567	33.72461	26.90484	21.68892	16.17166	10.48927	4.78535
2	50.0	65.17460	48.98662	44.05335	35.12008	28.00700	20.99565	13.66067	6.74174
2	50.0	68.53159	52.61764	47.54217	37.94669	30.62503	22.84032	14.85280	6.74792
2	60.0	88.71841	66.61450	60.02870	47.87621	38.23171	28.71844	18.75984	9.33580
2	60.0	93.34582	71.72270	64.92938	51.86858	41.91240	31.28052	20.35891	9.19861
2	65.0	101.17164	75.91939	68.46341	54.64487	43.66979	32.87003	21.58377	10.84211
2	65.0	107.65407	82.75004	74.99883	59.93376	48.46175	36.16539	23.52421	10.57073
2	70.0	112.72748	84.38213	76.12893	60.72230	48.44607	36.48854	24.06306	12.35724
2	70.0	121.97358	93.58413	84.74905	67.56218	54.41566	40.29524	25.79913	11.01833
2	75.0	123.56238	92.79164	83.83855	66.84003	53.37467	40.24390	26.67492	14.06772
2	75.0	132.08438	100.80912	90.94286	72.38265	57.80390	42.65031	26.49497	11.94049
2	80.0	135.24036	101.70549	91.62998	73.22732	58.75565	44.12243	29.21256	14.93718
2	80.0	136.54770	102.34552	91.33627	72.91284	59.05352	43.69304	28.14289	13.96952
2	85.0	138.59797	105.09207	94.57580	75.88121	62.05551	47.48758	32.29640	19.19767
2	85.0	137.22871	104.05425	93.49725	75.01848	61.07670	46.37544	30.99690	17.67939
2	90.0	143.65148	109.38605	98.78397	80.28287	65.62797	50.89135	36.12466	22.18218
2	90.0	145.85892	111.98538	101.64008	81.87629	67.36119	52.58658	37.31738	24.47028
2	100.0	149.90876	117.10564	105.88210	85.42047	70.27393	55.00503	40.97895	28.60067
2	100.0	153.74699	123.58328	113.39443	93.02331	76.87967	61.81540	45.94444	32.23326
2	110.0	156.81142	129.62368	119.15767	97.61163	83.61170	66.96067	50.88227	38.53596
3	10.0	8.73212	6.66136	5.90095	4.81919	3.89242	2.88984	1.77378	0.93236
3	10.0	9.63296	7.26863	6.40849	5.13242	4.12046	3.06315	1.89561	1.00866

3	20.0	19.00033	14.24935	12.64485	10.06409	8.09806	6.03709	3.84474	1.98675
3	20.0	17.84108	13.53758	12.07979	9.78938	7.92604	5.90237	3.72824	1.89388
3	30.0	31.50192	23.59581	20.99234	16.68077	13.43241	10.03528	6.47445	3.31358
3	30.0	30.16425	22.84328	20.45421	16.53342	13.40277	9.99494	6.39059	3.21079
3	40.0	46.64676	34.93562	31.15627	24.73889	19.93770	14.91853	9.68478	4.93404
3	40.0	45.37121	34.36505	30.84368	24.91832	20.21759	15.08752	9.70543	4.84543
3	50.0	64.06585	48.00731	42.88344	34.05440	27.47285	20.57115	13.43611	6.84427
3	50.0	63.99281	48.50559	43.63290	35.26393	28.63928	21.38843	13.80106	6.85749
3	60.0	86.90455	65.09802	58.22089	46.23417	37.33288	27.99156	18.34005	9.44716
3	60.0	87.46054	66.37441	59.83916	48.39762	39.36906	29.41723	19.01921	9.40609
3	65.0	98.68434	73.83609	66.08849	52.49108	42.44883	31.90237	21.02454	10.83592
3	65.0	99.52577	75.61834	68.25277	55.24867	44.98386	33.62023	21.74629	10.72663
3	70.0	109.82108	81.94855	73.38182	58.27450	47.15659	35.45409	23.46157	12.24592
3	70.0	114.06221	86.84019	78.57625	63.71034	51.98259	38.91471	25.22852	12.44559
3	75.0	121.94801	90.91740	81.48413	64.70317	52.53924	39.73169	26.61034	14.44179
3	75.0	125.84857	95.82556	86.78315	70.40299	57.45405	42.97645	27.80037	13.44790
3	80.0	133.26912	100.01133	89.83925	71.21358	57.34335	43.22001	28.77831	15.33234
3	80.0	133.81222	100.85395	90.76465	72.94146	58.82571	43.88654	28.76824	14.77328
3	85.0	137.60100	104.50762	93.89468	75.31708	61.53662	47.03068	32.21128	18.69090
3	85.0	137.36736	103.80135	93.25515	74.72858	60.88490	46.23801	31.31272	17.92300
3	90.0	143.80636	110.50838	99.92623	80.35197	65.96818	50.93274	36.09584	23.26333
3	90.0	143.05144	109.43195	98.69497	79.23968	64.87345	49.92194	35.05086	22.23052
3	100.0	153.61917	121.70321	111.41039	91.47960	77.28648	61.59794	45.46043	32.87421
3	100.0	151.15737	118.46335	107.95646	87.38722	72.04363	56.38782	41.16116	28.64399
3	110.0	155.91992	128.02531	118.22181	97.67642	83.67158	67.97444	51.42820	39.03196

Bibliography

[1] Churchill, S.W. and Usagi, R.: A general expression for the correlation of rates of transfer and other phenomena. *American Institute of Chemical Engineers Journal*, vol. 18, no. 6, pp. 1121 – 1128, 1972.

[2] Churchill, S.W. and Usagi, R.: A standardized procedure for the production of correlations in the form of a common empirical equation. *Industrial and Engineering Chemistry, Fundamentals*, vol. 13, no. 1, pp. 39 – 44, 1974.

[3] De Wet, P.D., Du Plessis, J.P., Mbiya, B.M. and Fester, V.G.: Power addition applied to non-Newtonian flow in a diaphragm valve. 2nd Southern African Conference on Rheology (SASOR), Cape Town, South Africa, 6 – 8 October 2008.

[4] De Wet, P.D., Halvorsen, B.M. and Du Plessis, J.P.: Powered addition applied to the fluidisation of a packed bed. In: Mammoli, A.A. and Brebbia, C.A. (eds.), *Computational Methods in Multiphase Flow V*, pp. 431 – 441. WIT Press, Southampton, UK, 15 – 17 June 2009.

[5] Churchill, S.W.: *The Interpretation and Use of Rate Data: The Rate Concept*. McGraw-Hill, New York, USA, 1974.

[6] Churchill, S.W.: Derivation, selection, evaluation and use of asymptotes. *Chemical Engineering and Technology*, vol. 11, pp. 63 – 72, 1988.

[7] Greenberg, M.D.: *Foundations of Applied Mathematics*. Prentice-Hall, Inc., Englewood Cliffs, USA, 1978.

[8] Myles, K.: *Knowing More About Valves*. K Myles and Associates cc, Northcliff, Johannesburg, South Africa, 2000.

[9] Mbiya, B.M.: *Predicting Pressure Losses in Straight-through Diaphragm Valves*. Ph.D. thesis, Cape Peninsula University of Technology, Cape Town, South Africa, 2007.

[10] Fester, V.G., Kazadia, D.M., Mbiya, B.M. and Slatter, P.T.: Loss coefficients for flow of Newtonian and non-Newtonian fluids through diaphragm valves. *Chemical Engineering Research and Design*, vol. 85, no. 9, pp. 1314 – 1324, 2007.

[11] Mbiya, B.M., Fester, V.G. and Slatter, P.T.: Evaluating resistance coefficients of straight-through diaphragm control valves. *The Canadian Journal of Chemical Engineering*, vol. 87, no. 5, pp. 704 – 714, 2009.

[12] Ward Smith, A.J.: *Pressure Losses in Ducted Flows*. Butterworth & Co (Publishers) Ltd, London, UK, 1971.

[13] Miller, D.S.: *Internal Flow: A Guide to Losses in Pipe and Duct Systems*. British Hydromechanics Research Association, Cranfield, UK, 1971.

[14] Streeter, V.L.: *Fluid Mechanics*. 4th edn. McGraw-Hill, New York, USA, 1966.

[15] Slatter, P.T.: The role of rheology in the pipelining of mineral slurries. *Mineral Processing and Extractive Metallurgy Review*, vol. 20, no. 1, pp. 281 – 300, 1999.

[16] Massey, B.S.: *Mechanics of Fluids*. 6th edn. Van Nostrand Reinhold (International), London, UK, 1989.

[17] Bird, R.B., Stewart, W.E. and Lightfoot, E.N.: *Transport Phenomena*. John Wiley & Sons, Inc., New York, USA, 1960.

[18] Happel, J. and Brenner, H.: *Low Reynolds Number Hydrodynamics with Special Applications to Particulate Media*. Martinus Nijhoff Publishers, The Hague, Netherlands, 1983.

[19] Tokaty, G.A.: *A History and Philosophy of Fluidmechanics*. G T Foulis & Co Ltd, Henley-on-Thames, Oxfordshire, UK, 1971.

[20] Bear, J. and Bachmat, Y.: *Introduction to Modeling of Transport Phenomena in Porous Media*, vol. 4 of *Theory and Applications of Transport in Porous Media*. Kluwer Academic Publishers, Dordrecht, Netherlands, 1991.

[21] Forchheimer, P.H.: Wasserbewegung durch boden. *Zeit. d. Ver. deutsch Ing.*, vol. 45, pp. 1782 – 1788, 1901.

[22] Woudberg, S.: *Laminar Flow through Isotropic Granular Porous Media*. Master's thesis, University of Stellenbosch, Stellenbosch, South Africa, 2006.

[23] Terblanche, L.: *The Prediction of Flow through Two-Dimensional Porous Media*. Master's thesis, University of Stellenbosch, Stellenbosch, South Africa, 2006.

[24] Niven, R.K.: Physical insight into the Ergun and Wen&Yu equations for fluid flow in packed and fluidised beds. *Chemical Engineering Science*, vol. 57, pp. 527 – 534, 2002.

[25] Churchill, S.W.: Similitude: Dimensional analysis and data correlation (Chapter 3). In: Kreith, F. (ed.), *Mechanical Engineering Handbook*, pp. 3–28 – 3–43. CRC Press LLC, Boca Raton, USA, 1999.

[26] Geldart, D.: Single particles, fixed and quiescent beds (Chapter 2). In: Geldart, D. (ed.), *Gas Fluidization Technology*, pp. 11 – 32. John Wiley & Sons, Inc., Chichester, UK, 1986.

[27] Du Plessis, J.P. and Masliyah, J.H.: Mathematical modelling of flow through consolidated isotropic porous media. *Transport in Porous Media*, vol. 3, pp. 145 – 161, 1988.

[28] Du Plessis, J.P.: Analytical quantification of coefficients in the Ergun equation for fluid friction in a packed bed. *Transport in Porous Media*, vol. 16, pp. 189 – 207, 1994.

[29] Du Plessis, J.P. and Diedericks, G.P.J.: Pore-scale modelling of interstitial transport phenomena (Chapter 2). In: Du Plessis, J.P. (ed.), *Fluid Transport in Porous Media*, pp. 61 – 104. Computational Mechanics Publications, Southampton, UK, 1997.

[30] Smit, G.F.J., Du Plessis, J.P. and Du Plessis (Sr.), J.P.: Modelling of airflow through a stack in a timber-drying kiln. *Applied Mathematical Modelling*, vol. 31, pp. 270 – 282, 2007.

[31] Woudberg, S., Du Plessis, J.P. and Smit, G.J.F.: Non-Newtonian purely viscous flow through isotropic granular porous media. *Chemical Engineering Science*, vol. 61, pp. 4299 – 4308, 2006.

[32] Du Plessis, J.P. and Woudberg, S.: Pore-scale derivation of the Ergun equation to enhance its adaptability and generalization. *Chemical Engineering Science*, vol. 63, no. 1, pp. 2576 – 2586, 2008.

[33] Crosnier, S., Du Plessis, J.P., Riva, R. and Legrand, J.: Modelling of gas flow through isotropic metallic foams. *Journal of Porous Media*, vol. 9, no. 1, pp. 35 – 54, 2006.

[34] Du Plessis, J.P., Montillet, A., Comiti, J. and Legrand, J.: Pressure drop prediction for flow through high porosity metallic foams. *Chemical Engineering Science*, vol. 49, no. 21, pp. 3545 – 3553, 1994.

[35] Davidson, J.F. and Harrison, D.: *Fluidised Particles*. Cambridge University Press, London, UK, 1963.

[36] Geldart, D.: Introduction (Chapter 1). In: Geldart, D. (ed.), *Gas Fluidization Technology*, pp. 1 – 10. John Wiley & Sons, Inc., Chichester, UK, 1986.

[37] Geldart, D.: Characterization of fluidized powders (Chapter 3). In: Geldart, D. (ed.), *Gas Fluidization Technology*, pp. 33 – 54. John Wiley & Sons, Inc., Chichester, UK, 1986.

[38] Sabiri, N.-E.: *Etude de l'Ecoulement de Fluides Newtoniens et Non Newtoniens a Travers les Milieux Poreux: Lits Fixes et Lits Fluidises*. Ph.D. thesis, Université de Nantes, Saint-Nazaire, France, 1995.

[39] Sabiri, N.-E. and Comiti, J.: Pressure drop in non-Newtonian purely viscous fluid flow through porous media. *Chemical Engineering Science*, vol. 50, no. 7, pp. 1193 – 1201, 1995.

[40] Ciceron, D.: *Etude de Fluidisation de Particules de Formes Diverses par des Liquides Non Newtoniens*. Ph.D. thesis, Université de Nantes, Saint-Nazaire, France, 2000.

[41] Richardson, J.F.: Incipient fluidization and particulate systems (Chapter 2). In: Davidson, J.F. and Harrison, D. (eds.), *Fluidization*, pp. 25 – 64. Academic Press, London, UK, 1971.

[42] Churchill, S.W.: Comprehensive correlating equations for heat, mass and momentum transfer in fully developed flow in smooth tubes. *Industrial and Engineering Chemistry, Fundamentals*, vol. 16, no. 1, pp. 109 – 116, 1977.

[43] Churchill, S.W.: Correlating equations for transitional behavior. *Industrial and Engineering Chemistry Research*, vol. 40, pp. 3053 – 3057, 2001.

[44] Chhabra, R.P. and Richardson, J.F.: *Non-Newtonian Flow and Applied Rheology: Engineering Applications*. 2nd edn. Butterworth-Heinemann, Oxford, UK, 2008.

[45] Hughes, W.F. and Brighton, J.A.: *Schaum's Outline of Theory and Problems of Fluid Dynamics*. 3rd edn. New York, USA.

[46] Incropera, F.P., Dewitt, D.P., Bergman, T.L. and Lavine, A.S.: *Fundamentals of Heat and Mass Transfer*. 6th edn. John Wiley & Sons, Inc., New Jersey, USA, 2007.

[47] Slatter, P.T.: *Transitional and Turbulent Flow of Non-Newtonian Slurries in Pipes*. Ph.D. thesis, University of Cape Town, Cape Town, South Africa, 1994.

[48] Slatter, P.T.: Sludge pipeline design. *Water Science and Technology*, vol. 44, no. 5, pp. 115 – 120, 2001.